*Volume 8, No. 3*

*May, 1961*

# THE SOVIET JOURNAL OF

# ATOMIC ENERGY

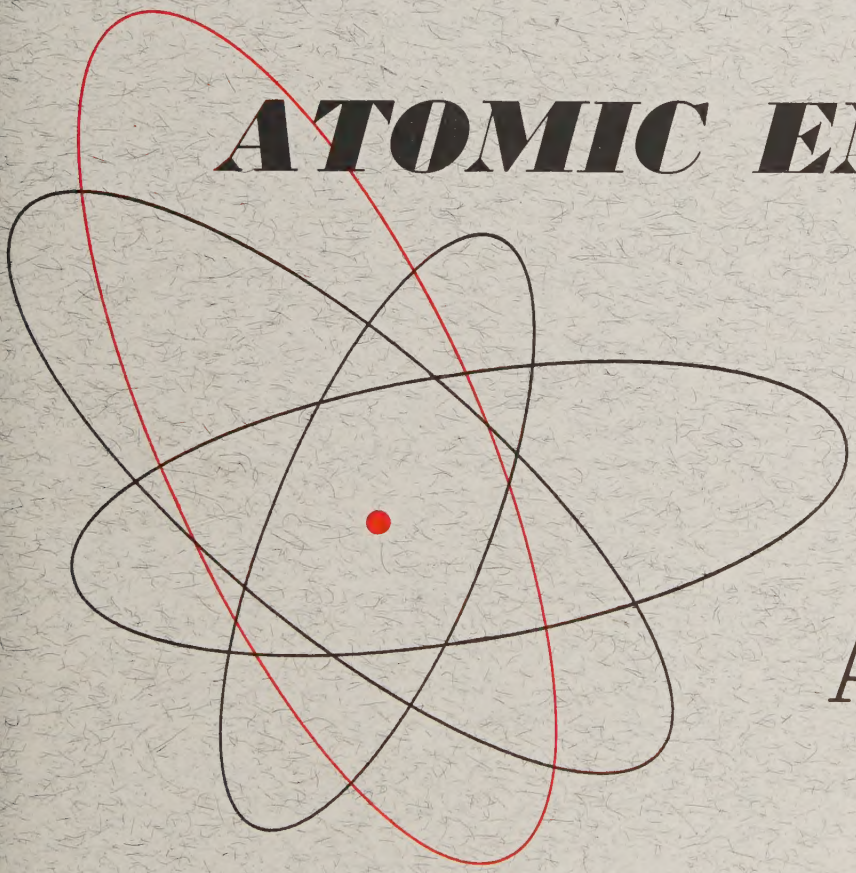

# Атомная энергия

TRANSLATED FROM RUSSIAN

CONSULTANTS BUREAU

THE SOVIET JOURNAL OF

# ATOMIC ENERGY

*A translation of ATOMNAYA ÉNERGIYA,*
*a publication of the Academy of Sciences of the USSR*

(Russian original dated March, 1960)

Vol. 8, No. 3 May, 1961

## CONTENTS



Annual subscription $75.00
Single issue 20.00
Single article 12.50

# CONTENTS (continued)



NOTE

The Table of Contents lists all material that appears in Atomnaya Énergiya. Those items that originated in the English language are not included in the translation and are shown enclosed in brackets. Whenever possible, the English-language source containing the omitted reports will be given.

Consultants Bureau Enterprises, Inc.

# THE LATE FRÉDERIC JOLIOT-CURIE
## (on the occasion of his sixtieth birthday)

March 19, 1960 marks the passage of sixty years from the time of the birth of the outstanding French scientist and physicist Fréderic Joliot-Curie, ardent fighter for peace and member of the French Communist Party. The name of this scientist is inscribed in gilded letters in the history of science. The most important stages of the development of nuclear physics in the first half of the XX Century are associated with his name.

Fréderic Joliot-Curie launched into the study of the physics of the atomic nucleus back in 1928, in collaboration with his wife Irene Joliot-Curie. In 1934 they discovered the phenomenon of artificial radioactivity. This discovery played an exceptionally great role in the development of concepts on the properties of atomic nuclei. The Joliot-Curies were jointly awarded the Nobel prize for this discovery, outstanding in its importance. The phenomenon of artificial radioactivity has come into advantageous use in our time on a broad and fruitful scale in almost all branches of science and in many branches of industry.

Joliot-Curie performed much important work preparatory to and conducive to the discovery of the neutron. He was the first to record and photograph the results of a neutron-proton collision in a Wilson cloud chamber. An important phase of Joliot-Curie's endeavors was also devoted to research on the formation by gamma photons of pairs of oppositely charged particles, the position and electron.

The outstanding scientist Joliot-Curie was one of the first to grasp the enormous significance of the discoveries of nuclear physics for the future of mankind. He took a firm stand against secrecy clouding research, and against military uses of nuclear research.

In 1946, soon after the liberation of France from the Hitlerite usurpers, Joliot-Curie became head of the Commissariat de l'Énergie Atomique, of which he was the founder, and on December 15, 1948, France's first nuclear reactor, named ZOE ("life" in Greek), was commissioned under his supervision.

In 1943, Joliot-Curie became a member of the Paris Academy of Sciences, and in 1947 became a Corresponding Member of the Academy of Sciences of the USSR.

Joliot-Curie was also very much active in public life. From 1946 on he was president of the World Federation of Scientific Workers, and from 1951 held the post of Chairman of the World Peace Council..

Joliot-Curie died on August 14, 1958.

Soviet scientists also found in Fréderic Joliot-Curie a true friend, and felt pride for his being an outstanding scientist and fighter for peace.

# A CYCLOTRON WITH A SPATIALLY VARYING MAGNETIC FIELD*

D. P. Vasilevskaya, A. A. Glazov, V. I. Danilov, Yu. N. Denisov,
V. P. Dzhelepov, V. P. Dmitrievskii, B. I. Zamolodchikov,
N. L. Zaplatin, V. V. Kol'ga, A. A. Kropin, Liu Nei-ch'uang
V. S. Rybalko, A. L. Savenkov, and L. A. Sarkisyan

Translated from Atomnaya Énergiya, Vol. 8, No. 3, pp. 189-200,
March, 1960
Original article submitted August 27, 1959

This article is devoted to the design of a cyclotron with a spatially varying magnetic field. The basic conclusions of the linear theory of motion of charged particles in a magnetic field of periodic radial and azimuthal structure are given. The theoretical and experimental results of the study of nonlinear resonance close to the center of the accelerator are presented. Formulas are obtained for the calculation of required magnetic field configurations. Methods of shimming, measurement, and stabilization of the magnetic field are suggested. An accelerator designed with pole faces of diameter 120 cm was used for modeling the ion phase motion and for investigating spatial stability. Deuterons were accelerated to an energy of 13 Mev at an accelerating voltage of 5 kv.

## Introduction

The idea of using a spatially varying magnetic field in cyclical accelerators to provide stable motion of the particles was first expressed in 1938 [1]. This idea was not further developed at that time because the limitation on the energy attainable in the cyclotron was caused by the phase motion of the ions, and the proposed method removed this limitation only in a narrow region of accelerated ion energies. As a result of the discovery of the autophasing principle in 1944-1945 by V. I. Veksler [2] and E. McMillan [3], the energy limitation in cyclical accelerators was removed. There arose, however, serious difficulties of a technical and economic nature in the design of accelerators for energies of the order of 10-15 Bev and above.

The application of magnetic fields with a varying gradient in ring accelerators [4] permitted a decrease in the volume of the magnetic field in which the acceleration of the particles takes place and an increase in the energy of the accelerated protons to several tens of billion electron-volts [5-7]. The pulse character of the operation of these accelerators, however, greatly restricts the average accelerated particle current and, to a considerable degree, narrows the possibilities of their use in nuclear research.

The proposed application of colliding beams of particles for the study of nuclear processes, the exceptional importance of investigations of nuclear reactions produced by secondary particles ($\pi$, $\mu$, K, $\tilde{p}$, $\Sigma$, etc.), the constantly increasing requirements of experimental accuracy all lead to the need of increasing the particle beam intensity obtained from the accelerators. In this connection, there is a pressing need for a detailed investigation of new possibilities of accelerating technique [8, 9] involving nonhomogeneous structures of stationary magnetic fields.†

In 1955, there was suggested a magnetic field whose intensity varies periodically in both the azimuthal and radial directions [12]. Theoretical investigations of the particle dynamics in such fields indicated that these fields are more advantageous than the magnetic fields suggested in [1]. For cyclical accelerators these advantages lead to an increase in the limiting energy of the accelerated particles and also to a considerable decrease in the required amplitude of variation (flutter) of the magnetic field intensity. For accelerators of the phasotron type, such fields permit one to obtain dy-

* A brief account of the starting up of this accelerator appeared in the journal Atomnaya Energiya 6, 6, 657 (1959). [Original Russian pagination. See. C. B. translation]

† Here we shall not consider questions related to the use of the properties of relativistic plasma [10] for accelerators or the possibilities of a coherent method of acceleration [11], since this goes beyond the scope of our discussion.

namically similar orbits during the entire acceleration cycle and also to "accomodate" a large range of pulses of particles in a relatively narrow ring-shaped zone of the magnetic field.

During 1955-1958, in the Nuclear Problems Laboratory of the Joint Institute of Nuclear Studies investigations of spiral-ridge magnetic fields were carried out on an accelerator of the cyclotron type designed and built on the basis of the theory of spatial stability developed at Dubna [13-15] and Harwell [16-18].

Linear Theory

The motion of a charged particle in a magnetic field is described by the equations (in the cylindrical coordinate system)

$$\left.\begin{aligned} r''-\frac{2r'^2}{r}-r &= -\frac{e}{mc}\frac{\sqrt{r'^2+r^2+z'^2}}{v}\left(rH_z-z'H_\varphi-\frac{z'r'}{r}H_r+\frac{r'^2}{r}H_z\right);\\ z''-\frac{2r'z'}{r} &= -\frac{e}{mc}\frac{\sqrt{r'^2+r^2+z'^2}}{v}\left(r'H_\varphi-rH_r-\frac{z'^2}{r}H_r+\frac{z'r'}{r}H_z\right), \end{aligned}\right\} \quad (1)$$

where r' and z' denote differentiation with respect to $\varphi$; $H_z$, $H_r$, $H_\varphi$ are the components of the magnetic field intensity; mv is the momentum of the particle.

We represent the magnetic field of a cyclotron in the median plane in the form

$$H_z = H(r)[1+\varepsilon f(r,\varphi)], \quad (2)$$

where $\epsilon$ is the flutter of the magnetic field; $f(r, \varphi)$ is a periodic function of r and $\varphi$ with an average value of zero.

After inserting (2) into (1), we obtain the following system of equations, which describes the motion of particles of momentum

$$p = mv = \frac{e}{c}H(R)R \quad (3)$$

apart from terms higher than the second order:

$$\left.\begin{aligned} &\varrho''+\left[1+n+\varepsilon R\frac{\partial f}{\partial r}+(2+n)\varepsilon f\right]\varrho+\\ &+\left[\frac{d}{R}+\frac{1}{R}+\frac{2n}{R}+\frac{\varepsilon}{R}(1+2n+d)f+\right.\\ &\left.+\varepsilon(2+n)\frac{\partial f}{\partial r}+\frac{\varepsilon R}{2}\frac{\partial^2 f}{\partial r^2}\right]\varrho^2-\\ &-\left[\frac{1}{2R}-\frac{3}{2}\frac{\varepsilon}{R}f\right]\varrho'^2-\frac{1}{2}\left[\frac{2d}{R}+\right.\\ &+\frac{2d}{R}\varepsilon f+2n\varepsilon\frac{df}{dr}+\varepsilon\frac{\partial f}{\partial r}+\frac{n}{R}(1+\varepsilon f)+\\ &\left.+\frac{\varepsilon}{R}\frac{\partial^2 f}{\partial\varphi^2}+\varepsilon R\frac{\partial^2 f}{\partial r^2}\right]z^2-\frac{\varepsilon}{R}\frac{\partial f}{d\varphi}zz'+\\ &+\frac{1}{2R}(1+\varepsilon f)z'^2=-\varepsilon Rf;\\ &z''-\left[n+\varepsilon nf+\varepsilon R\frac{\partial f}{\partial r}\right]z-\\ &-\left[\frac{2}{R}(n+d)+\frac{2\varepsilon}{R}(n+d)f+\right.\\ &+2\varepsilon(1+n)\frac{\partial f}{\partial r}+\varepsilon R\left.\frac{\partial^2 f}{\partial r^2}\right]z\varrho+\\ &+\frac{\varepsilon}{R}\frac{\partial f}{\partial\varphi}z\varrho'-\left[\frac{1}{R}-\frac{\varepsilon}{R}f\right]z'\varrho'=0, \end{aligned}\right\} \quad (4)$$

where $\varrho = r - R$; $n = \frac{R}{H(R)}\frac{dH(r)}{dr}\Big|_{r=R}$; $d = \frac{1}{2}\times$ $\times\frac{R^2}{H(R)}\frac{d^2H(r)}{dr^2}\Big|_{r=R}$; the values of the function $f$ and its partial derivatives are taken at r = R.

The equation of the closed orbit in the linear approximation obtained from (4) has the form

$$\varrho''+\left[1+n+\varepsilon R\frac{\partial f}{\partial r}+(2+n)\varepsilon f\right]\bar{\varrho}=-\varepsilon Rf. \quad (5)$$

Denoting by $\rho$ the particular solution of the inhomogeneous equation (5), we obtain a linearized equation of oscillations with respect to the closed orbit:

$$\left.\begin{aligned} &\varrho''+\left[1+n+\varepsilon R\frac{\partial f}{\partial r}+(2+n)\varepsilon f+\right.\\ &+\frac{2}{R}(1+2n+d)\bar{\varrho}+2\varepsilon(2+n)\bar{\varrho}\frac{\partial f}{\partial r}+\\ &\left.+\frac{2\varepsilon}{R}(1+2n+d)f\bar{\varrho}+\varepsilon R\bar{\varrho}\frac{\partial^2 f}{\partial r^2}\right]\varrho-\\ &-\frac{1}{R}(1-3\varepsilon f)\bar{\varrho}'\varrho'=0;\\ &z''-\left[n+\varepsilon nf+\varepsilon R\frac{\partial f}{\partial r}+\frac{2}{R}(n+d)\varrho+\right.\\ &+\frac{2\varepsilon}{R}(n+d)\bar{\varrho}f+2\varepsilon(1+n)\bar{\varrho}\frac{\partial f}{\partial r}+\\ &\left.+\varepsilon R\bar{\varrho}\frac{\partial^2 f}{\partial r^2}-\frac{\varepsilon}{R}\frac{\partial f}{\partial r}\bar{\varrho}'\right]z-\\ &-\frac{1}{R}(1-\varepsilon f)\bar{\varrho}'z'=0. \end{aligned}\right\} \quad (6)$$

We shall consider a case encountered in practice in which the lines of the extreme values of the vertical component of the magnetic field intensity are Archimedes spirals:

$$f=\sin\left(\frac{r}{\lambda}-N\varphi\right), \quad (7)$$

where $2\pi\lambda$ is the radial pitch and N is the periodicity of the magnetic field structure.

Since in a cyclotron ($\omega_0$ = const) the exponent of the field n should vary as $\beta^2/(1-\beta^2)$, then the choice of the magnetic field structure in which the extreme values of the intensity are distributed over a logarithmic spiral [16] is impractical.

For the cyclotron under consideration the basic focusing action is determined by terms containing the ratio $R/\lambda$. For a nonconservative choice of parameters [19], this ratio considerably exceeds unity throughout the range of radii, except for a small zone at the center

of the accelerator where the employed linear theory is inapplicable.

After neglecting small terms and reducing the system (6) to canonical form, we can write

$$\left.\begin{aligned} \varrho'' + (a_r + 2q\cos 2\xi)\,\varrho = 0; \\ z'' + (a_z - 2q\cos 2\xi)\,z = 0, \end{aligned}\right\} \qquad (8)$$

where

$$a_r = \frac{4}{N^2}\left\{1 + n - \frac{\varepsilon^2 R^2}{2\lambda^2 [N^2 - (1+n)]}\right\};$$

$$a_z = -\frac{4}{N^2}\left\{n - \frac{\varepsilon^2 R^2}{2\lambda^2 [N^2 - (1+n)]}\right\};$$

$$q = \frac{2\varepsilon R}{N^2 \lambda};$$

$$2\xi = \frac{R}{\lambda} - N\varphi.$$

From (8) it follows that for cyclotrons the intial values of the coefficients in the Mathieu equations are $a_r = 4/N^2$, $a_z = 0$, $q = 0$, i.e., the working point lies in the first stability band [20]. The width of this band for $q < 1$ is given to an accuracy of a few percent by

$$-\frac{1}{2}q^2 \leqslant a_{r,\,z} \leqslant 1 - q - \frac{1}{8}q^2. \qquad (9)$$

From inequalities (9) it follows that for the vertical oscillations the restriction imposes only the lower boundary of the stability band ($-1/2q^2$) and for radial oscillations, only the upper boundary ($1 - q - 1/8q^2$).

The first restriction is written in the form

$$\varepsilon \geqslant \frac{N\lambda}{R}\sqrt{n}\sqrt{\frac{N^2 - (1+n)}{N^2 - \frac{1}{2}(1+n)}}, \qquad (10)$$

and the second

$$\varepsilon \leqslant \frac{N^2\lambda}{2R}\left\{\frac{4[N^2-(1+n)]}{3N^2+(1+n)} - \sqrt{\frac{16[N^2-(1+n)]^2}{(3N^2+n+1)^2} - \frac{8[N^2-(1+n)]}{3N^2+n+1} + \frac{32(1+n)[N^2-(1+n)]}{N^2(3N^2+n+1)}}\right\}. \qquad (11)$$

Comparing (10) and (11) for a given N, one may determine the limiting values of the quantity n, and, consequently, the limiting energy which can be obtained in the cyclotron with a magnetic field of the form (7):

$$E_{\text{kin}} = E_0\left(\sqrt{n+1} - 1\right). \qquad (12)$$

For accelerators whose free frequencies of oscillation change during the acceleration process, the limiting energy is determined not by the boundaries of the stability band but by the resonance values of the free frequencies of oscillation.

From the system of equations (8), it follows that the free frequencies of oscillation are

$$Q_{z,\,r} = \frac{N}{2}\mu_{z,\,r}, \qquad (13)$$

where the values $\mu_z$ and $\mu_r$ for the Mathieu equations are determined from the expression

$$\cos\mu\pi = \cos\pi\sqrt{a} - \frac{\pi^2}{4}\frac{\sin\pi\sqrt{a}}{\pi\sqrt{a}}\frac{q^2}{1-a}. \qquad (14)$$

This expression is sufficiently accurate for practical calculations over the entire range of variation of the free oscillation frequencies.

If $q \ll 1$, then from (8), (13), and (14) it follows that

$$Q_r = \sqrt{1+n} + \frac{3}{4}\frac{1}{N^3}\left(\frac{\varepsilon R}{\lambda N}\right)^2 \frac{1 - \frac{4}{3}\frac{1+n}{N^2}}{1 - \frac{1+n}{N^2}}, \qquad (15)$$

where for $n \ll N^2$

$$Q_z = \sqrt{\left(\frac{\varepsilon R}{N\lambda}\right)^2 - n}. \qquad (16)$$

Thus, the initial frequencies of the free oscillations in cyclotrons are $Q_z = 0$ and $Q_r = 1$. In the acceleration process these frequencies increase. If we exclude resonance excitation of oscillation in the central region of the accelerators, then the first linear resonance excitation of the oscillations of the first and third harmonics of the magnetic field are possible in the zones where $Q_z = 0.5$ and $Q_r = 1.5$, respectively.

Data on the passage of particles through parametric resonance are given in [15]. The calculations carried out for an increase in the amplitudes of oscillation close to the resonance regions $Q_r = 2$ and $Q_z = 1$ for a periodicity of the magnetic field structure N equal to 4, 6, 8, and $\infty$ indicate possible limiting energies‡ of 500, 790, 850, and 938 Mev, respectively for protons.

## Nonlinear Effects

The presence in the magnetic field structure (2) and (7) of the small parameter $\varkappa$ increases the influence of nonlinear effects in such accelerators.

By analogy with systems considered in [21], it should be expected that the investigated systems (1), (2), (7) are excited to frequencies $Q_{r,z} = l\,N/q$, where $l$ and $q$ are integers. Thus, in the central region of the accelerator ($Q_r = 1$, $l = 1$, $q = N$) a nonlinear resonance effect is possible if the initial amplitude is larger than some quantity determined by the parameters of the chosen magnetic field structure. In order to find this amplitude it is necessary to solve (1) at $z = 0$.

$$r'' - \frac{2r'^2}{r} - r = -\frac{e}{pc}\frac{(r'^2 + r^2)^{3/2}}{r}H_z(r, \varphi). \qquad (17)$$

‡ The resonance $Q_z = 1$ and also the resonance for the linear interaction $Q_r + Q_z = 1$, $Q_r + Q_z = 2$ occur only in the event of disturbance of the mirror symmetry of the magnetic field $\left.\frac{\partial H_z}{\partial z}\right|_{z=0} \neq 0$.

Here

$$H_z(r, \varphi) = H_0(1 + \alpha r^2)\left[1 + \varepsilon \sin\left(\frac{r}{\lambda} - N\varphi\right)\right],$$

where

$$\alpha = \frac{1}{2r_\infty^2}\left(r_\infty = \frac{E_0}{eH_0}\right).$$

For the central region of the accelerator $\alpha r^2 \ll 1$ and $\epsilon \ll 1$; therefore for the unperturbed solution of (17) one may take

$$r = s\cos(\varphi - \psi) + \sqrt{R^2 - s^2\sin^2(\varphi - \psi)}, \quad (18)$$

where s and $\psi$ are the coordinates of the center of curvature of the radius

$$R = \frac{pc}{eH_0}. \quad (19)$$

Since the appearance of a nonlinear resonance effect for $\epsilon \ll 1$ is expressed as a displacement of the instantaneous center of curvature of the orbit, the solution of (17) should also be sought in the form (18), where $s = s(\varphi)$ and $\psi = \psi(\varphi)$.

The relation between the coordinates of the particles (r, $\varphi$) and the coordinates of the center of curvature (s,$\psi$) for motion in the magnetic field $H_z(r, \varphi)$ can be represented in the form

$$\left.\begin{aligned} \frac{ds}{d\varphi} &= \frac{pc}{e}\frac{H_z'}{H_z^2\sqrt{r'^2 + r^2}} \times \\ &\times [r\cos(\varphi - \psi) + r'\sin(\varphi - \psi)]; \\ s\frac{d\psi}{d\varphi} &= \frac{pc}{e}\frac{H_z'}{H_z^2\sqrt{r'^2 + r^2}} \times \\ &\times [r\sin(\varphi - \psi) - r'\cos(\varphi - \psi)], \end{aligned}\right\} \quad (20)$$

where $H_z'$ denotes the total derivative with respect to $\varphi$. Inserting (18) into (20) and using the method introduced in [21] of averaging over $\varphi$ for the condition $s_{max} < \lambda \ll R$, we obtain for even structures ($N = 2k$)

$$\left.\begin{aligned} \frac{ds}{d\varphi} &= (-1)^{N/2}\varepsilon R\frac{1}{(N-1)!\,2^N} \times \\ &\times \left(\frac{s}{\lambda}\right)^{N-1}\sin\left(N\psi - \frac{R}{\lambda}\right); \\ \frac{d\psi}{d\varphi} &= -\alpha R^2 + (-1)^{N/2}\frac{\varepsilon R}{\lambda} \times \\ &\times \frac{1}{(N-1)!\,2^N}\left(\frac{s}{\lambda}\right)^{N-2}\cos\left(N\psi - \frac{R}{\lambda}\right). \end{aligned}\right\} \quad (21)$$

From (21) it follows that the boundary separating operation with precession of the center of curvature from operation with azimuthal motion of the center of curvature limited by the angle $\pi / N$ is characterized by the inequality

$$\alpha R^2 > \frac{\varepsilon}{2^N(N-1)!}\frac{R}{\lambda}\left(\frac{s_{max}}{\lambda}\right)^{N-2}. \quad (22)$$

The experimental investigation of nonlinear resonance was carried out with an accelerator model for N = 4, $\lambda$ = 1.34 cm, $\epsilon$ = 0.02. The displacement of the centers of instantaneous orbits for various radii are seen in Fig. 1, where the points denote the positions of the centers of orbits and the numbers, their radii. The theoretically calculated maximum displacements of the centers for the case $s > \lambda$ are in agreement with experiment.

For the choice of the parameters of the magnetic field for which nonlinear resonance will not occur, it is sufficient to use (22), where instead of $s_{max}$ it is necessary to insert the maximum initial amplitude of oscillations for the given accelerator.

On the basis of the analysis, a magnetic field structure with the following parameters was produced: N = 6, $\lambda$ = 2.7 cm, $\epsilon$ = 0.066. Inserting these parameters in (22), one can see that it is satisfied starting with a radius of R = 2 cm. The experimental determination of the center of curvature of the orbits for

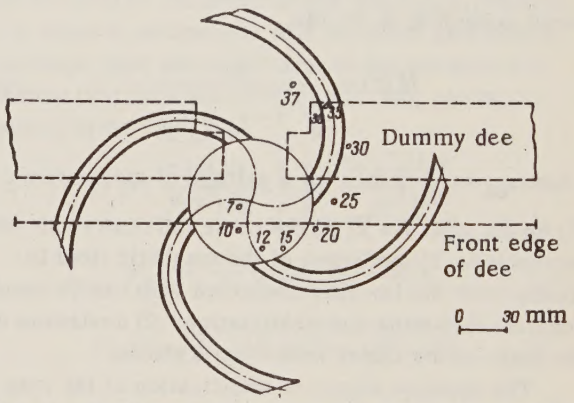


Fig. 1. Position of the centers of instantaneous orbits for N = 4.

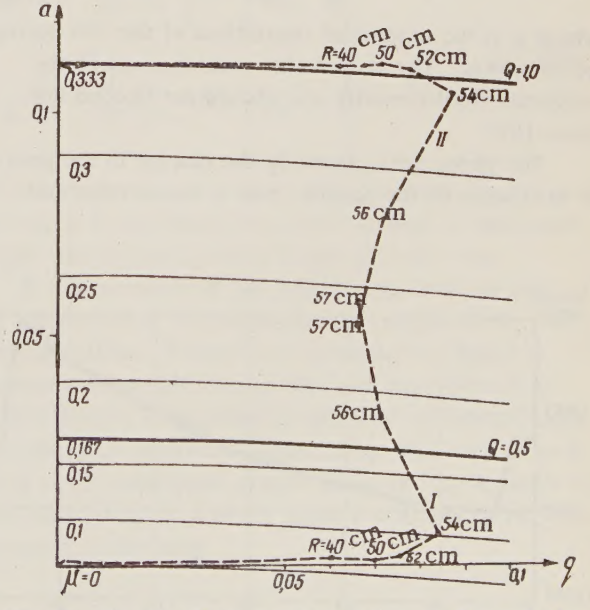


Fig. 2. Motion of the working points in the stability band. I) For vertical oscillations; II) for radial oscillations.

this case showed that the displacement of the orbits does not exceed the displacements resulting from the lower harmonics in the magnetic field structure; in absolute value these displacements do not exceed 2 cm.

The motion of the working point in the stability band characterizing the change in the free oscillation frequencies in the acceleration process is shown in Fig. 2.

For the design of an accelerator of such a type for phasotron energies, the choice of operation for the motion of the working point in the stability band will largely depend on the results of investigations of the passage of particles through the regions of nonlinear resonances $N/(N-1)$, $N/(N-2)$, . . . to $N/(N-0.5N) = 2$ for radial oscillations and also through the coupling oscillation zone.

## Phase Motion

If the mean value of the magnetic field intensity varies according to the law

$$H(r) = \frac{H_0}{\sqrt{1-\left(\frac{r}{r_\infty}\right)^2}}, \qquad (23)$$

where $r_\infty = \frac{E_0}{eH_0}$, then for a particle of momentum $p$ (3) on the orbit $R + \bar{\rho}(\varphi)$ the phase shift can result from two factors: 1) deviations of the magnetic field intensity from the law (23) connected with insufficiently accurate shimming and stabilization; 2) deviations of the shape of the closed orbit from a circle.

The required degree of stabilization of the magnetic field should not be less than

$$\frac{\Delta H}{H} = \frac{1}{4\nu}, \qquad (24)$$

where $\nu$ is the number of revolutions of the ion during acceleration. The error in the measurement of the magnetic field intensity also should not exceed this value [22].

The phase shift caused by the change in the period of revolution of the particle over a closed orbit under a change in energy can be calculated from the formula

$$\Delta\omega = \frac{v}{R} - \frac{2\pi v}{\int_0^{2\pi} \sqrt{r'^2 + r^2}\, d\varphi}. \qquad (25)$$

Using the solution of (5), we obtain

$$\frac{\Delta\omega}{\omega} = \frac{\varepsilon^2}{2}\left\{\frac{2+n}{(1+n)\,N^2-(1+n)]} - \frac{N^2}{2[N^2-(1+n)]^2}\right\}. \qquad (26)$$

From (26), it follows that the value of the correction to the law (23) is of the order $(\epsilon / N)^2$. For $\epsilon > 0.1$ it is necessary to introduce a correction to the law (23).

Phase operation in the cyclotron was checked on the six-spiral magnetic field structure for the acceleration of deuterons to an energy of 13 Mev. The minimum accelerating voltage on the dee for the magnetic field H(r), a graph of which is shown in Fig. 3, turned out to be 5 kv. Here, the ions underwent approximately 2500 revolutions.

The energy of the accelerated particles at the limiting radius (54 cm) was determined by two methods: measurement of the mean radius of curvature of the orbit by means of three probes and measurement of the length of path of the accelerated deuterons in aluminum foil. The experiments were carried out at an external beam intensity not exceeding 1 $\mu$a, and therefore the activity of the internal parts of the chamber was slight.

Figure 4 shows a plot of the internal beam intensity versus the accelerator radius at an accelerating voltage of 11 kv on the dee. At all radii, the beam was well focused and the half-width of its vertical distribution was less than 1 cm.

## Calculation and Shimming of the Magnetic Field

The magnetic field in the median plane of the electromagnet gap (pole-face diameter 120 cm, distance between poles $2h_m$ = 22 cm) of (2) was produced by means of shims of rectangular cross section bent into Archimedes spirals $r = \varkappa N \varphi$ and a system of ring shims.

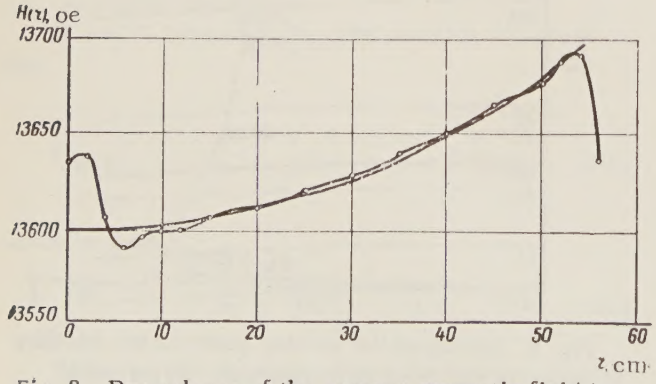


Fig. 3. Dependence of the average magnetic field intensity of the cyclotron on the radius for N = 6.

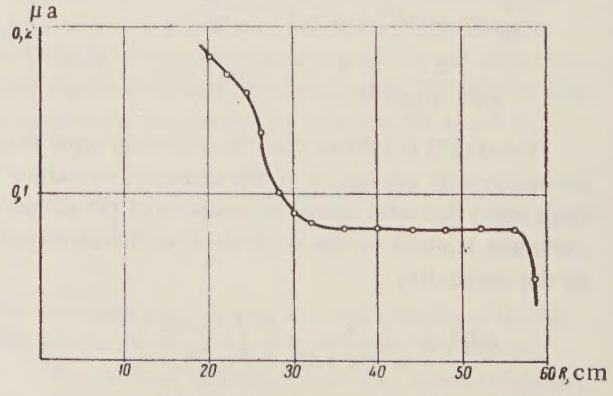


Fig. 4. Particle beam current at different radii ($V_0$ = 11 kv).

In the choice of the parameters of the spiral shims (the ratio between the width and height), it was assumed that the magnetization of the shim volume in the direction of the vertical component of the field was close to saturation. Here, the obtaining of the required magnetic field law can be separated into two practically independent problems. The first problem involves the production of the necessary variation of the field $\epsilon$, and the second involves the formation of the axial symmetric field H(r).

The components of the field from shims of arbitrary configuration are found from the expression

$$\left.\begin{aligned} \Phi &= M\frac{\partial}{\partial z}\int\limits_{V'}\frac{1}{\varrho}\,dV';\\ \vec{H} &= -\operatorname{grad}\Phi, \end{aligned}\right\} \qquad (27)$$

where $\Phi$ is the scalar magnetic potential; $M = M_z$ is the average intensity of magnetization of the sample along the z axis; $\rho$ is the distance between the point of observation of the field (r, $\varphi$, z) and a variable point (r', $\varphi'$, z') of volume V'.

From (27), using the well-known integral representation [23]

$$\frac{1}{\varrho} = \int\limits_0^\infty e^{-\tau|z-z'|} I_0(\tau r)\, I_0(\tau r')\, d\tau + 2\sum_{m=1}^{\infty}{}' \cos m(\varphi-\varphi') \int\limits_0^\infty e^{-\tau|z-z'|} \times I_m(\tau r)\, I_m(\tau r')\, d\tau, \qquad (28)$$

one may find the magnetic field of an arbitrary system of curvilinear shims in the form of a Fourier series

$$H_z(r, \varphi, z) = H_z(r, z) + \sum_{m=1}^{\infty} H_{mN}(r, z)\sin[\beta_{mN}(r, z) - mN\varphi]. \qquad (29)$$

Here, $2\pi/N$ is the period of the field structure; $H_N = \epsilon H(r)$ is the amplitude of the fundamental harmonic, which is chosen to correspond to the conditions in (10) and (11). It should be noted that if the amplitudes of the higher harmonics in the magnetic field law are not large, then the stability condition is not violated [24].

The shim system giving the required distribution of $H_z$ in the form (29) consists of 2N identical shims distributed symmetrically with respect to the median plane of the electromagnet gap (z = 0) and displaced from one another by an angle of $2\pi/N$. For a system of spiral shims of unlimited height and with a thickness that is small in comparison with the other parameters, the average field and amplitudes of the harmonics in expansion (29) for z = 0, by (27) and (28), can be represented in the form [25]

$$H(r)\,\frac{2M\delta N h_1}{\pi r\sqrt{r\lambda N}}\int\limits_{\varphi_b}^{\varphi_e}\sqrt{\frac{1+\varphi'^2}{\varphi'^3}}\times\left[-\frac{d}{dx}Q_{-1/2}(x)\right]d\varphi'; \qquad (30)$$

$$H_k(r) = \sqrt{[H_k^c(r)]^2 + [H_k^s(r)]^2}. \qquad (31)$$

Here, k = mN (m = 1, 2, 3, . . .);

$$\left.\begin{aligned} H_k^c(r) &= \frac{4M\delta N h_1}{\pi r\sqrt{r\lambda N}}\int\limits_{\varphi_b}^{\varphi_e}\sqrt{\frac{1+\varphi'^2}{\varphi'^3}}\cos k\varphi'\left[-\frac{d}{dx}Q_{k-\frac{1}{2}}(x)\right]d\varphi';\\ H_k^s(r) &= \frac{4M\delta N h_1}{\pi r\sqrt{r\lambda N}}\int\limits_{\varphi_b}^{\varphi_e}\sqrt{\frac{1+\varphi'^2}{\varphi'^3}}\sin k\varphi'\left[-\frac{d}{dx}Q_{k-\frac{1}{2}}(x)\right]d\varphi', \end{aligned}\right\} \qquad (32)$$

where $Q_{k-\frac{1}{2}}(x)$ is a spherical Legendre function of the second kind with the argument

$$x = \frac{h_1^2 + r^2 + \lambda^2 N^2 \varphi'^2}{2r\lambda N\varphi'};$$

$\varphi_e - \varphi_b$ is the azimuthal distance; $\delta$ is the shim thickness; $2h_1$ is the gap between shims in the vertical direction; $M = \frac{21{,}000}{4\pi}$ oe.

The field of a system of shims limited in height can readily be obtained from (30) and (32) as the difference in the fields from shim systems of unlimited height with $h_1$ and $h_2$ (shim height $2b = h_2 - h_1$).

If the curvature of the spiral shims tends to zero, the amplitudes of the harmonics (29) attain their limiting values. These limiting values are equal to the harmonic amplitudes in the field expansion of an infinite system of rectangular shims of unlimited length with the same transverse dimensions. The field of such shims in the coordinate system shown in Fig. 5, under the conditions $(\delta/h_1) \ll 1$ in the plane z = 0, can be represented in the form

$$H_z(y) = \frac{2Mh_1\delta}{(2\pi\lambda)^2}\sum_{s=-\infty}^{s=\infty}\left[\frac{1}{\left(\frac{h_1}{2\pi\lambda}\right)^2+\left(\frac{y}{2\pi\lambda}+s\right)^2} - \frac{1}{\left(\frac{h_1+2b}{2\pi\lambda}\right)^2+\left(\frac{y}{2\pi\lambda}+s\right)^2}\right]. \qquad (33)$$

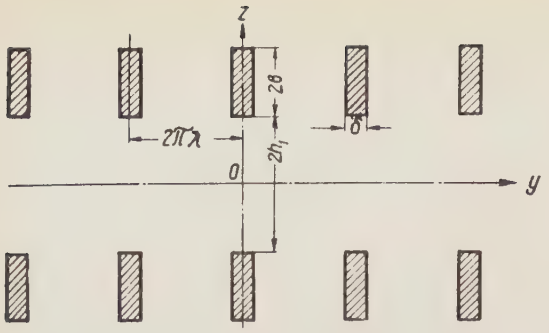


Fig. 5. System of rectangular shims.

Carrying out the summation over S in (33) and expanding the obtained result in a Fourier series, we find the following expression for the harmonic amplitudes [26]:

$$H_k^* = 4M\frac{\delta}{\lambda}e^{-k\frac{h_1}{\lambda}}\left(1-e^{-k\frac{2b}{\lambda}}\right). \qquad (34)$$

Formula (34) was used for the preliminary choice of the parameters of the spiral shim system.

The influence of the pole pieces on the field of the shims is taken into account in the assumption of the infiniteness of the pole pieces on the basis of image theory [27].

For the case in which the magnetic permeability of the pole $\mu \gg 1$ and for an electromagnet gap $2h_M = 2(h_1 + 2b)$, we obtain for the harmonic amplitudes

$$H_k^* = 4M\frac{\delta}{\lambda}e^{-k\frac{h_1}{\lambda}}\frac{1-e^{-k\frac{4b}{\lambda}}}{1-e^{-k\frac{2h_M}{\lambda}}}. \qquad (35)$$

From (35) it is seen that for $h_M > \frac{2\pi\lambda}{4}$ the calculation of the amplitudes of the field harmonics can be carried out with sufficient accuracy for practical purposes without taking into account the influence of the pole pieces by assuming the shim to be of unlimited height. This leads to a considerable simplification of the calculations by formulas (32) of the dependence of the amplitude and phase of the fundamental harmonic of the magnetic field on the radius.

The investigated magnetic field structure was produced by means of a system of spiral shims with the following parameters:

1) $N=4$, $\lambda=1.34$ cm, $\delta=1.2$ cm, $h_1=4$ cm, $2b=4$ cm,
2) $N=6$, $\lambda=2.7$ cm, $\delta=2.5$ cm, $h_1=4$ cm, $2b=3$ cm,

The calculated curve and the experimental values of the amplitude of the fundamental harmonic for the first variant is shown in Fig. 6. In this figure the deviations of the phase of the fundamental harmonic $\beta_4$ from the ideal phase $r/\lambda$ are shown. The change in sign of the deviation leads to an effective increase in $\lambda$ at the final radii, which causes a local increase in amplitude at these radii. For an optimum choice of $\lambda$ (from the condition that the limiting amplitude be a maximum) this effect decreases appreciably. This is seen from analysis of the data shown in Fig. 7, in which the variation of the amplitude and phase of the fundamental harmonic with the radius is shown for the variant N = 6, where $\lambda$ was chosen close to the optimum.

The pole pieces with spiral shims for this variant are shown in Fig. 8. In the interval of radii 20-50 cm, the ratio of the harmonic amplitudes in the expansion of the field corresponds to the calculated value (34). The amplitude of the eighth harmonic in the first variant and of the twelfth harmonic in the second is 5 and

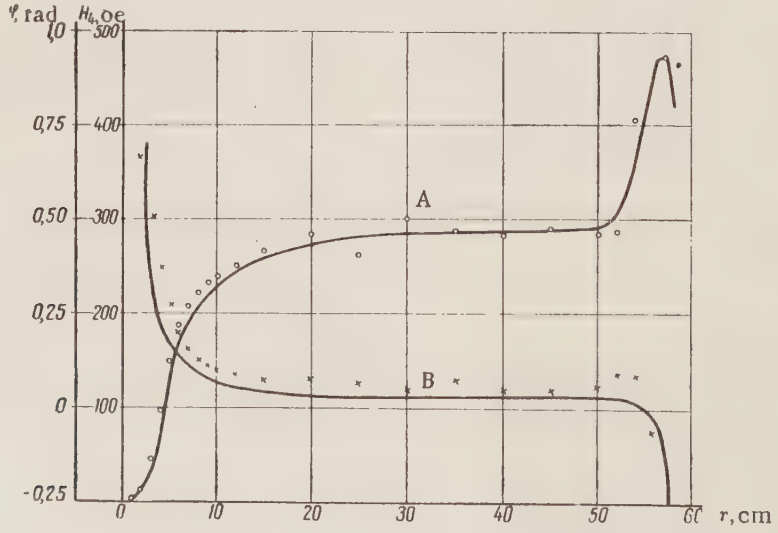


Fig. 6. A) Variation of the amplitude of the fourth harmonic of the magnetic field $H_4$ with the radius (solid curve – calculated, circles – experimental data); B) deviation of the phase of the fourth harmonic of the magnetic field from a spiral (solid curve – calculated; crosses – experimental data).

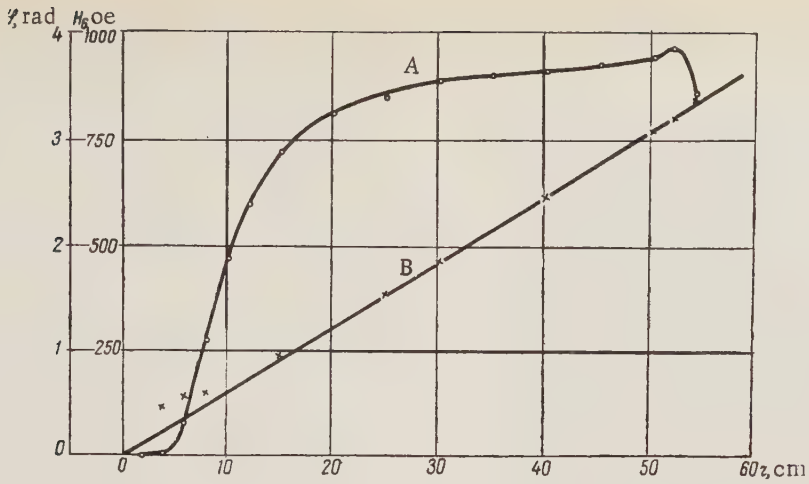


Fig. 7. A) Variation of the amplitude of the sixth harmonic of the magnetic field $H_6$ with the radius; B) Variation of the phase $\varphi$ of the spiral shim with the radius (solid curve – calculated, crosses – experimental data).

25%, respectively, of the fundamental harmonic amplitude.

The formation of the resonance average field was effected by ring shims; the calculation of their magnetic field was carried out under the assumption of a uniform axial magnetization [28]. The value of the magnetization intensity M was found from the curves of [29] and the magnetometer demagnetization factor [28].

Preliminary experiments carried out with thin, single ring shims showed that the deviation between the calculated and experimental curves from the maximum value of the shim field did not exceed 10%, and, within the limits of this accuracy, the principle of superposition of the fields from the single shims holds. For more accurate shimming of the average field, steel cylinders of small diameter (0.8 cm) were used. A redistribution of the cylinders along the azimuth was used to decrease the amplitudes of the first and second harmonics, whose behavior in the expansion of the field is accounted for by errors in the geometry of the shims of about 0.01 cm in the prepared set of spiral shims and the misalignment of the pole faces, which did not exceed 0.05 cm. The values of the amplitudes of the first and second harmonics for $0 < r < 50$ cm did not exceed 15 oe.

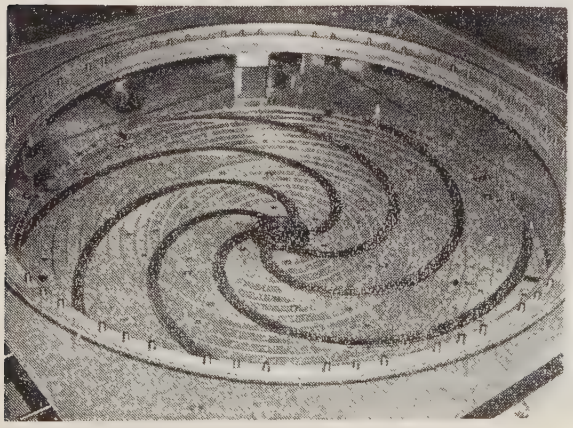

Fig. 8. Pole piece with spiral shims.

In order to improve the initial formation of the beam in the central region of the accelerator, a small increase in the average field was employed. In the interval of radii 8–52 cm, the deviation of the average field from the resonance field did not exceed $2 \cdot 10^{-2}$% (see Fig. 3, in which the curve with the dots represents the experimentally obtained average field).

## Measurement and Stabilization of the Magnetic Field Intensity

The absolute value of the intensity of the inhomogeneous magnetic field of the accelerator was measured by specially designed magnetometers based on the Hall effect [30] and the phenomenon of nuclear magnetic resonance [31, 32].

With the aid of a nuclear magnetometer, the absolute value fof the magnetic field intensity in the range of 250 – 24,000 oe with a gradient of 5 – 10% of $H_0$ (to 1000 – 1200 oe/cm) can be measured to an accuracy of ±0.01%. The volume of substance in the magnetometer detector was $2 \cdot 10^{-4}$ cm$^3$. At the same time the value of the gradient of the magnetic field intensity at the point of measurement and its direction can be determined to an accuracy of ±1%.

The special fitting on which the detectors were placed permitted the latter to be set at a point at any radius or height to an accuracy of ±0.01 cm, and azimuth to an accuracy of ±0.1°.

Employed in the nuclear magnetometer were a remote-controlled system of coarse and fine tuning of

the regenerative signal detector oscillation circuit and semi-automatic remote-controlled azimuthal positioning of the detector.

The magnetic field intensity of the cyclotron was stabilized to an accuracy of 0.005% by a nuclear stabilizer in which the resonance signal was observed by means of the nuclear induction method [33].

## High-Frequency System and Generator

The high-frequency system of the cyclotron consisted of a coaxial four-conductor resonance line (W = = 64 cm), one side of which was terminated by a movable disc and the other by the dee–chamber load capacity [34].

The shifting of the disc tuned the system in the 7.6 – 12 Mc range at a working frequency of 10.5 Mc.

A special feature of the high-frequency system was the use of only one dee and small gaps between the dee and the chamber (1.5 – 2 cm). The high-frequency probe between the dee and the chamber limited the highest possible accelerating voltage to 40 kv. The small size of the gaps were the cause of considerable detuning of the system under load, which led to the necessity of taking special steps to keep the free frequency constant. The dee radius was 57.5 cm and the aperture was 4 cm. In order to increase the working aperture, cooling tubes were located along the lateral sides of the dee outside the working radii.

The generator output stage, working in a grounded-grid circuit, was connected to two GU-12A tubes connected in parallel. Its anode circuit consisted of a high-frequency system with conductive coupling through a short air-filled coaxial line with a wave resistance of 64 ohms. During the operation of the generator with an independent excitation the shift in the resonance frequency of the high-frequency system resulting from the loading led to a change in the accelerating voltage. The oscillation frequency (the amplitude of the accelerating voltage) was maintained constant by means of an automatic amplitude stabilization system by a change in the capacity between the dee and an auxiliary electrode introduced into the accelerator chamber. The stabilization system maintained the accelerating voltage constant over the adjustable range to an accuracy of 1.5%.

## Chamber and Ion Source

The accelerator vacuum chamber has a shape of a rectangular parallelepiped of size 158 × 154 × 33.5 cm. In order to decrease the undesired radioactive background from long-lived isotopes accumulated in the chamber under the action of the accelerated particles, this chamber, except for the cylindrical steel covers, was made from an alloy of the "Avialite" type. The chamber and the outer tube of the resonance line formed one vacuum volume evacuated by three oil vapor pumps of the H-5T type. The working vacuum in the system was $(1\text{-}2) \cdot 10^{-5}$ mm Hg for a gas flow into the source of about 2-5 $cm^3$/min.

A discharge of the Penning type, used as the ion source, made it possible to eliminate considerable design difficulties connected with the heating of the cathode and the cooling of the various parts of the ion source. The source was designed so that it was possible to displace it sideways and lengthwise without disturbing the vacuum in the system. The chamber was provided

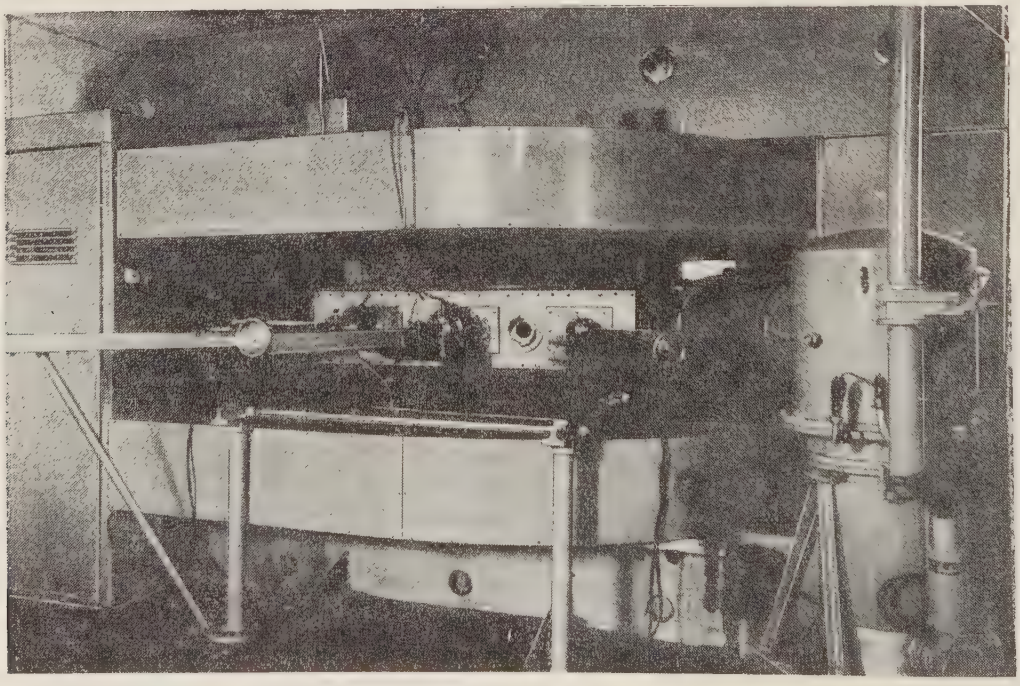

Fig. 9. General view of the accelerator from the side of the ion source and probes.

with three probes with quartz targets as beam indicators. A fine tungsten wire wound on the quartz targets permitted the measurement of the beam current of accelerated particles simultaneously with visual observation.

A general view of the accelerator from the side of the ion source and probes is shown in Fig. 9.

## Conclusions

From the work on setting into operation and the study of the accelerator with a spatially varying magnetic field, the following conclusions can be made:

1) The linear theory of spatial stability developed in connection with these accelerators has been experimentally confirmed in the given range of variation of the free frequencies of oscillation of the particles.

2) The nonlinear resonance effect at the center of the accelerator was investigated theoretically and experimentally; the values of the parameters for the magnetic field structure at which this effect is practically absent were found.

3) The methods developed for producing variation of the magnetic field intensity provide the necessary accuracy for practical cases and can be used for constructing accelerators of this type.

4) The theoretical and experimental investigations that were made, the apparatus designed for measurement and stabilization of magnetic fields of complex configuration, and the methods of shimming the average field make it possible to produce the resonant acceleration of particles with cyclotrons of appropriate dimensions to energies obtained at the present time on phasotrons with beam currents of hundreds of microamperes.

The authors highly appreciate the great amount of work and effort on the part of the personnel of the experimental shop, designing office, electronic and electrical departments of the Nuclear Problems Laboratory of the Joint Institute of Nuclear Studies. The authors are deeply grateful to these personnel and to their chiefs K. A. Baicher, N. I. Frolov, M. F. Shul'ga, F. V. Chumakov for their aid, valuable discussions, and suggestions in solving many technical problems. The authors express their gratitude to D. I. Blokhintsev, D. V. Efremov, K. N. Meshcheryakov, V. N. Sergienko for constant interest and assistance, which greatly facilitated the work, to E. G. Komar, I. F. Malyshev, L. N. Fedulov for constructing and preparing the chamber and the magnet of the accelerator, to A. V. Chestnyi for help during the first stage of setting up the technical problem.

## LITERATURE CITED

1. L. Thomas, Phys. Rev. 54, 580 (1938).
2. V. I. Veksler, Doklady Akad. Nauk SSSR 43, 346 (1944).
3. E. McMillan, Phys. Rev. 68, 143 (1945).
4. N. Christophilos (unpublished); E. Courant, M. Livingston, and M. Snyder. Phys. Rev. 88, 1190 (1952) (1952).
5. V. Vladimirski, E. Komar, and A. Mints, CERN Symposium 1, 122 (1956).
6. Collection: Proton synchrotron for 25 Bev [in Russian] (Izd. Glavnogo. Upravleniya po Ispol'zovaniyu Atomnoi Énergii pri Sovete Ministrov SSSR, No. 1, 1956).
7. Annual Report of Brookhaven National Laboratory (July 25, 1958) Vol. 1.
8. M. S. Kozodaev and A. A. Tyapkin, Nuclear Problems Institute Report [in Russian] (AN SSSR, 1953) 1953); A. A. Kolomenskii, V. A. Petukhov, and M. S. Rabinovich, Acad. Sci. USSR Report, (1953) and collection: Some Problems of the Theory of Cyclical Accelerators [in Russian] (Moscow, Izd. AN SSSR, 1955) p. 7.
9. E. M. Morz and M. S. Rabinovich, Pribor i Tekh. Éksp. 1, 15 (1957).
10. G. I. Budker, Atomnaya Énerg. 5, 9 (1956).**
11. V. I. Veksler, Atomnaya Énerg. 2, 5, 427 (1957).**
12. D. Kerst, K. Terwilliger, K. Symon, and L. Jones, Bull. Am. Phys. Soc. 30, No. 1 (1955).
13. V. P. Dmitrievskii, On the Limiting Energy of Particles in Accelerators of the Cyclotron Type with a Spatially Varying Magnetic Field [in Russian] (OIYaI, 1955).
14. V. V. Kol'ga, Application of Periodical Magnetic Fields of Special Form in Accelerators [in Russian] (Otchet Lab. Yad. Problem OIYaI, 1956).
15. V. V. Kol'ga, Effect of Perturbations on the Stability of Orbits in a Cyclotron with a Periodic Magnetic Field [in Russian] (Otchet Lab. Yad. Problem OIYaI, 1956).
16. P. Dunn, L. Mullett, T. Pickavance, W. Walkinshaw, and J. Wilkins, CERN Symposium 1, No. 9 (1956).
17. W. Walkinshaw and N. King, "Linear Theory in S/R Cyclotron Design", AERE, GP/R 2050 (1956).
18. N. King and W. Walkinshaw, Nuclear Instr. 2, No. 4 (1958).
19. D. Kerst, H. Hausman, R. Haxby, L. Laslett, F. Mills, T. Ohkawa, F. Peterson, A. Sessler, J. Snyder, and W. Wallenmeyer, Rev. Sci. Instr. 28, 11, 970 (1957).
20. MacLaughlin, Theory and Application of the Mathieu Equation [Russian translation] (IL, Moscow, 1953).
21. N. N. Bogolyubov and Yu. A. Mitropol'skii, Asymptotic Methods in the Theory of Nonlinear Oscillations [in Russian] (Gostekhizdat, Moscow, 1953).
22. V. P. Dmitrievskii and V. V. Kol'ga, Phase Motion in a Cyclotron with a Periodic Field [in Russian] (Otchet Lab. Yad. Problem OIYaI, 1958).

* Original Russian pagination. See C. B. translation.

23. N. N. Lebedev, Special Functions and Their Application [in Russian] (Gostekhizdat, Moscow, 1953).

24. V. V. Kol'ga, Effect of Higher Harmonics on the Motion of Particles in Accelerators with a Periodic Magnetic Field [in Russian] (Otchet. Lab. Yad. Problem OIYaI, 1958).

25. V. I. Danilov, N. L. Zaplatin, and V. S. Rybalko, A Method of Calculation of Magnetic Fields for an Accelerator with a Spatially Varying Magnetic Field [in Russian] (Otchet. Lab. Yad. Problem OIY OIYaI, 1956).

26. V. I. Danilov, V. P. Dmitrievskii, N. L. Zaplatin, V. V. Kol'ga, Liu Nei-ch'ang, V. S. Rybalko, and L. A. Sarkisyan, Magnetic Field of a Cyclotron Model with a Spatial Variation [in Russian] (Otchet. Lab. Yad. Problem OIYaI, 1958).

27. W. Smythe, Static and Dynamic Electricity [Russian translation] (Moscow, IL, 1954).

28. V. I. Danilov, N. L. Zaplatin, V. S. Rybalko, and L. A. Sarkisyan, Formation of Axially Symmetric Magnetic Fields by Means of Ring Shims [in Russian] (Preprint) (OIYaI, 1959) p. 334.

29. I. V. Antik, E. I. Kondorskii, E. P. Ostrovskii, and B. A. Sadikov, Magnetic Measurements [in Russian] (Moscow, 1959).

30. D. P. Vasilevskaya, Yu. N. Denisov, Pribor. i Tekh. Éksp. No. 3 (1959).

31. Yu. N. Denisov, Pribor. i Tekh. Éksp., 5, 67 (1958).

32. Yu. N. Denisov, Pribor. i Tekh. Éksp., 1 (1960).

33. Yu. N. Densiov, Pribor. i Tekh. Éksp., 1, 36 (1959).

34. A. A. Glazov, V. A. Kochkin, B. N. Marchenko, and A. L. Savenkov, Radio-frequency System of a Cyclotron Model with a Spatially Varying Magnetic Field [in Russian] (Otchet Lab. Yad. Problem, 1959).

# ACCELERATION OF IONS IN A CYCLOTRON WITH AN AZIMUTHALLY VARYING MAGNETIC FIELD

R. A. Meshcherov, E. S. Mironov, L. M. Nemenov,
S. N. Rybin, and Yu. A. Kholmovskii

Translated from Atomnaya Énergiya, Vol. 8, No. 3, pp. 201-208,
March, 1960
Original article submitted August 6, 1959

This article describes experiments on the acceleration of charged particles in an azimuthally varying magnetic field on the 1½-meter cyclotron of the Atomic Energy Institute of the Academy of Sciences, USSR [1].

The production of a magnetic field of the sector type with a coarse variation of ~±15% at a potential of ~15 kv between the dees made it possible to accelerate deuterons to an energy of 19 Mev. Investigation of the motion of the ions at the final orbits showed that it was possible to eject a large part of the ion beam with an energy considerably exceeding 20-22 Mev by means of an electrostatic deflecting system. Curves characterizing the acceleration process in an azimuthally varying magnetic field were plotted. Valuable data was obtained on the correction to the form of the magnetic field by current coils distributed inside the accelerating chamber.

## Introduction

In order to produce vertical stability of accelerated ions in an ordinary cyclotron, it is necessary that the magnetic field intensity decrease as a function of the radius. As early as 1938, however, L. Thomas [2] showed that it is also possible to have stable motion of charged particles when an increase in the magnetic field intensity with the radius is accompanied by an azimuthal variation. Thomas's suggestion opened up new perspectives in the acceleration of the charged particles to high energies at high currents, but it was not developed further, since the production of a magnetic field of required form presented at that time an exceptionally complex problem and the discovery by V. I. Veksler (1944) and E. McMillan (1945) of the principle of autophasing diverted the attention of physicists from this suggestion.

In recent years, many authors have investigated theoretically and experimentally the motion of charged particles in a cyclotron with an azimuthally varying field [3-6].* A number of theoretical studies has also been made at the Atomic Energy Institute of the Academy of Sciences, USSR.

In 1957, experiments were set up on a model of a 1½-meter cyclotron (1/5 natural size) on the modeling of the azimuthally varying magnetic field of the sector type. The combined action of the iron and current correcting elements, which is of considerable interest in the development of a cyclotron with adjustable energy, was studied on the same model. The experiment showed that the combination of the iron and current correcting elements made it possible to produce a given form of the field over a wide range of magnetic fields.

The azimuthal variation of the magnetic field with a flutter of about ±15% was produced by three sectors. This type is the simplest from the point of view of the technology of construction.

Preparations for the acceleration of ions on the 1½-meter cyclotron were begun in 1958 after completion of experiments on the model. New covers for the accelerating chamber, sectors, and all necessary iron and current correcting elements were prepared.

The design of the cyclotron resonance line did not permit a high-frequency voltage wavelength less than 26.7 m. This circumstance was determined by the limiting energy to which deuterons and ions of molecular hydrogen could be accelerated.

## Constructive Elements

The new covers of the accelerating chamber were 1500 mm in diameter and 80 mm in thickness. The covers were machined flat to a tolerance of 0.08 mm. The tolerance on the machining of the iron sectors of height 30 mm and angular width of ~60° was 0.1 mm. All iron parts were made to the same tolerance. In order to eliminate high-frequency losses in the iron parts, their surfaces were electrolytically coated with a copper layer ~70 μ thick.

* The cyclotron with a "spiral" magnetic field will not be considered in the present article.

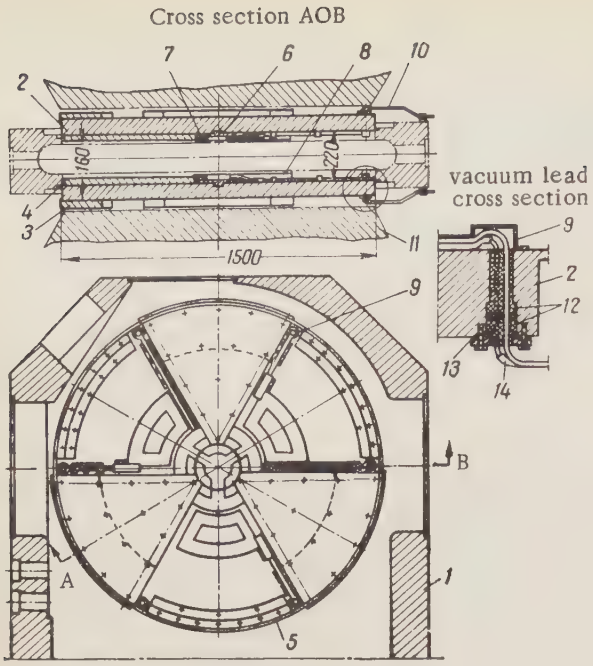


Fig. 1. Accelerating chamber covers with correcting iron elements and current correcting coils. 1) Accelerating chamber; 2) accelerating chamber covers; 3) outer correcting elements; 4) sectors; 5) inner correcting elements; 6) central disks; 7) central correcting coils; 8) correcting coils in gaps; 9) copper shields; 10) vacuum lead for energizing the coils; 11) electromagnet pole piece; 12) insulators; 13) rubber packing; 14) vinyl-chloride tube.

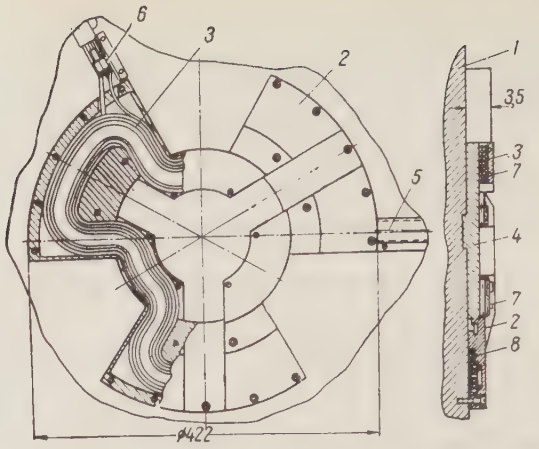


Fig. 2. Central correcting coil. 1) Accelerating chamber cover; 2) coil form; 3) copper tube coil; 4) central disks; 5) copper shield; 6) detachable vacuum coupling; 7) tubes for water cooling of form; 8) clamping plate.

Figure 1 shows a sketch of the accelerating chamber with covers. The covers were sealed in the usual way. Sectors 4 were fastened to the covers 2 by means of screws. The outer 3 and inner 5 iron correcting elements (the outer correcting elements were of larger size) were fastened in the same way. As seen from the diagram, elements 5 were set in the gaps between sectors and served to increase the magnetic field intensity on the periphery. In the center of the covers were iron disks 6 of diameter 200 mm. In order to make a fine correction at radii of 190-260 mm, the sectors had threaded openings into which could be screwed screws with heads in the shape of a small disk serving as a correcting element. Any of the screws fastening the sector to the cover could be replaced, when necessary, by a screw with the head in the shape of a disk. Attached to the inner surface of each over were four correcting coils. The central correcting coil had two sections (each with seven turns) with a separate power supply. One of the sections permitted the magnetic field intensity in the central part to be changed, the other shifted the median magnetic plane.

Figure 2 shows two projections of the central correcting coil. The form 2 for the coil was milled from brass and cooled by water by means of copper tubes. To prevent the zinc from melting during spark-overs the form was electrolytically coated with a thin copper layer. Seen in the figure are both sections of the copper tubes, one next to the other. The detachable vacuum coupling 6 made it possible, when necessary, to remove the coil together with the form. Coils 8 (each with 14 turns, see Fig. 1) placed in the gaps made it possible to correct the first harmonic of the magnetic field nonhomogeneity.

Figure 3 shows a view and section of a similar coil. All coils are made from copper tubes 4 × 0.5 mm in diameter set in two rows and cooled by water. The coil form was also water cooled. All coils were insulated by a vinyl-chloride tube whose gas release proved to be quite acceptable.

Figure 1 shows a separate section of the vacuum lead. All leads from the coils were covered with copper shields screwed on to the chamber covers. Thus, owing to the presence of the coil form and shields, the coils were completely shielded from the effect of high-frequency currents and spark-overs. Figure 4 shows the accelerating chamber with the upper cover removed and Fig. 5 shows the upper cover set in position.

In order to take the characteristics of the beam of accelerated ions, two shielded probes were designed and prepared. Before falling on the measuring electrode, the ions passed through an aluminum filter which prevented low-energy charged particles from falling on the measuring electrode. Knowing the filter thickness, one can estimate with sufficient accuracy the ion energy at any radius of acceleration. A shortcoming of the shielded probe is the "blind" space formed by the

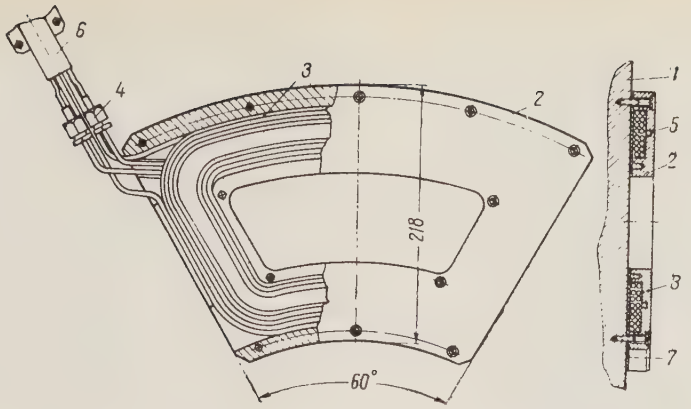


Fig. 3. Correcting coils in the gaps. 1) Accelerating chamber cover; 2) coil form; 3) coil; 4) detachable vacuum coupling; 5) water-cooling tube for coil form; 6) copper shield; 7) coil form cover.

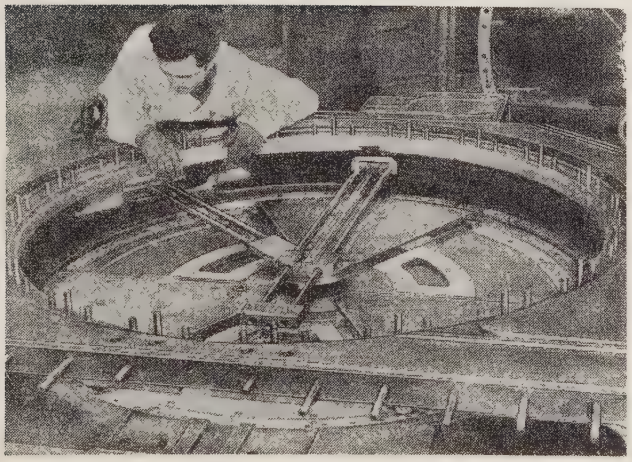

Fig. 4. Accelerating chamber with upper cover removed. An instrument for measuring the magnetic field is seen.

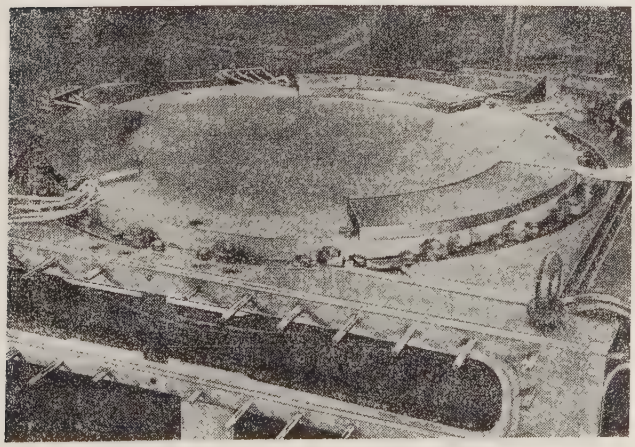

Fig. 5. Accelerating chamber. Seen on the upper cover are the coil leads and the outer correcting iron elements.

front wall of the coil form and the gap between this wall and the measuring electrode. This blind space reduces the probe indication by cutting off about 1.5 mm of the initial part of the beam. A probe located inside one of the dees was also used in the experiments. This probe could serve both for measurement of the current and for shielding the beam during the determination of the zone of the centers of trajectory by the three-probe method. In order to investigate the distribution of the ion beam intensity along the vertical, a multi-electrode probe with a slotted copper screen behind which thermocouples were placed, was used. The thermocouples were connected to the measuring instrument by means of a telephone switch.

An ordinary ion source of the open type was used to obtain ions. The intensity of the high-frequency field for drawing the ions from the source was increased by mounting a flange of length 200 mm on the dees. The ions were drawn off in both dees.

To decrease the activation of the elements of the accelerating chamber, all experiments were carried out under pulsed operation with a duty ratio of 5 to 500. The ion currents in the pulses were measured by means of a calibrated oscillograph and the value of the mean current, by either an integrator or a thermal method. In all the measurements, the values of the currents in the pulse were used. To study the motion of ions at large radii in the region of action of the scattering field of the electromagnet, the deflecting system was removed from the dees.

## Characteristics of the Magnetic Field and and Acceleration of Ions

To measure the vertical component of the magnetic field intensity in the median plane, an ordinary circuit with two coils connected in opposition was used.

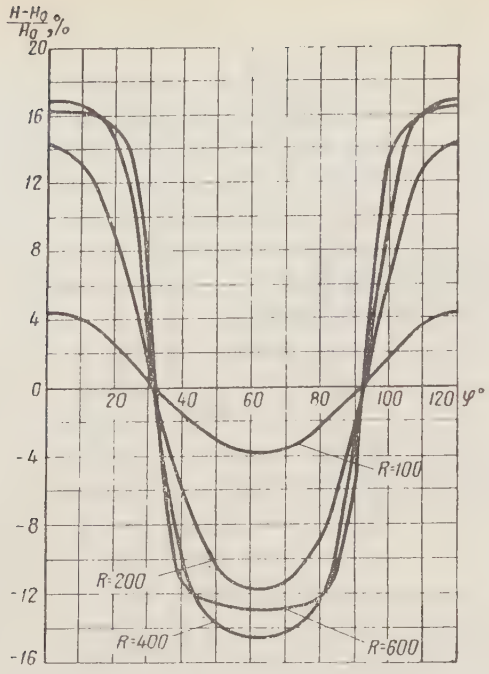


Fig. 6. Variation of the magnetic field intensity with the angle $\varphi$.

The measuring instrument was a ballistic galvanometer. The accuracy of the measurement was 0.05% of the value of the intensity at the center of the field $H_0$.

Figure 6 shows a plot of the magnetic field intensity versus the azimuthal angle $\varphi$ at different radii R. From these curves the variation of $f(R)$ and the amplitude of the fundamental harmonic $\Phi_1(R)$ shown in Fig. 7 were obtained.

The quantity

$$f(R) = \frac{1}{2\pi} \int_0^{2\pi} \frac{H(R, \varphi) - H_0}{H_0} d\varphi$$

characterizes the change in the average value of the magnetic field intensity in the median plane.

It should be noted that there was good agreement between the results of the measurements made on the cyclotron magnet and the data obtained on the model. This agreement made it possible to accelerate ions without any alterations in the design of the covers, sectors, and correcting elements.

The acceleration of ions of molecular hydrogen and and deuterons took place under two conditions of operation differing in the character of the variation of the average magnetic field intensity as a function of the radius of acceleration. (The acceleration of molecular hydrogen ions was convenient, since they produce a much smaller activity of the elements in the accelerating chamber). Two different types of magnetic fields were chosen in order to determine the influence of the law of the magnetic field increase on the motion of the accelerated ions.

In Fig. 8, the curve 2 depicts the variation of the current with radius for a cyclotron with an azimuthal variation of the magnetic field. Shown in the same figure is a similar curve 1 taken on the same cyclotron under the same conditions, but without an azimuthal variation.

The relatively small drop in the current with radius in the cyclotron with an azimuthal variation is accounted for by the absence of phase losses and stronger vertical focusing.

The vertical distribution of the beam current and the position of the median magnetic plane were investigated by means of a multi-electrode thermocouple

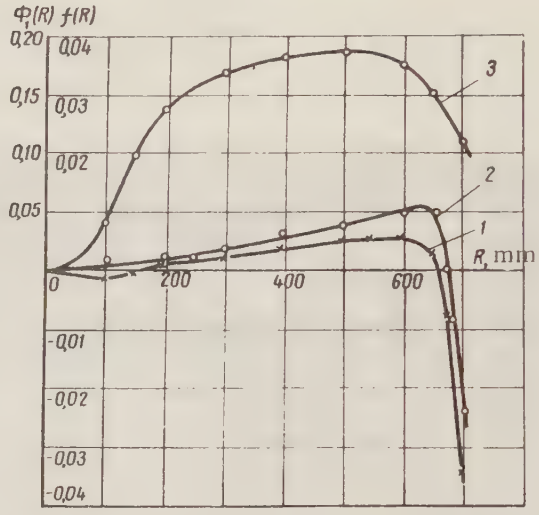


Fig. 7. Variation of the mean value of the magnetic field intensity and amplitude of the fundamental harmonic with the radius: 1) f(R) for $H_0$ = 14.7 koe; 2) f(R) for $H_0$ = 14.koe; 3) $\Phi_1(R)$ for $H_0$ = 14.7 koe.

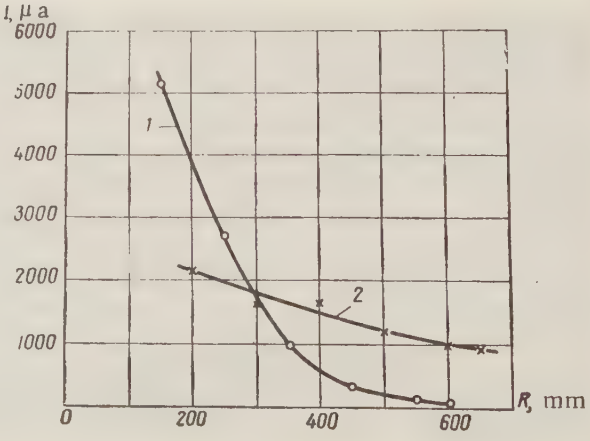


Fig. 8. Variation of the current with the radius at the probe position. 1) For an ordinary cyclotron; 2) for a cyclotron with an azimuthally varying magnetic field.

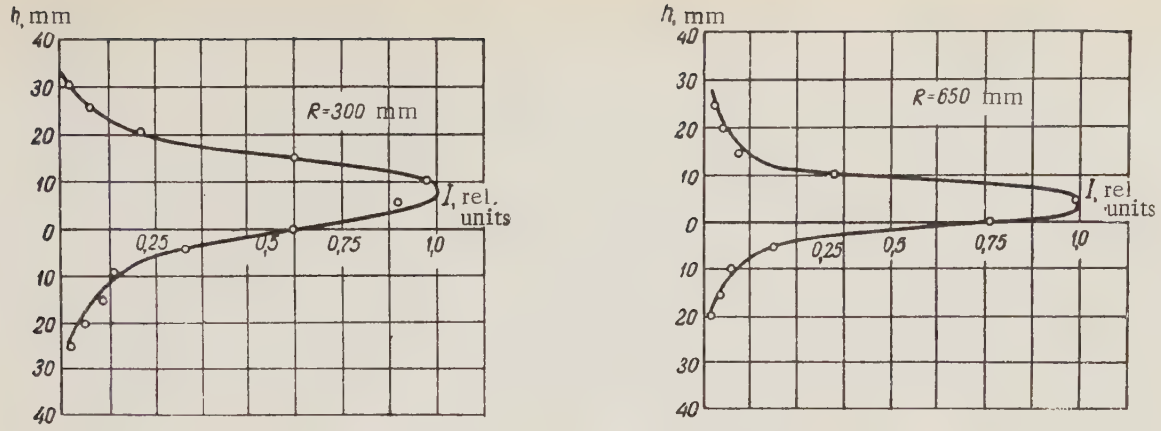


Fig. 9. Vertical distribution of the ion beam intensity.

probe. In Fig. 9, curves of this type are shown for two values of the radius.

It should be noted that the tolerances to which the covers and sectors were made turned out to be sufficient to obtain high currents at the final radii immediately after assembly, without any correction to the magnetic field.

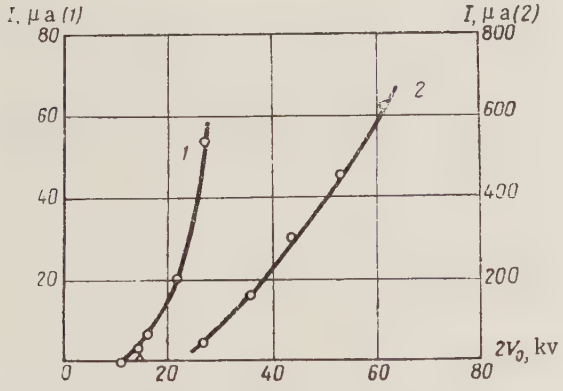


Fig. 10. Variation of probe current with dee voltage (2); initial segment of curve on expanded scale (1).

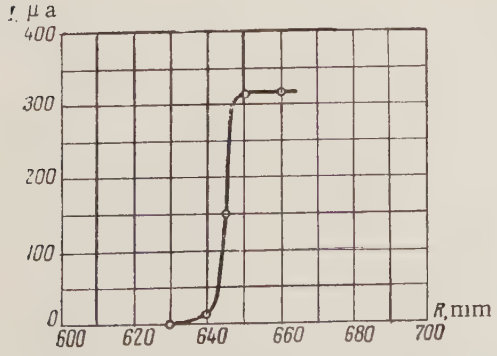


Fig. 11. Absorption curve taken with an aluminum filter.

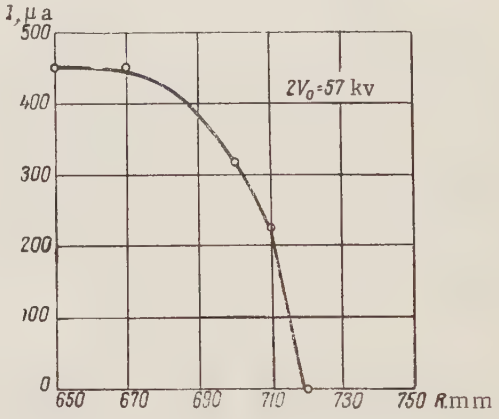


Fig. 12. Variation of the current with the radius at the probe position.

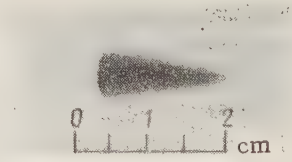


Fig. 13. Photograph of beam obtained by placing a copper plate irradiated by deuterons on photographic emulsion.

Figure 10 shows the variation of the ion current with the accelerating voltage ("control characteristic") taken for an energy of 19 Mev at $H_0$ = 14.0 koe. The energy of the accelerated ions in the given case was computed on the average orbit radius measured by means of three probes. The point with the triangle corresponds to the control voltage calculated under the assumption that the initial phase is +45°. The control characteristic for the same ion energy at a magnetic field intensity $H_0$ = 14.7 koe is practically the same as the curve shown.

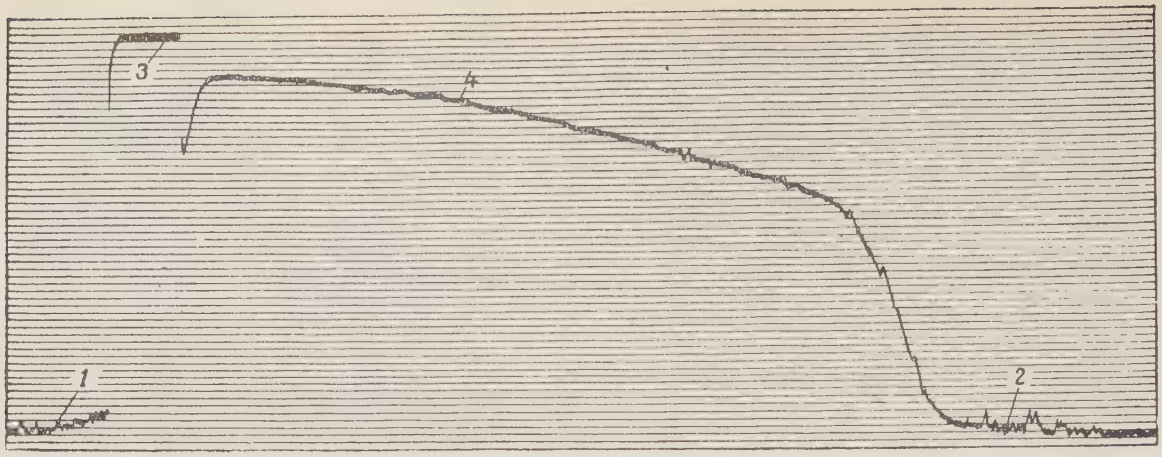


Fig. 14. Results of photometric measurement of the beam imprint. 1 and 2) Photographic film background; 3) reference mark obtained with covered photocell; 4) darkening curve.

The action of the central correcting coils on the ion acceleration process was studied. By using these coils, we could study the effect of a rise or drop in the average field value at small radii of acceleration. Whenever the increase in the field produced by the coils at the center of the chamber did not exceed +0.5% of $H_0$, the increase in probe current was slight. For larger changes of the field at the center (both signs), the probe current, as a rule, decreased.

To verify the value of the accelerated ion energy computed at the average orbit radius, the orbits for a given range of ions in aluminum were established. The measuring electrode of the probe was covered with a layer 190 mg/cm$^2$ thick. The absorption curve taken under these conditions is shown in Fig. 11. The value obtained for the mean energy was 21.5 Mev. The calculations agreed with experiment to an accuracy of 3%. The ion energy spread determined from this curve was ~± 1.5%. It should be noted that for ordinary cyclotrons this value is ~± 3%.

The motion of ions at large radii was studied. Figure 12 shows the variation of the accelerated ion current with the radius.

Figure 13 shows the beam shape at a radius of 700 mm obtained by placing an irradiated copper plate on photographic emulsion. The very small height of this beam is striking. Figure 14 shows a curve obtained from the photometric measurement of the beam imprint. The sharp break in the darkening from the right-hand side (Figs. 13 and 14) results from the fact that the accelerated ions at this point began to fall on the front part of the dee. The large beam width (more than 15 mm) is explained by the disturbance of the radial stability of the ion motion due to the sharp drop in the magnetic field intensity.

This circumstance made it possible to eject the beam by means of an electrostatic deflecting system at electric field intensities considerably less than in the ordinary cyclotrons. Consequently, ions could be ejected from the accelerating chamber of the cyclotron with an azimuthally varying magnetic field at an energy considerably exceeding the energy of ions obtained in ordinary cyclotrons (22-24 Mev).

## Conclusions

The experiments on the study of ion motion in the 1½-meter cyclotron with an azimuthally varying magnetic field gave the following results which are of great value for the design of similar accelerators:

1. For a difference in potential of 80 kv between the dees it was possible to accelerate molecular hydrogen ions and deuterons to an energy of ~21 Mev at an ion current of ~1000 μa at the final radius of acceleration. At the maximum energy 23.7 Mev, the accelerated particle current was ~200 μa.

2. It was shown that the produced form of the magnetic field completely coincided with the form of the field obtained on the model that was 1/5 of the natural size. This also applies to the iron correcting elements, including the fine correction by screws with heads in the shape of a disk.

3. Current correcting elements in the form of coils were introduced into the vacuum volume and worked reliably during all experiments. The magnetic fields produced by these coils were investigated.

4. As a result of the study of the change in ion current at large radii of acceleration, valuable data was obtained for effecting the beam ejection. On the basis of these data, it can be stated that an electrostatic system can be used to eject ions of energy considerably greater than the ion energy obtained in ordinary cyclotrons.

5. Experiments on the determination of the ion energy at the final radius of acceleration by means of aluminum filters showed that the energy spread of ions in the beam was ~± 1.5%.

In conclusion, the authors thank N. D. Fedorov, A. P. Babichev, A. S. Knyazyatov, and V. K. Anokhin for taking part in the magnetic measurements, S. I. Prokof'ev for active aid in the preparation of the covers of the accelerating chamber, N. N. Khaldin for valuable advice and participation in the fabrication planning, N. I. Venkov and all personnel servicing the cyclotron setup, I. M. Shnaptsev and H. G. Yadykin for making the vacuum tests, M. A. Egorov, V. M. Komarov, V. I. Andreev, and V. S. Kalyaev for their outstanding work on assembling the mechanical parts.

## LITERATURE CITED

1. L. M. Nemenov, S. P. Kalinin, L. F. Kondrashev, E. S. Mironov, A. A. Naumov, V. S. Panasyuk, N. D. Fedorov, N. N. Khaldin, and A. A. Chubakov, Atomnaya Énerg. 2, 1, 36 (1957).†
2. L. Thomas, Phys. Rev. 54, 580 (1938).
3. E. M. Moroz and M. S. Rabinovich, Pribor. i Tekh. Éksp. 1, 15 (1957).†
4. E. Kelly, R. Pyle, and L. Thornton, Rev. Sci. Instr. 27, 493 (1958).
5. F. Heyn, Khoe Kong Tat, Rev. Sci. Instr. 29, 662 (1958).
6. H. Blosser, R. Worsham, C. Goodman, R. Livingston, J. Mann, H. Moseley, G. Trammel and T. Welton, Rev. Sci. Instr. 29, 819 (1958).

†Original Russian pagination. See C. B. translation.

# METHOD OF OBTAINING AN AVERAGE VALUE FOR THE NUCLEAR CONSTANTS INVOLVED IN FAST REACTOR CALCULATIONS, TAKING INTO ACCOUNT THE NEUTRON VALUES

A. I. Novozhilov and S. B. Shikhov

Translated from Atomnaya Énergiya, Vol. 8, No. 3, pp. 209-213,
March, 1960
Original article submitted January 8, 1959

In this paper we present a method of finding the average value of multiple-group constants so that we may use the values in single-group calculations to determine the critical dimensions or the critical mass of a two-zone fast reactor. The accuracy of the method, as verified by means of an example involving the solution of nine-group space problems, turns out to be so high that it becomes unnecessary to solve the multiple group space problem in order to compute the critical mass of a thick-screen, two-zone reactor. The results of these calculations are given in this paper. This method provides a basic simplification of the necessary calculations involved in the design of fast reactors as compared to those required when using the multiple-group space diffusion method.

## Introduction

The neutron spectrum in a fast reactor represents a neutron fission spectrum softened by the effects of elastic and inelastic retardation due to the heavy and average nuclei of the substances composing the active zone of the reactor and its sheath.

For neutrons having an energy of ~0.1 Mev there is practically no inelastic scattering due to the fact that the neutrons comprising the basic portion of the spectrum have an energy close to 0.1 Mev, which permits us to use the simple homogeneous method of calculation in order to compute the critical volume or critical mass of the reactor. The accuracy of the computation depends upon a correct choice for the cross section of the single group.

Usually, when we compute the single-group cross section, we make an approximate evaluation by integrating separately the spectrum in the active zone and in the sheath and then the initial multiple-group constants are averaged on the basis of these spectra. The results of calculations show that the critical mass as determined with the aid of multiple-group constants averaged over the neutron spectra is from 10-20% lower than the critical mass obtained by solving the multiple-group space diffusion system of equations. This discrepancy is due to the fact that this method of averaging does not take into account the different reactive contributions of the neutrons in the various groups due to their different values.

We now examine a method of averaging the constants which practically removes the indicated error in the single-group computation.

## Initial Equations and Method of Calculation

Let us examine the total neutron balance and the values of the neutrons in a finite volume regardless whether the volume is located in the active zone or in the shield. The following equations hold

$$-J_k-\Sigma_{cf}^{(k)}I_k-\left(\Sigma_{\text{hr}}^{(k)}I_k-\sum_{j=1}^{k-1}\Sigma_{\text{hr}}^{kj}I_j\right)+\chi_k\sum_{l=1}^{m}\frac{\nu_f^{(l)}\Sigma_f^{(l)}I_l}{K_{\text{eff}}}=0; \tag{1}$$

$$-J_k^+-\Sigma_{cf}^{(k)}I_k^+-\left(\Sigma_{\text{hr}}^{(k)}I_k^+-\sum_{j=k+1}^{m}I_j^+\Sigma_{\text{hr}}^{jk}\right)+\frac{\nu_f^{(k)}\Sigma_{(f)}^{(k)}}{K_{\text{eff}}}\sum_{l=1}^{m}\chi_l I_l^+=0 \tag{2}$$

(k = 1, 2, . . . , m).

Here

$$I_k=\int_V\Phi_k\,dV \text{ and } I_k^+=\int_V\Phi_k^+\,dV$$

are the integrals giving the flux and values of the neutrons in the kth group of the volume under study; $J_k$, $J_k^+$ are the total neutron leakages and values for the

volume under study; the indices "c", "$f$", "hr" for the macroscopic cross sections denote the respective radiation capture, fission and total elastic and inelastic removals for the given group; $\Sigma_{hr}^{kj}$ denotes the macroscopic cross section of the heat removal from the jth group to kth group,

$$\Sigma_{hr}^{(h)} = \sum_{j=k+1}^{m} \Sigma_{hr}^{jk},$$

where $\chi_k$ is the portion of the fission neutrons arriving in the kth group, then $\sum_{k=1}^{m} \chi_k = 1$; $\nu_f^{(k)}$ denotes the number of fission neutrons per fission resulting from the neutrons in the kth group. The number of groups in (1) increases as the neutron energy decreases.

The values of $K_{eff}$ in (1) and (2) coincide, as we know, since these equations are conjugate. The spectra of the neutron flux and the neutron values which are determined from these equations will be used to obtain the average values of the constants separately in the active zone and in the sheath, and the single-group constants obtained will enable us to successfully calculate the critical reactor loading without having to solve the multiple-group space diffusion problem.

For an active zone of given dimensions it is simplest to evaluate the spectra by calculations based upon the bare (unshielded) reactor where the radius $R_r$ of the reactor is determined either with the aid of the effective supplement (the orientation of the supplement is always known), or by means of an approximate estimate of the critical mass.

In the first case we know the radius of the equivalent bare reactor; this determines the value of

$$\varkappa^2 = \left(\frac{\pi}{R_r}\right)^2.$$

and

$$J_{k,\text{a.z.}} = \varkappa^2 D_k I_k; \quad D_k = \frac{1}{3\Sigma_{tr}^{(k)}}. \tag{3}$$

Then we can solve (1), starting with the first group and proceeding to the last group inclusive, but we must assume that

$$\frac{\sum_{l=1}^{m} \nu_f^{(l)} \Sigma_f^{(l)} I_l}{K_{eff}} = 1, \tag{3a}$$

where the volume of the basic fissionable isotope (i.e., the volume ratio) is chosen so that $K_{eff} = 1$.

In the second case the volume of the basic fissionable isotope is given and we must choose $R_r$ so that $K_{eff} = 1$. We can do this most conveniently if we use the formula given below, based upon perturbation theory, for finding the critical radius $R_{cr}$ of the bare reactor

$$R_{cr} = -\frac{R}{\sqrt{1+\frac{\Delta k}{J}}}, \tag{4}$$

where

$$J = \sum_{k=1}^{m} J_{k,\text{a.z.}},$$

and $\Delta K = K_{eff} - 1$; this corresponds to the value of R used in the calculation.

The system of value equations is solved in an analogous manner for the value of $R_r = R_{cr}$ which we have found, starting with the last group and working towards the first group, inclusive; in this process we must assume in (2) that

$$\left.\begin{aligned} J_{k,\text{a.z.}}^{+} &= \varkappa^2 D_k I_k^{+}; \\ \sum_{l=1}^{m} \varkappa_l I_l^{+} &= K_{eff}. \end{aligned}\right\} \tag{5}$$

When we satisfy the latter relation we verify the correctness of the solution of (1) and (2).

In order to compute the integral spectra for the neutron flux and the neutron values in the shield we should in (1) and (2) assume that the space leakages are equal to zero (for a sufficiently thick shield) and consider the leakage from the equivalent bare reactor as supplementary (outer) sources for the sheath, or in other words we should make the following substitutions in (1) and (2):

$$-J_k = J_{k,\text{a.z.}} \qquad -J_k^{+} = J_{k,\text{a.z.}}^{+}$$

Then the solution of (1) may be written in the form proposed by L. N. Usachev

$$J_k = N_k + M_k \frac{\sum_{j=1}^{m} \nu_f^{(j)} \Sigma_f^{(j)} N_j}{1 - K_\infty}, \tag{6}$$

where

$$K_\infty = \sum_{j=1}^{m} \nu_f^{(j)} \Sigma_f^{(j)} M_j. \tag{7}$$

The value of $M_k$ represents the neutron flux in the kth group of an infinite medium with fission neutrons as sources, and is computed by solving equation

$$-\Sigma_{cf,hr}^{(k)} M_k + \sum_{j=1}^{k-1} \Sigma_{hr}^{kj} M_j + \chi_k = 0$$
$$(k = 1, 2, \ldots m),$$

where $N_k$ is the neutron flux in an infinite medium with external sources which represent a leakage from the active zone, and which is calculated by solving equation

$$-\Sigma_{cf,hr}^{(k)} N_k + \sum_{j=1}^{k-1} \Sigma_{hr}^{kj} N_j + J_{k,\text{a.z.}} = 0.$$

The solution of (2) for the sheath is written in an analogous manner.

## Obtaining the Average Values of the Constants and the Single-Group Method of Determining the Critical Loading

The spectra obtained are used to find the average values of the constants in the following manner.* We substitute (3) into (1) and then multiply (1) by $I^+_k$; we then sum over all the groups. The result of the summation may be written in the form

$$\frac{1}{K_{\text{eff}}} = \frac{\varkappa^2 \sum_{k=1}^{m} D_k I_k I_k^+ + \sum_{k=1}^{m} \Sigma_{cf}^{(k)} I_k I_k^+ + \sum_{k=1}^{m} I_k^+ \left( \Sigma_{\text{hr}}^{(k)} I_k - \sum_{j=1}^{k-1} \Sigma_{\text{hr}}^{kj} I_j \right)}{\left( \sum_{k=1}^{m} I_k^+ \chi_k \right) \left( \sum_{l=1}^{m} \nu_f^{(l)} \Sigma_f^{(l)} I_l \right)} . \tag{8}$$

At the same time we have for one group

$$\frac{1}{K_{\text{eff}}} = \frac{\varkappa^2 \overline{D} + \overline{\Sigma}_a}{\overline{\nu_f \Sigma_f}} . \tag{9}$$

Inasmuch as we wish that the reactivity computed by means of the single-group method coincide with the reactivity obtained using the multiple-group calculations, it is natural to use the following scheme for obtaining the average values of the constants

$$\overline{D} = \frac{\sum_{k=1}^{m} D_k I_k I_k^+}{\sum_{k=1}^{m} I_k I_k^+} ; \tag{10}$$

$$\overline{\Sigma}_a = \overline{\Sigma}_{cf} + \overline{\Sigma}_{\text{eff}} ; \tag{11}$$

$$\overline{\Sigma}_{cf} = \frac{\sum_{k=1}^{m} \Sigma_{cf}^{(k)} I_k I_k^+}{\sum_{k=1}^{m} I_k I_k^+} ; \tag{12}$$

$$\overline{\Sigma}_{\text{eff}} = \frac{\sum_{k=1}^{m} I_k^+ \left( \Sigma_{\text{hr}}^{(k)} I_k - \sum_{j=1}^{k-1} \Sigma_{\text{hr}}^{kj} I_j \right)}{\sum_{k=1}^{m} I_k I_k^+} ; \tag{13}$$

$$\overline{\nu_f \Sigma_f} = \frac{\left( \sum_{k=1}^{m} I_k \chi_k \right) \left( \sum_{l=1}^{m} \nu_f^{(l)} \Sigma_f^{(l)} I_l \right)}{\sum_{k=1}^{m} I_k I_k^+} . \tag{14}$$

The effective cross section is determined from (13) which characterizes the reactive input due to the fact that after being scattered the neutron passes over into a state which has a different value. Formulas (10)-(14) then transform into the usual formulas for obtaining the average value from the neutron spectrum, if we assume that the values of the neutrons in all the groups are equal.

For the active zone, where the spectrum evaluation is based upon the spectrum of the bare reactor, (14) takes the form

$$\overline{\nu_f \Sigma_f} = \frac{k_{\text{eff}}^2}{\sum_{k=1}^{m} I_k I_k^+} . \tag{14a}$$

The single-group cross sections, computed in the indicated manner, must give a reactivity, calculated using (9), that coincides with that computed by means of the multiple-group formula of perturbation theory, (8).

This serves as the basis which permits us to use the single-group formula for the critical dimension in the two-zone reactor calculations, and thus to entirely omit the calculation of the space distribution of the neutrons

$$\frac{\operatorname{tg} \varkappa R_a}{\varkappa R_a} = \frac{1}{1 - \frac{\overline{D}'}{\overline{D}} (\varkappa' R_a \operatorname{cth} \varkappa' d + 1)} , \tag{15}$$

where the magnitudes designated by the dash on top refer to the shield, and

$$(\varkappa')^2 = \frac{\overline{\Sigma}'_a - \frac{\overline{\nu_f \Sigma'_f}}{K_{\text{eff}}}}{\overline{D}'} ; \tag{16}$$

$$\varkappa^2 = \frac{\frac{\overline{\nu_f \Sigma_f}}{K_{\text{eff}}} - \overline{\Sigma}_a}{D} \tag{17}$$

($R_a$ is the radius of the active zone and d, the thickness of the shield).

* We wish to note that a method of obtaining the average values of the constants, taking the values of the neutrons into account, was proposed independently of the solution given by the authors of this paper, in [1]. G. I. Marchuk has made known that he has found an iterative method of reducing the multiple-group diffusion problem to an equivalent single- or two-group problem which may be used in multiple-zone reactor calculations. The method was developed in order to determine the higher order corrections for the diffusion approximation. In contrast to the method proposed in the present paper he requires a preliminary understanding of the space distribution in similar reactors.

TABLE 1

Composition of the Active Zone of the Reactor

| Fractional volume of the element | Reactor variation | | |
|---|---|---|---|
| | I | II | III |
| $\epsilon$ alloy | 0.33 | 0.35 | 0.31 |
| $\epsilon$ Na | 0.50 | 0.53 | 0.57 |
| $\epsilon$ Fe | 0.17 | 0.12 | 0.12 |

Remarks: 1) The fuel used in reactor variations I and II was the alloy $U^{238}$ + $Pu^{239}$, the fuel used in variation II was $U^{238}$ + $U^{235}$. 2) The radius of the active zone $R_a$ was for variation I, 36.55 cm, for variation II, 60.35 cm, for variation III, 58.15 cm. 3) The shield thickness was 60 cm for all three reactors. 4) The volume of the sheath was equally composed of: $\epsilon_u$ = = 0.7; $\epsilon_{Na}$ = 0.2 and $\epsilon_{Fe}$ = 0.1 and was the same for all reactors.

The single-group macroscopic active zone cross sections in (17) represent the sum of the single-group cross sections of the individual isotopes, i.e.,

$$\overline{\Sigma} = \sum_m \sigma_m N_m \varepsilon_m = \varepsilon_f A + B.$$

From this expression we can obtain the fraction of the volume occupied by the fissionable isotope $\epsilon_f$.

For a given $R_a$ we usually determine the value of $\kappa$ and substituting this value in (17) find $\epsilon_f$ for $K_{eff}$ = = 1. If the value of $\epsilon_f$ coincides with the value assumed in the calculation for the bare reactor then we consider that we have solved the problem of determining the critical mass of the reactor. If there is a substantial difference then the computation of the spectra and of the single-group constant should be repeated using the newly obtained volume fraction. In this process it is not necessary to recompute the sheath spectra and constants since they are insensitive to the composition and dimensions of the active zone.

The value of critical mass obtained in this manner is in good agreement with the critical mass computed with the aid of the set of equations for a nine-group diffusion system. In addition, we can obtain as a result of these computations the effective supplement $\delta_{eff}$ which is equal to the difference between the critical radius of the bare reactor $R_{cr}$ and the radius of the active zone, $\delta_{eff} = R_{cr} - R_a$.

## Discussion of the Results and Conclusions

The proposed method was verified by a series of calculations for fast reactors of varying dimensions

TABLE 2

Average Values of Single-Group Cross Sections Obtained by Taking Account of and Not Taking Account of Neutron Values

| Reactor variations | Method of averaging | Active zone | | | | | Sheath | |
|---|---|---|---|---|---|---|---|---|
| | | $\overline{\Sigma_f \nu_f}$ | $\overline{\Sigma}_{cf}$ | $\overline{\Sigma}_{eff}$ | $\overline{D}$ | $\varkappa$ | $\overline{D}'$ | $\varkappa'$ |
| I | with neutron values | 0,0176 | 0,0085 | 0,0019 | 1,96 | 0,062 | 1,30 | 0,090 |
| | without neutron values | 0,0154 | 0,0084 | — | 1,65 | 0,060 | 0,88 | 0,086 |
| II | with neutron values | 0,0133 | 0,0085 | 0,0018 | 1,98 | 0,041 | 1,27 | 0,095 |
| | without neutron values | 0,0119 | 0,0083 | — | 1,62 | 0,040 | 0,95 | 0,089 |
| III | with neutron values | 0,0118 | 0,0067 | 0,0020 | 1,84 | 0,042 | 1,17 | 0,087 |
| | without neutron values | 0,0099 | 0,0072 | — | 1,58 | 0,043 | 0,96 | 0,085 |

TABLE 3

Fractional Volumes of the Basic Fissionable Isotope $\epsilon_f$ in Three Reactor Variations for $K_{eff}$ = 1

| Method of computation | Reactor variations | | | Difference between the single-group and space calculation results in % |
|---|---|---|---|---|
| | I | II | III | |
| Nine-group space . . . . . | 0.0512 | 0.0464 | 0.0300 | – |
| Single-group, not taking account of neutron values . . . . . | 0.0460 | 0.0400 | 0.0260 | –(10-14) |
| Single-group taking account of the neutron values . . . . . | 0.0510 | 0.0466 | 0.0300 | $\lesssim 1$ |

and having active zones and shields of varying composition. In all cases the critical mass as calculated by the single-group method, taking into account the values of the neutrons, agreed well with the critical mass obtained from the multiple-group space calculations.

In Table 1 we give the composition of the active zone and shield for three fast reactors.

The integral spectra of the neutron fluxes $I_k$ and the neutron values $I_k^+$ were found using the nine-group approximation. The group constants for these calculations were taken from [2].

We see from Table 2 that the single-group cross section, computed taking and not taking the neutron values into account, can differ quite significantly; in the first case we systematically add the effective cross section of the heat remover to the capture cross section.

The values of the fraction of the basic fissionable isotope obtained by means of the single-group method discussed in this paper, and a comparison with the values obtained by means of the nine-group space calculations are given in Table 3.

As we see from Table 3, the result obtained using the proposed method coincides very closely with the solution of the nine-group space problem (the difference in the results lies within the limits of accuracy of the computations); this is due to the correct method of obtaining the average cross section which reduces the multiple-group reactivity equations (8) to a single-group equation (9).

The accuracy of the method turns out to be sufficiently high so that it is no longer necessary in multiple-group space calculations to compute the critical mass of a fast reactor with a thick sheath.

The method herein considered for calculating the critical loading of fast reactors has been applied and verified for the following conditions:

1. The sheath must be thick, of the order of two-three effective diffusion lengths $L_{eff} = 1/\kappa'$, in order that we can neglect the space leakage.

2. There must not be an edge effect in the sheath. In fast reactors, using only heavy nuclei, there is no edge effect; however it may occur in the shield where hydrogen-containing media and other good moderators are used. Such reactors are of the fast-interval type and our method has not been verified for this type of reactor.

3. The single-group method of calculating the critical mass is applicable to active zones of any size. However, if its dimensions are less than 4-5 single-group neutron mean free paths, we must introduce a correction in (15) for the gas-transport effect.

4. We must consider that this method has only been verified for reactors containing not more than two active zones (an active zone and a production zone).

## LITERATURE CITED


1. G. I. Marchuk, Numerical Methods of Nuclear Reactor Calculation [in Russian] (Atomizdat, Moscow, 1958).
2. A. I. Leipunskii et al., Atomnaya Énerg. 5, 3, 277 (1958).†


†Original Russian pagination. See C. B. translation.

# THE FEASIBILITY OF USING ORGANIC LIQUIDS HEATED IN NUCLEAR REACTORS AS WORKING FLUIDS IN TURBINES, FROM THE THERMODYNAMICAL STANDPOINT

P. I. Khristenko

Translated from Atomnaya Énergiya, Vol. 8, No. 3, pp. 214-218,
March, 1960
Original article submitted April 11, 1959

This article examines, in principle, the possibility of employing heated organic fluids as working fluids for tubines. The organic liquids considered for such applications are diphenyloxide, diphenyl, Dowtherm, etc. Heating takes place inside power-reactor circuits, with evaporation possible in the turbine nozzle. The vapors of these liquids become superheated in adiabatic expansion, although the vapor temperature drops in the process. As an example, we consider data on the thermodynamic cycle of a power reactor using Dowtherm as coolant medium.

Some organic coolants (for example, diphenyloxide) have the capability of setting a turbine into motion directly by application of the organic liquid heated inside the reactor, bypassing the steam system.

It is known that when the saturated vapor of any liquid expands adiabatically, the vapor state during the expansion depends on the physical properties of the liquid, i.e., on the relationship between the specific heat of the liquid and its latent heat of vaporization ([1], p. 72). If, for instance, saturated water vapor or saturated mercury vapor is allowed to expand adiabatically, it will pick up moisture as it expands. On the other hand, saturated diphenyloxide vapor will become superheated during adiabatic expansion, despite a concurrent drop in temperature.

Analytically, this phenomenon may be described as follows:

$$S'' = S' + \frac{r}{T},$$

where S" is the entropy of the dry saturated vapor; S' is the entropy of the liquid, r is the latent heat of vaporization; T is the absolute temperature of the saturated vapor. By differentiating this equation with respect to the temperature T, we get

$$\frac{dS''}{dT} = \frac{1}{T}\left(C_L + \frac{dr}{dT} - \frac{r}{T}\right)$$

(since $TdS' = C\,dT$).

If the specific heat $C_L$ of the liquid is smaller in absolute value than the expression $\frac{dr}{dT} - \frac{r}{T}$, the entropy increment of the saturated vapor will be negative as the temperature goes up, corresponding to curve 1 in Fig. 1. In that case, the curve will go to the right of ordinate KA drawn through the critical point. This slope of the curve corresponds to saturated water or mercury vapor which would pick up moisture during adiabatic expansion. If the value of $C_L$ is larger in absolute value than the expression $\frac{dr}{dT} - \frac{r}{T}$, then the curve will pass to the left of ordinate KA (curve 2, in Fig. 1). The entropy increment of the saturated vapor will then be positive; this vapor will become superheated during adiabatic expansion.

The behavior of saturated diphenyloxide vapor gives us reason for supposing that heated diphenyloxide will prove useful as the direct working fluid for setting turbines into action. Figure 2 is a T-S diagram for diphenyloxide. When diphenyloxide heated to a temperature $T_1$ is directed into a nozzle within which it expands adiabatically until it reaches a temperature $T_2$, then a jet of superheated saturated vapor, or slightly moist vapor, will issue from the nozzle (if the latter is

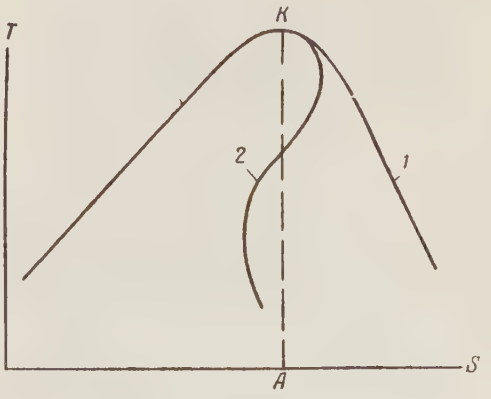


Fig. 1. T-S diagram for water and diphenyloxide.

of sufficient length), and this jet may be directed at the turbine blades directly, and later condensed in the condenser system. It is obvious that the heated liquid must come to a boil and pass over into superheated vapor while in the nozzle.

The constraint $C_L > \left|\frac{dr}{dT} - \frac{r}{T}\right|$, which characterizes the property of some liquids to vaporize completely in the course of adiabatic expansion, as does diphenyloxide, is satisfied by quite a few other liquids.

Figure 3 shows a T-S diagram ([1], p. 82) for diphenyloxide, kerosene, and ethyl ether. In addition to these liquids, we might also mention Dowtherm (eutectic mixture of diphenyloxide and diphenyl), and, apparently, n-hexane, acetic acid, and naphthalene.

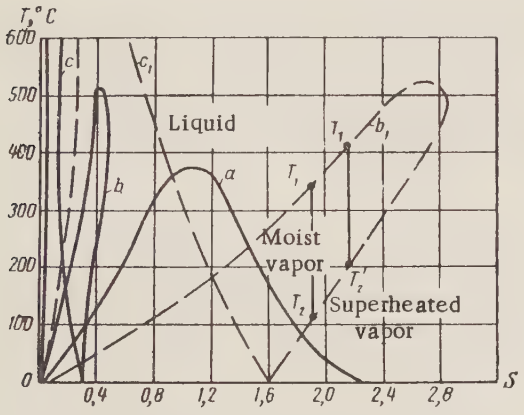


Fig. 2. T-S diagram for water, diphenyloxide, mercury: a) water; b) diphenyloxide; c) mercury (scaled to 1 kg saturated vapor); $b_1$) diphenyloxide; $c_1$) mercury (scaled to 6 kg saturated vapor).

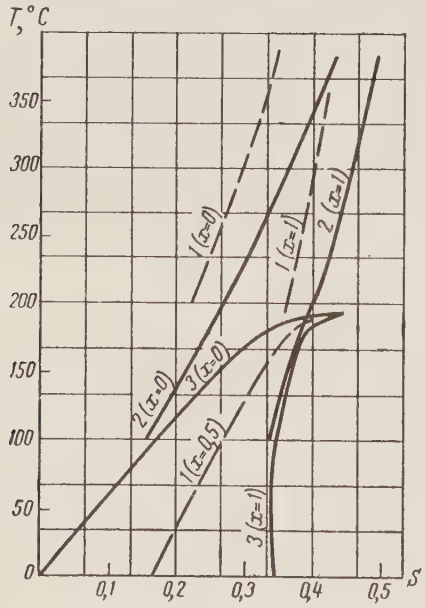


Fig. 3. T-S diagram for diphenyloxide, kerosene, and ethyl ether: 1) Diphenyloxide; 2) kerosene; 3) ethyl ether.

The thermodynamic cycle of a heat engine making direct use of a heated liquid is shown in Fig. 4. The isobar AB (coinciding with the lower limit of the curve) characterizes the heat transfer of the liquid, while the adiabatic line BC gives the liquid expansion in the turbine nozzle, and the isotherm CA gives the vapor condensation.

If the working fluid satisfies the condition $C_L > \left|\frac{dr}{dT} - \frac{r}{T}\right|$, then (assuming a long enough nozzle) vapor or a two-phase liquid will emerge from the nozzle. This cycle could be termed a boiling-liquid cycle.

The efficiency of this cycle (assuming the specific heat of the liquid to be constant) is

$$\eta_t = 1 - \frac{T_2 \ln \frac{T_1}{T_2}}{T_1 - T_2}, \qquad (1)$$

where $T_1$ is the peak temperature of the cycle, and $T_2$ is the low-point temperature of the cycle (temperature in the condenser).

If we take advantage of the fact that the lower limiting curve coinciding with the isobar in the T-S diagram is quite close to linear over a limited temperature range (say, to 100°C, for water), we can then derive the formula giving an approximation to the cycle efficiency:

$$\eta_t = \frac{T_1 - T_2}{T_1 + T_2}. \qquad (2)$$

Comparing the efficiency of this boiling-liquid cycle to the Carnot cycle efficiency

$$\eta_t = \frac{T_1 - T_2}{T_1} \qquad (3)$$

for the same temperatures $T_1$ and $T_2$ in both cycles, we find that a machine operating on the Carnot cycle uses almost double the amount of heat of a machine operating on the boiling-liquid cycle. But the thermal effi-

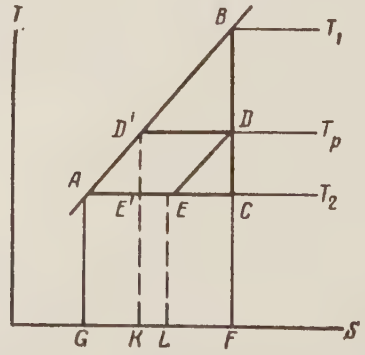


Fig. 4. T-S diagram of cycle of boiling liquid with regeneration.

ciency of the boiling-liquid cycle may be raised appreciably (and even brought close to a Carnot cycle) by resorting to heat regeneration.

The theoretical regenerative boiling-liquid cycle with an infinite number of bleed stages is indicated on the T-S diagram (Fig. 4) by the figure ABDE, or the figure D'BCE'.

Cycle ABDE may be brought about for either a boiling liquid in droplet form or for a gas. It constitutes a thermodynamic cycle similar to that achieved in a gas turbine with gas heated under constant pressure in a regenerative heater and combustion chamber (lines AD' and D'B), under adiabatic expansion of a gas in a turbine (line BD), with the gas cooled under constant pressure in a regenerative heater (line DE), and in the case of isothermal compression of the gas in a compressor (line EA).

For a heat engine operating on a boiling-liquid regime, lines AD' and D'B correspond to the case of a liquid heated in a multistage regenerative heater and heat generating unit, lines BD and DE correspond to adiabatic expansion of the liquid without bleed-off and with multistage extraction of the working fluid, while EA corresponds to condensation of the vapor.

The cycle D'BCE' represents a cycle obtainable in a gas turbine with heating under constant pressure (line D'E), adiabatic expansion of the gas (line BC), and isothermal and adiabatic compression of the gas (lines CE' and E'D', respectively).

Denoting as $T_r$ the regeneration temperature, the efficiency of the cycle with regeneration will then appear, under the conditions assumed earlier, viz., C = const and C dT = T dS, in the form

$$\eta_t = 1 - T_2 \frac{\ln\left(\frac{T_1}{T_r}\right)}{T_1 - T_r}. \qquad (4)$$

The approximate value of the above is given by

$$\eta_t = 1 - \frac{2T_2}{T_1 + T_r}.$$

Consider the use of diphenyloxide, heated inside the reactor loop, as the working fluid for a steam tubine. The critical temperature of diphenyloxide is 530°C, the pressure at that point being 32.7 atm , and accordingly: 6 atm at 350°C, 16.5 atm at 450°C, 0.05 atm at 150°C. Pure diphenyloxide melts at 28°C, and melts at much lower temperatures in the presence of trace impurities, while diphenyloxide decomposes at high temperature. Experience has shown that 1-2% of the diphenyloxide decomposes when exposed to 15 atm and 440°C for 700 hours [2].

The limits of application of diphenyloxide may be found from inspection of the T-S diagram. For the initial temperature of the liquid at entry into the machine, the range is 300–400°C (points $T_1$ and $T_1'$), and for the final temperature the range is 120 -200°C (points $T_2$ and $T_2'$). This corresponds to initial pressures of 2.0-16.5 atm, and final pressures of 0.015-0.15 atm. Since the final temperature of diphenyloxide vapor after discharge from the turbine remains high (120 - -200°C), these machines must be used only as first-stage units. The remaining heat must be utilized either for industrial process needs or to drive the second stage of turbines operating on low-pressure steam.

In the latter case, use of heat from a reactor will proceed along a two-stage thermodynamic cycle, a flow-chart for which appears in Fig. 5, along with a T-S diagram. The first stage of this cycle is indicated by the figure D'BD, bounded by the isobar D'B, along which heat is delivered to the liquid diphenyloxide in the reactor 1 (Fig. 5a), by the adiabatic line BD', along which the heated diphenyloxide expands with vaporization in the nozzle of the single-pressure-stage turbine 2, and by the isotherm DD', along which diphenyloxide vapor condenses in the condenser 3. This condenser

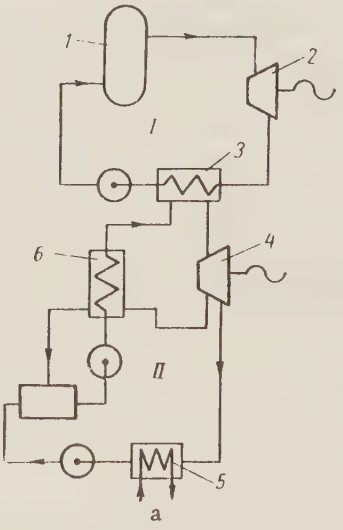


Fig. 5. Flowchart (a) and T-S diagram (b) of the dual cycle: Stage I) heated diphenyloxide; Stage II) saturated steam; 1) reactor; 2,4) turbines; 3,5) condensers; 6) regenerative feed heater.

at the same time functions as an evaporator unit to produce saturated steam, the working fluid for the second second stage of the dual cycle. The second stage of the cycle is illustrated graphically by the figure D'DEA, bounded by the isotherm D'D, along which vaporization of the water in the condenser 3 takes place, to yield saturated steam, by the line DE, depicting adiabatic expansion of the steam in the steam turbine 4, which has multistage bleed-offs for regenerative feed heating, by the isotherm EA and isobar AD', along which condensation of steam in condenser 5 and heating of feedwater in regenerative feed heater 6 take place respectively, heat rejected from the bled-off steam being used to heat the feedwater.

The thermal efficiency of the binary cycle using liquid diphenyloxide (stage I) and steam (stage II) is 0.43 (at temperatures $t_1 = 350°C$, $t_r = 200°C$, and cooler temperature $t_c = 35°C$). If we assume the internal turbine efficiency $\eta_0 = 0.75$, the mechanical efficiency $\eta_M = 0.96$, the electrical efficiency $\eta_E = 0.97$, and the theoretical cycle efficiency $\eta_{th} = 0.9$, then the plant may attain an efficiency as high as 27%. This would be a very high efficiency, considering that the diphenyloxide pressure does not exceed 6 atm, with the temperature at 350°C.

In some cases, as for instance in designing a nuclear propulsion engine for transportation purposes, where weight and size of the plant are prime considerations, design may be limited to include one turbine using an organic fluid as working fluid. In that case, the thermal efficiency of the thermodynamical cycle of the plant would be $\eta = 0.2$-$0.3$, and the total plant efficiency would be $\eta_{pl} = 0.13$-$0.2$.

The organic coolant media which have been most thoroughly investigated, and which are currently least expensive, are diphenyl, diphenyloxide, and their eutectic mixture, Dowtherm.

For example, by using Dowtherm as the working fluid with initial temperature $t_i = 300°C$ and enthalpy $H_i = 149.5$ cal/kg (or $t_i = 400°C$ and $H_i = 219$ cal/kg), and taking into account expansion of the fluid in the turbine nozzle to a state of saturated or slightly moist vapor, then we shall obtain, at turbine exit, either vapor at pressure $P_{vap} = 0.017$ atm with specific volume $v = 11.5$ m$^3$/kg and enthalpy $H = 149.5$ cal/kg, or vapor at pressure $P_{vap} = 0.25$ atm with $v = 1.0$ m$^3$/kg and $H_{vap} = 219$ cal/kg.

The heat drop during adiabatic expansion of the liquid to a state of saturated vapor will be approximately $\Delta H_1 = 25$ and $\Delta H_2 = 55$ cal/kg, and the speed at which the vapor leaves the turbine nozzle $c_1 \simeq 450$ and $c_2 \simeq$ $\simeq 600$ m/sec. The value of these speeds, as well as the need to expand the boiling liquid to a state of saturated vapor within the entrance nozzle of the turbine, govern design considerations. The design would apparently be a velocity-stage impulse turbine with one or more (depending on power rating) two-row or three-row discs.

If we bear in mind the comparative low speeds at which the vapor leaves the turbine nozzle, the low pressures, and the specific volumes of the organic vapors, then the design of turbines for several hundred to several tens of thousands of kilowatt ratings will be within reach. The cost of turbines based on this principle should not exceed the cost of conventional units.

We must also bear in mind the fact that the use of turbines operating in a direct cycle with liquid organic coolants heated in-pile would obviate the need for installing a first stage of steam generating units with pressure 30-40 atm.

A thermodynamical cycle utilizing heat rejected from nuclear reactors would depend largely on the method of heat removal.

In one case, where coolant heated in-pile retains its original state of aggregation, the energy of the coolant alone may be used to perform work, by cooling the coolant medium in the engine and extracting work from the higher temperature imparted to it in the reactor to the lower temperature corresponding to the cold source. The theoretical thermodynamical cycle for such (nonboiling) reactors must of necessity be the cycle considered here.

In another case, where the coolant suffers a change in its state of aggregation while in the reactor (the liquid being converted to vapor), the latent heat of vaporization of the liquid may be utilized to perform work, i.e., vapor produced in-pile is allowed to expand adiabatically in the engine. A part of the heat rejected by this vapor is transformed into work, and the vapor is then condensed in the condenser. The theoretical thermodynamical cycle for such (boiling) reactors must of necessity be a cycle bounded by two isobars and two isotherms. The efficiency of this cycle will be equal to the efficiency of the Carnot cycle.

An intermediate position between boiling reactors and nonboiling reactors is occupied by the uranium-graphite reactor now being built by the USSR, which features superheated high-pressure steam. In this reactor, a conventional regenerative thermodynamical cycle with steam superheat, common for modern steam heat-power installations, is achieved.

As we have shown, a theoretical cycle for coolants heated inside the reactor loop is realizable with the aid of liquids which are fully capable of vaporizing during adiabatic expansion.

## LITERATURE CITED


1. V. Shyule, Engineering Thermodynamics [in Russian] (Goséngergoizdat, Moscow-Leningrad, 1934) Vol. I, book 2.
2. Petrorius, "Efficiency and increased power in back-pressure machines," Verein deutscher Ingen. 7, No. 6 (1927).

# SOME FORCE AND DEFORMATION CHARACTERISTICS IN THE METAL FORMING OF URANIUM

I. L. Perlin, I. D. Nikitin, V. A. Fedorchenko,
A. D. Nikulin, and N. G. Reshetnikov

Translated from Atomnaya Énergiya, Vol. 8, No. 3, pp. 219-227,
March, 1960,
Original article submitted February 23, 1959

To determine the system of metal forming of uranium in order to produce sheets, bars, tubes, etc., an investigation was made of the force and deformation characteristics in rolling, extruding, wire-drawing, and stamping of uranium. Determinations were made of the relationship between rollability of uranium and the temperature and between the average specific pressure of uranium on the rolls, the absolute widening and the degree of reduction (from 10 to 50%), and the temperature (from 400 to 1000°C). A calculation of the average specific pressure of uranium on the rolls according to the analytical formula of A. I. Tselikov [1] showed good agreement between the calculated data and the experimental results.

A study was made of the dependence of the extrusion stress on the drawing (up to 54), the temperature (from 250 to 800°C), and the scale factor (the ratio of diameters of the containers equal to 5). The concepts are introduced of extrudability and the modulus of the extrusion stress, methods are proposed for calculating them, and the dependence is determined on the temperature of extrudability and the modulus. A study is made of the dependence of the wire drawing stress and the safety coefficient on the degree of deformation (from 5.5 to 34%).

The metal forming of uranium differs in that, in contrast to a number of industrial nonferrous metals, uranium has a strong similarity to oxygen and to the metals of the iron group. Additional difficulties in the selection of optimum thermomechanical systems for processing uranium are caused by the fact that it undergoes three allotropic transformations with the formation of modifications which have very different plastic and strength characteristics.

Due to the large thermal effect during processing caused by the high resistance of uranium to deformation and its low specific heat, cases are found in practice where, during extrusion and rolling with high reductions and speeds, the metal is heated due to the heat of deformation and is converted from the $\alpha$-phase to the $\beta$-phase.

Oscillograms of the temperature changes inside an uranium billet during the process of upsetting on a friction press showed that at 420°C during deformation of specimens from 90 to 60 mm in one impact, the temperature of the metal is increased by 90-100°C. A similar effect is also observed at other temperatures.

The intensive oxidation of uranium also affects the change in temperature of the metal during processing.

Bearing in mind the possibility of a considerable increase in temperature due to the thermal effect of deformation and oxidation, with appropriate control of the heating it might be possible to select a system of deformation in which the temperature remained practically constant, i.e., an " isothermal " process might be established.

It is mainly these considerations which determine the methods used in the metal forming of uranium.

Methods have been developed for preparing uranium components with all types of metal-forming processes. Success has been achieved in the production of bars, profiles, tubes, wire, various sheets, strip, and also components with a more complex configuration.

## Rolling

The maximum permissible reductions in the rolling of uranium ($\epsilon_{max} = \frac{H-h}{H} 100\%$) cannot be determined simply on the basis of the mechanical characteristics of uranium (relative elongation, impact toughness, etc.), since during rolling, as in any other metal-forming process, the stress state has a complex form. The rollability (or plasticity of the metal during rolling) is therefore usually determined by rolling wedge-shaped specimens into a strip of equal thickness. Figure 1 shows the influence of temperature on the maximum permissible reduction per pass in the rolling of cast uranium specimens of 15 mm width. It can be seen from the diagram that in the temperature ranges 500-600° and 770-1000°C, the uranium permits reductions during the

TABLE 1

Relationship between the Average Specific Pressure of the Metal on the Rolls and the Initial State of Uranium, Reduction and Rolling Temperature

| Initial state of uranium | Initial thickness H, mm | Final thickness h, mm | Initial width B, mm | Relative reduction $\epsilon$, % | Rolling temperature t, °C | Average specific pressure $p_{av}$, kg/mm$^2$ |
|---|---|---|---|---|---|---|
| Cast | 10.2 | 9.3 | 30.0 | 8.8 | 20 | 163 |
| The same | 10.3 | 8.2 | 30.0 | 20.4 | 20 | 175 |
| Rolled in the $\alpha$-phase | 7.0 | 6.4 | 27.8 | 8.6 | 20 | 558 |
| The same | 7.0 | 6.45 | 28.5 | 7.8 | 20 | 512 |
| Rolled in the $\gamma$-phase | 25 | 10 | 100.0 | 60 | 950 | 2.5 |
| The same | 25 | 10.3 | 100.0 | 58.5 | 850 | 3.1 |

pass equal to > 80%. Below 300°C the rollability of the uranium falls sharply. At temperatures of 300-500°C the permissible reductions are 50-75%. If the temperature is accurately controlled, $\beta$-uranium can be rolled with reductions up to 30%. Temperatures close to the transformation points $\alpha \rightarrow \beta$ and $\beta \rightarrow \gamma$ are the most dangerous from the point of view of breakdown in the rolled components. The obtained relationship is approximate for the development of the method, since plasticity during rolling depends on the character of the stress state and, consequently, on the deformation conditions (the shapes of the components and billets, ratios of width to thickness, type of groove design, etc.).

In connection with the considerable anisotropy of the properties and the reduced plasticity at temperatures from 20 to 200-250°C, uranium is exceptionally sensitive to unevenness in the distribution of deformation in the rolled component. For example, thin uranium strips (0.05-0.20 mm) can be obtained by rolling in the cold, with a total reduction of 80-85% and better for one pass without breakdown. The increased plasticity in this case is due to the low degree of unevenness in the distribution of deformation in the rolled strip. When rolling thin plates in the cold with a change in the rolling direction, the resultant unevenness in deformation along the width causes the metal to break. Reduced plasticity is observed at temperatures up to 250°C in all cases where the metal is deformed with a high degree of unevenness (for example, when rolling bars into strip).

Resistance to deformation. An investigation of the change in the average specific pressure of the metal on the rolls ($p_{av}$) in relation to various factors was carried out on a two-high mill with rough ground steel rolls of 220 mm diameter. The pressures on the clamping screws were determined by means of inductive or graphite pickups and an MP-02 loop oscillograph. Two series of experiments were carried out. In the first series, cast and mechanically machined specimens with initial thickness H = 10 mm and width B = 25 mm were rolled in one pass with various reductions. In the second series, specimens of varying thickness (8-14 mm), quench-hardened from the $\beta$-phase, were rolled to the same final thickness h = 7 mm. Rolling in the $\gamma$-phase was carried out on specimens measuring 10 × 100 × 180 and 25 × 100 × 180 mm.

The average specific pressure of the metal on the rolls falls sharply with the rolling temperature (Fig. 2) and increases considerably on transformation to the $\beta$-phase. The greater pressures for the same reductions in the second series of experiments (compared with the first) are due to the use of quench-hardened specimens.

The average specific pressures of the metal on the rolls at room temperature can exceed the pressures in the $\gamma$-phase by more than 80-100 times (Table 1).

The dependence of the average specific pressure on the reductions during the pass for various temperatures is different (Fig. 3). The drop in the value of the average specific pressure with increase in reduction at temperatures of 100, 200, 300 and 700°C is mainly due to the increase in temperature of the metal during rolling from the heat of deformation. Increase in temperature of the metal during rolling at t = 630°C causes transformation to the $\beta$-phase, which is recorded on the oscillograms in the form of sudden changes in the curves.

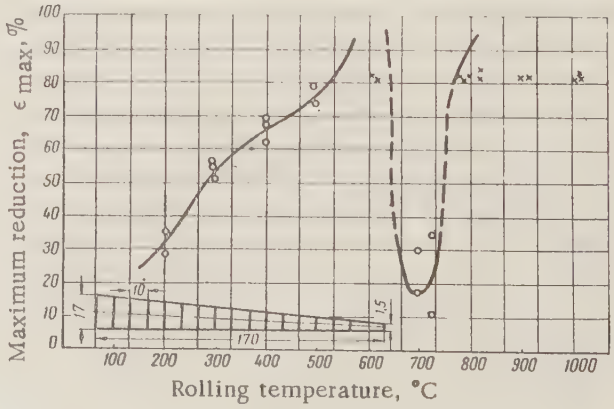


Fig. 1. The effect of temperature on the rollability of uranium: × ) no breakdown observed in the specimens.

TABLE 2

Mechanical Properties of Extruded Uranium

| Initial state of uranium | Yield strength, $\sigma_b$, kg/mm² | Relative elongation $\delta$, % | Necking of the transverse section $\psi$, % |
|---|---|---|---|
| Extruded at 350°C . . . . . | 143.0 | 9.2 | 8.9 |
| Extruded at 730-750°C . . . . . | 61.3 | 9.2 | 4.1 |
| Extruded at 900°C . . . . . | 80.9 | 7.6 | 4.0 |
| Extruded in the $\alpha$-phase with subsequent quench hardening from the $\beta$-phase . . . . . | 75.0 | 7.0 | 6.0 |

Remarks: 1) Each number is the arithmetic mean of three measurements. 2) Small specimens were used in the tests.

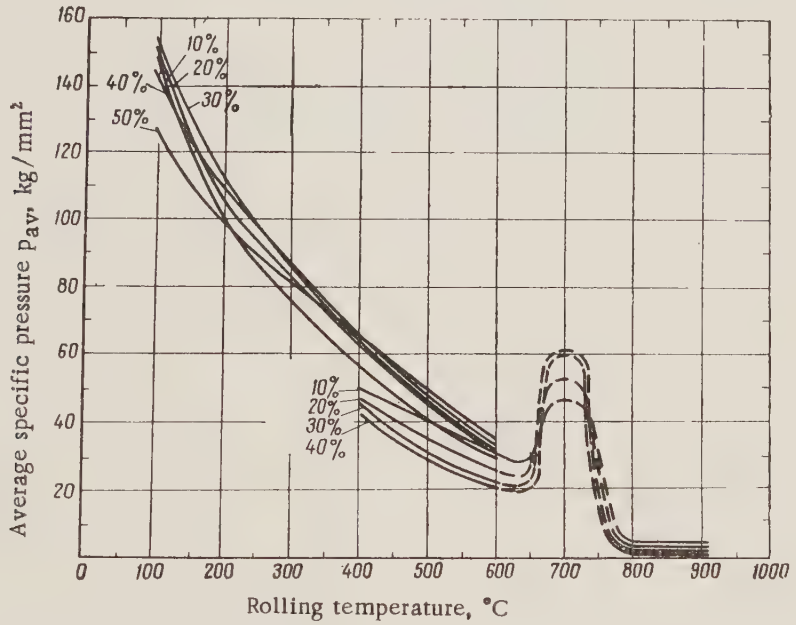


Fig. 2. The relationship between the average specific pressure of the metal on the rolls and the temperature: ——— the first series of experiments; — — — — — the second series of experiments.

The calculation of average specific pressures from the Tselikov analytical formula [1] showed good agreement between the calculation data and the experimental results:

$$p_{av} = k\frac{2(1-\varepsilon)}{\varepsilon(\delta-1)}\left(\frac{h_H}{H}\right)\left[\left(\frac{h_H}{H}\right)^{\delta}-1\right],$$

where $\epsilon = \frac{H-h}{H}$ is the relative reduction; $h_H$ is the height of the strip in the neutral section; $\delta = \mu\sqrt{\frac{2D}{\Delta h}}$ ($\mu$ is the coefficient of friction, D is the diameter of the rolls); $k = 1.15 n_\gamma \sigma_s$ ($n_\gamma$ is the coefficient of hardening, $\sigma_s$ is the yield stress at high plastic deformations).

Two curves of Fig. 3 were plotted on the basis of a calculation according to this formula. In the calculations, the coefficient of hardening for all reductions was taken constant and equal to 1.3 for t = 600°C and 1.5 for t = 200°C. However, as the investigations showed, it changes in relation to the reduction and temperature. The following hardening coefficients are recommended when calculating with the Tselikov formula [1]: 1 at 760-1000°C; 1.2-1.4 at 500-650°C; 1.4-1.6 at 200-500°C. The last two values of the hardening coefficient increase with the reduction.

For a more correct approach to the calculation of roll groove designs in the rolling of uranium it is essential in the first place to know the widening.

Figure 4 shows the relationship between the absolute widening $\Delta b = B_1 - B$ and the temperature during the rolling of a square billet measuring 21 x 21 x 180 mm on 220 mm diameter rolls. The presence of a max-

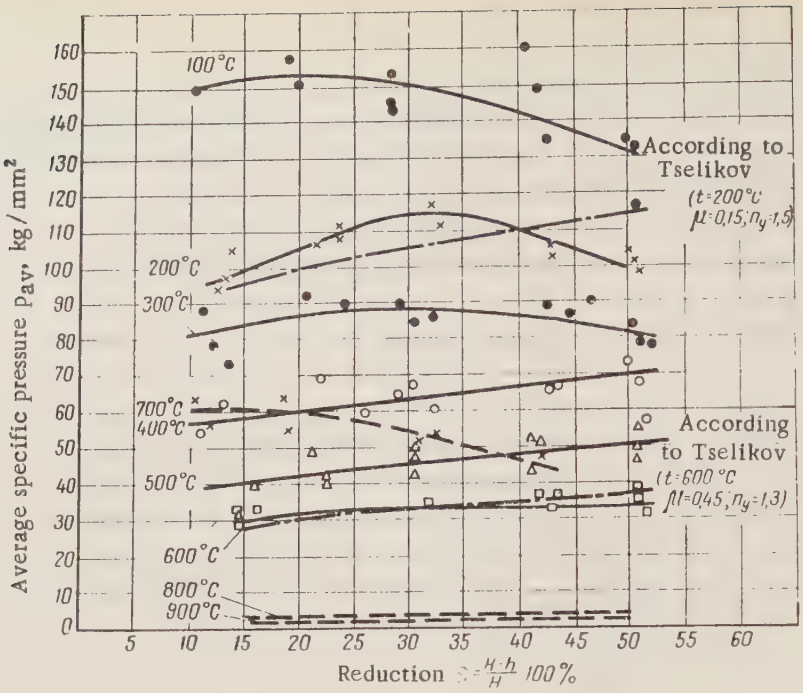


Fig. 3. The relationship between the average specific pressure of the metal on the rolls and the reductions per pass— — — — first series of experiments.

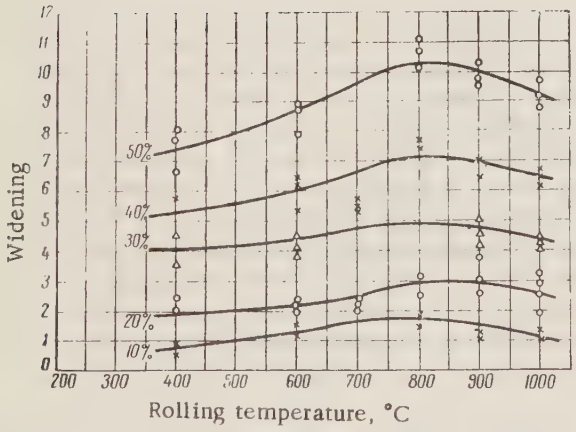


Fig. 4. Relationship between the absolute widening of the billet and the rolling temperature.

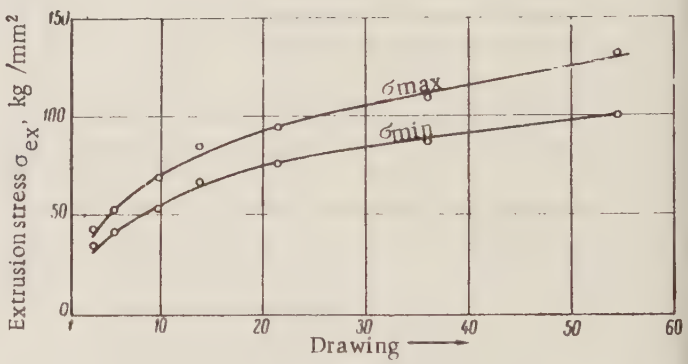


Fig. 5. Relationship between the extrusion stress of uranium and drawing.

imum on the curves at t≃800°C is connected with the presence of a maximum for the coefficient of friction at this temperature. When t = 900-950°C, the coefficient of friction (determined from the maximum angle of bite) when rolling with steel rolls is equal to 0.4-0.45. The differences in the value of widening for t ≃ 600 and t ≃ 1000°C are very small, especially with reductions up to 30%. It follows that with the same groove design it is possible to roll uranium at t ≃ 600 and t ≃ 900-1000°C.

## Extrusion

Uranium is extruded with varying degrees of difficulty in the temperature range 250-1000°C.

Gamma-uranium is extremely plastic and is extruded with very small extrusion stresses, but readily fuses with the components of the extrusion tool (iron, nickel and cobalt), forming low melting eutectics. Gamma-uranium is extruded in a graphite shell using a carbide or steel tool with special coatings (for example, molybdenum or chromium) and various lubricants. Good results are obtained using ceramic tools.

Under ordinary extrusion conditions, α-uranium binds strongly with the steel extrusion tool. In the extrusion of α-uranium, as in the extrusion of γ-uranium, it is essential to avoid contact of the uranium with the steel tool and with air. To achieve high quality in

the components and a good yield of useful metal in the extrusion of α-uranium it is essential to ensure conditions of fluid friction at the contact surfaces. As a rule, α-uranium is extruded in various metal and nonmetallic shells (for example, in copper, zirconium, nickel and graphite) or without a shell using lubricants with fillers which are resistant to extrusion. In the extrusion of α-uranium, the tool is of heat-resistant steels, carbides, or ceramics. When the billets are heated before extrusion in a salt bath, the fused salt serves not only as a heating medium, but also as a lubricant in the extrusion.

Uranium components are made by both forward and backward extrusion. Alpha-uranium is extruded with rates of 1-400 mm/sec and greater, depending on the shape and dimensions of the component. The rate of extrusion of γ-uranium is practically unlimited.

When α- or γ-uranium are extruded without a shell, the components are often cooled in water immediately after leaving the die in order to reduce oxidation and to improve the structure of the metal.

Extrusion stress. The methods for calculating the working stresses during extrusion involve the selection of difficultly determined coefficients. In order to make these coefficients more precise, as well as data on the mechanical properties of uranium at high temperatures, it is therefore necessary to know experimentally determined values of the working stresses during the extrusion of uranium.

At temperatures of 600-650°C, α-uranium can be extruded with high degrees of deformation (99.5% and better).

Figure 5 shows the relationship between the extrusion stress and the drawing. The extrusion was carried out at temperatures of 600-560° with a hydraulic press. For all billets, the length was three times the diameter. The force of extrusion was recorded by a self-recording manometer. With increase in degree of deformation the extrusion stress increases smoothly. The scale factor has a considerable effect on the extrusion stress. With decrease in the diameter of the container the extrusion stress increases, and vice versa.

The extrusion stress of uranium also depends on the uniformity of heating of the billets. Sometimes the heating of the billets (for example, by high frequency induction) is best carried out so that the surface layers have a higher temperature than the inner layers. The higher temperature of the surface layers then compensates their cooling due to contact with the tool during extrusion.

The extrusion stress also increases, other conditions being equal, with increase in the length of the billet (during the isothermal extrusion of α- and γ-uranium a length of the billet which is between three and five times the diameter of the container has no noticeable effect on the extrusion stress).

Figure 6 gives the relationship between the extrusion stress of uranium and the temperature. There is an increase in the extrusion stress in the β-phase region. When the surface layers of the billet cool during extrusion from the temperatures of γ-uranium to those of β-uranium, the component cracks – a "jag" is formed (periodic disturbances in the continuity of the component). When the surface layers of the billet cool from the temperatures of β-uranium to those of α-uranium, no "jag" forms. In this case, the hard and brittle β-uranium is pressed into the soft and plastic shell of α-uranium, which means that in the core consisting of β-uranium there are no tensile stresses.

It can be seen from Fig. 7 that the relationship between the extrusion stress and the integral index of the degree of deformation i ($i = \ln\mu$) in semilogarithmic coordinates is expressed by a straight line passing through the origin.

The experimentally found regularities in the change in extrusion stress as a function of the degree of deformation and temperature are in full agreement with the theoretical principles, which means that a nomogram can be drawn to determine extrusion stresses (Fig. 8). The dotted line corresponds to an extrusion stress equal to 150 kg/mm²; the crosshatched area shows the effect

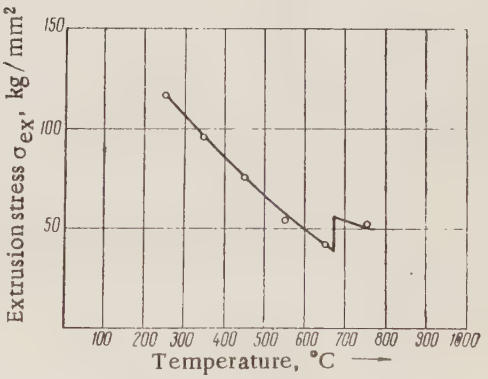


Fig. 6. Relationship between the extrusion stress for uranium and the temperature.

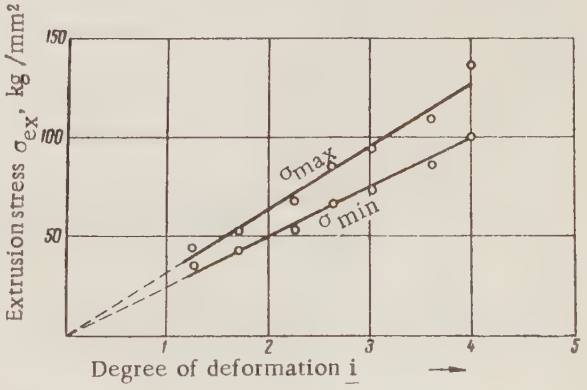


Fig. 7. The relationship between the maximum and minimum extrusion stresses and the integral index of the degree of deformation.

of the scale factor on the extrusion stress with a ratio of the container diameters equal to five.

Modulus of extrusion stress. Certain data were published in [2, 3] on the extrusion constant of uranium, determined from the formula

$$K = \frac{P}{F_H \ln \mu},$$

where K is the extrusion constant; P is the force of extrusion; $F_H$ is the area of cross section of the container; $\mu$ is the drawing.

Some papers mention that the value of K depends on the state of the contact surfaces, the lubricant and the length of the ingot [3] and also on the degree of deformation [2]. Consequently, the value P expresses the total force of extrusion determined in the general case by the formula [4]:

$$P = R_M + T_s + T_M + T_f,$$

where $R_M$ is the force on the press plate needed to provide the basic deformation without allowing for the contact friction forces; $T_s$ is the force on the press plate needed to overcome the friction forces arising on the side surface of the container; $T_M$ is the force on the press plate needed to overcome the friction of the deformed metal against the surface of the die; $T_f$ is the force on the press plate needed to overcome the friction forces on the surface of the sizing flange of the die.

In our experiments it was found possible to neglect the forces of contact friction (before the center of deformation) in view of their small values. As can be seen from Fig. 7, with increase in the degree of deformation the extrusion stress increases according to a linear law and the straight line passes through the origin. The total extrusion stress is then determined from the formula

$$\sigma_{ex} = \frac{R_M + T_M}{F_H} = M_{ex} i,$$

where $\sigma_{ex}$ is the extrusion stress.

The value $M_{ex}$, which is the coefficient of proportionality in the formula connecting the stress and deformation, by analogy with the modulus of elasticity we have called the modulus of extrusion stress.

Figure 9 shows the relationship between the modulus of the uranium extrusion stress and the temperature. In the $\beta$-phase region there is an increase in the modulus of the stress. In $\gamma$-uranium the stress modulus is approximately six times smaller than in $\alpha$-uranium at ~650°, and approximately twenty times smaller than for $\alpha$-uranium at 300°C.

Extrudability. The extrudability (resilience) of a metal is a value determined for a general case from the formula

$$i_{ex} = \frac{\sigma_{ex}}{M_{ex}},$$

where $i_{ex}$ is the extrudability with extrusion stress $\sigma_{ex}$.

Of interest is the maximum extrudability of a metal, which is determined at an extrusion stress which is equal to the permissible yield strength of the press tool material, i.e., 150 kg/mm². From the maximum extrudability it is possible to evaluate the capacity of a metal to deform by extrusion at a given temperature. Figure 10 shows the effect of extrusion temperature on the extrudability of uranium. The upper curve shows the change in the maximum extrudability and the lower curve the change in extrudability for

$$\sigma_{ex} = 15 \text{ kg/mm}^2.$$

In the region of the $\beta$-phase there is a considerable reduction in the extrudability of uranium; $\gamma$ uranium has a very high extrudability (~35), which corresponds to an extremely high degree of drawing (more than $1.5 \cdot 10^{15}$).

The mechanical properties of extruded uranium. Components extruded in the region of the $\alpha$-phase have a fibrous macrostructure and porcelain-like fractures. Components extruded in the $\gamma$- and $\beta$-phases have a granular macrostructure, whereas the fracture of uranium extruded in the $\beta$-phase is coarser grained than the fracture extruded in the $\gamma$-phase. The mechanical properties of extruded uranium correspond to the grain sizes (Table 2). As can be seen from the table, uranium extruded in the $\alpha$-phase has a higher yield strength and

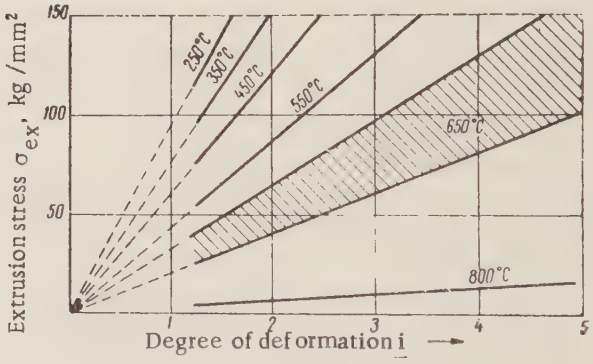


Fig. 8. Nomogram for determining extrusion stresses.

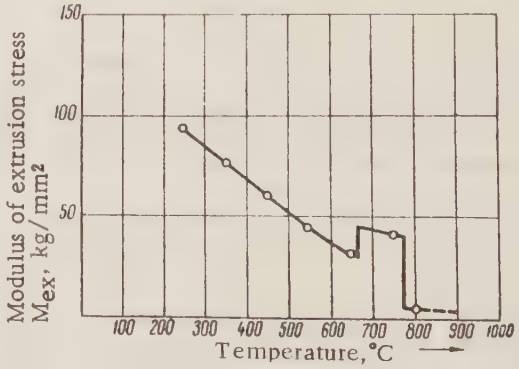


Fig. 9. Relationship between the modulus of the uranium extrusion stress and the temperature.

TABLE 3

Relationship Between Drawing Stress and Reduction

| Initial state of uranium bar | Initial diameter $d_i$, mm | Final diameter df, mm | Reduction per pass δ, % | Drawing force $P_{dr}$, kg | Drawing stress $\sigma_{dr}$, kg/mm² |
|---|---|---|---|---|---|
| Annealed | 11.45 | 10.7 | 12.7 | 1950 | 21.7 |
| Preliminarily deformed | 10.3 | 9.8 | 10.0 | 1700 | 22.5 |
| | 9.5 | 8.5 | 20. | 2650 | 47 |

a considerable necking of the transverse section compared with uranium extruded in the γ-phase. Heat treatment of uranium extruded in the α-phase reduces the yield strength, the relative elongation and the necking of the transverse section.

## Wire Drawing

Uranium wire and other components can be obtained by drawing in the cold state or with heating. When drawing bars in the cold state the lubricant can be a graphite preparation with various fillers; the material is applied to the bar before drawing and is dried. This lubricant has good covering power and is not pressed out of the die plate, clings firmly to the bar and gives a bright smooth surface. An additional thin layer of lubricant must be applied to the bar before each pass.

In the cold drawing of a bar the reduction per pass can be 10-20%. In some cases the partial deformation can be increased. During the drawing the coefficient of friction in the couple uranium – metal of the die plate is fairly high. Using from [5] the formula for determining the drawing stress

$$\sigma_{dr} = \frac{1}{\cos^2\left(\frac{\alpha+\varrho}{2}\right)} \sigma_{TC} \frac{a+1}{a} \times$$

$$\times \left[1 - \left(\frac{S_K}{S_H}\right)^a\right] + \sigma_q \left(\frac{S_K}{S_H}\right)^a$$

and the corresponding experimental data we found that in the couple uranium – carbide with a graphite lubricant the friction coefficient is equal to 0.2-0.25.

Table 3 gives some results for the cold drawing of uranium bars.

The investigations showed that in the drawing of the uranium in the cold state it is necessary to have intermediate annealings and to have special electrolytic coatings on the wire and the self-drawing should be carried out with small rates and small reductions per pass.

Wire should be made by drawing with heating over a wide range of temperatures up to 600°C. Measures should then be taken to prevent oxidation of the metal. With this method, tubes and bars can be made with varying sizes and shapes. The hot drawing of uranium wire can be carried out with reductions per pass of 13-20%, but the uranium permits reductions of up to 30-35% also (Table 4).

Figure 11 shows the relationship between the drawing parameters and the degree of deformation per pass. In this case the wire in the initial state is annealed, the wire drawing should be carried out through the same die plate and the necessary reductions per pass are achieved by different initial diameters of the wire. It follows from the diagram that the force and stress increase regularly with increase in the degree of deformation but lag behind its growth. This lag is uniform and is due to the fact that on the one hand the intensification of the drawing process reduces the relative losses on external friction and on the other hand that the yield strength of the uranium wire, having an effect on the value of the drawing force, increases along a gently decaying curve with increase in the degree of deformation.

Drawing with heating makes it possible to prepare uranium wire with 2 mm diameter and smaller. With certain changes in the heating conditions it is possible to prepare fine wire with diameter down to 0.1 mm.

## Stamping

Uranium is satisfactorily stamped in hammers and high speed presses at the temperatures of α- and γ-

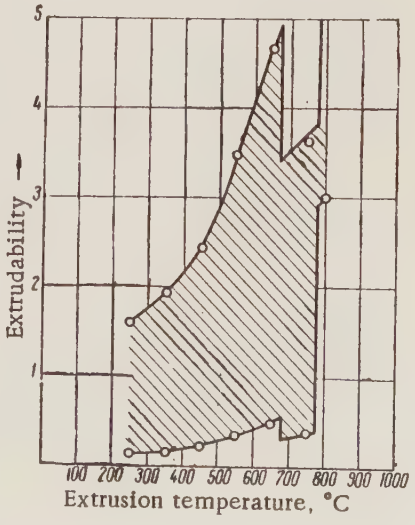


Fig. 10. Relationship between extrudability of uranium and the temperature.

TABLE 4

Parameters for Drawing Wire with 3-7 mm Diameter

| Reduction per pass $\delta$, % | Drawing stress $\sigma_{dr}$, kg/mm$^2$ | Safety factor during drawing $K_s$ | Coefficient of friction $f_N$ |
|---|---|---|---|
| 5.5 | 14 | 6.0 | 0.2 |
| 13 | 24 | 3.7 | 0.22 |
| 28 | 38 | 2.47 | 0.25 |
| 34 | 39.4 | 2.4 | 0.25 |

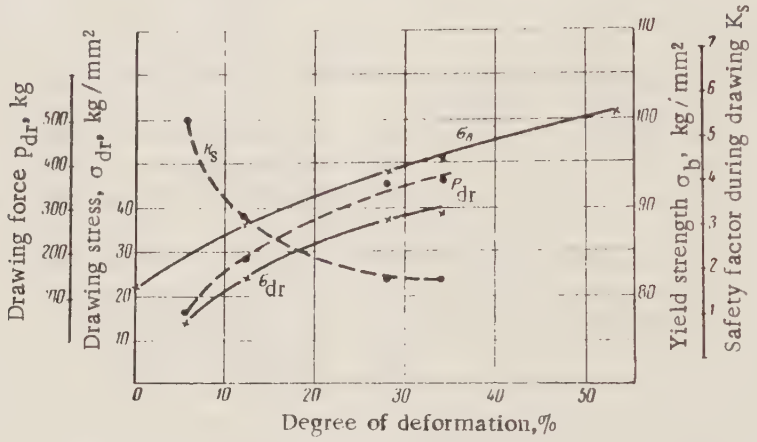


Fig. 11. Relationship between the drawing parameters and the degree of deformation per pass.

regions. Alpha-uranium at temperatures of 600-650°C can be stamped with speeds of hammer-working stroke of 6000-7000 mm/sec. If the billets are overheated to the temperature of the $\beta$-phase during stamping with high rates the uranium cracks. Serious cooling of the billets can also lead to cracking. When stamping in the $\gamma$-phase, cooling of the uranium to the $\beta$-phase state leads to breakage of the components.

Uranium components can be deep-drawn at temperatures of 200-600°C using special lubricants. The forces in drawing and also compression obey the same laws as the forces in the drawing of steel and copper; the values of the forces are about the same as for steel. When developing a drawing method it is essential to allow for the anisotropy of the properties of $\alpha$-uranium and a special rolling method must be used to remove the festoons.

## Forging

Billets can be prepared by the usual manual and machine free forging in the $\alpha$- and $\gamma$-phases. In a number of cases it is convenient to use rotation forging of uranium components at room temperatures and high temperatures. The standard equipment and tools are used for rotation forging. The reductions per pass are 10-25%. To improve the conditions of rotation forging and to reduce oxidation (when forging at 500-600°C) the components should be coated with a graphite lubricant. Rotation forging is also used when forging the ends of uranium components which are intended for drawing.

## LITERATURE CITED


1. A. I. Tselikov, Rolling Mills [in Russian] (Metallurgizdat, 1947).
2. D. Howe, Materials of the International Conference on the Peaceful Uses of Atomic Energy (Geneva, 1955) [Russian translation] (Goskhimizdat, Leningrad, 1958) Vol. 9, p. 221.
3. Kaufmann, Materials of the International Conference on the Peaceful Uses of Atomic Energy (Geneva, 1955) [in Russian] (Goskhimizdat, Leningrad, 1958), Vol. 9, p. 261.
4. I. L. Perlin, Tsvetnye Metal. 9, 73 (1957).
5. I. L. Perlin, The Theory of Wire Drawing [in Russian] (Metallurgizdat, Moscow, 1957).

# PROSPECTING CRITERIA FOR URANIUM DEPOSITS

M. M. Konstantinov*

Translated from Atomnaya Énergiya, Vol. 8, No. 3, pp. 228-238, March, 1960,
Original article submitted November 20, 1959

The author discusses criteria which can be used for assessing the possible occurrence of uranium in a particular region and for prospecting for uranium deposits and individual ore bodies.

In the Soviet Union prospecting criteria are considered to include all geological laws (both particular and general), natural phenomena, and historical data which in the final analysis can be used for discovering workable accumulations of mineral products.

Some investigators distinguish in prospecting criteria between geological grounds for prospecting and prospecting indicators [1]. Prospecting criteria are generally subdivided, according to their nature, into structural, petrographic, mineralogical, etc.

The grouping we have adopted is an attempt to classify prospecting criteria on the basis of problems solved by means of particular criteria or, to be more accurate, on the basis of the "geological objective" for which they are intended (see table).

The arbitrary nature of the boundaries between individual groups of prospecting criteria should be noted. There are also all-purpose criteria, which are suitable both for the determination of the uranium content of a particular ore field and an assessment of the prospecting possibilities of large regions. One of the most important criteria – the presence of a uranium ore occurrence or deposit – is included in such criteria. But the majority of present-day prospecting criteria fall within our system, which is not to deny the usefulness of other classifications. Practical geologists frequently request scientific workers engaged on metallogeny, geochemistry and other studies to develop prospecting criteria, but they are dissatisfied with the results of their investigations because they have been given prospecting criteria of a scope of application different from that requested. Our proposed assessment of the scope of prospecting criteria will make it possible to introduce clarity into some of the problems of their development and utilization.

## Theoretical Criteria Based on Regional Geology (A)

This category includes geological factors which make it possible to assess the prospects of large geological regions. From this aspect the following are the most essential criteria:

1. The location of provinces in zones linking Archean massifs with Proterozoic folded structures. These zones are located along the marginal areas of

* Deceased.

System of Grouping Prospecting Criteria

| Categories of prospecting criteria | Types of ore concentrations – objects for prospecting and assessment | Problems solved by means of prospecting criteria |
|---|---|---|
| A (Theoretical criteria based on regional geology) | Metallogenic province. Ore zone. | General assessment of the prospecting possibilities |
| B (Field criteria based on regional geology) | Ore complex. Ore field. | Distinguishing of the ore-bearing sites for carrying out prospecting. |
| C (local-prospecting). | Deposit. Ore body. | Discovery of deposits and ore bodies. |
| D (prospecting-surveying) | Ore chutes. | Discovery of workable concentrations within prospected and worked deposits. |

shields (Canadian, Australian) or in the inner regions of shields (Baltic, Indian) (Fig. 1). It is this factor which is the principal criterion for a positive assessment of the prospects of finding uranium in Precambrian shields.

2. In addition to this structural factor, a specific metallogenic appearance, inherent in the main uranium provinces of Precambrian shields, should be noted. This specific character consists in the presence of thick stratiform deposits of iron, copper, cobalt and nickel ores (southern sector of the Canadian belt, the South African belt and the Bihar belt of India).

3. The following must be considered as favorable conditions for prospecting endogenic deposits of uranium in folded regions: a) the presence of rigid massifs with a Precambrian base, compressed by young folds (Fig.2); b) the presence of young, markedly differentiated intrusive activity; c) the presence of large disruptive intrusions of a different type.

4. Certain authors emphasize the great importance of an arid climate for the formation of sedimentary uranium deposits [2, 3]. But examination of the paleoclimatic conditions of a number of sedimentary uranium deposits shows that they are more probably correlated with zones transitional between a humid and arid climate, characterized by instability and frequent change of the climatic conditions.

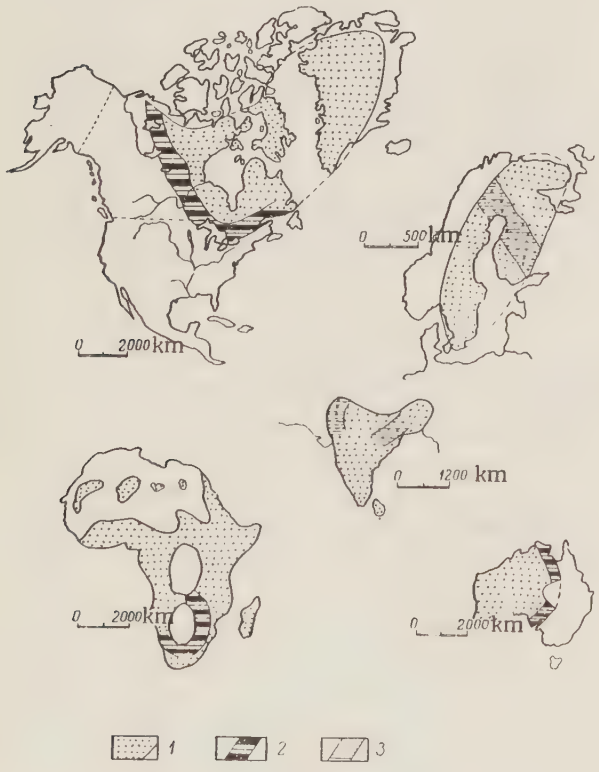


Fig. 1. Location of uranium-bearing belts in Precambrian shields: 1) Precambrian shields; 2) ore belts with large uranium deposits; 3) ore belts with slight uranium mineralization.

5. Marginal troughs of platforms, extended zones of intermontane depressions, where the uranium concentration may be associated with phosphorite deposits, fish bones, residual petroleum products and organic matter of various origins are favorable for the prospecting of uranium deposits of the sedimentary type.

6. The presence of specific epochs of formation of uranium deposits may be used as a criterion for the assessment of a number of regions. Thus, for Western Europe, higher uranium concentrations in deposits of Cambrian-Silurian age are characteristic; for the Mediterranean folded region the higher uranium concentrations are found in Permian-Carboniferous (Alps) and Cretaceous deposits (Morocco) (the phosphorites of Morocco, Israel, etc.), while in the American sector of the Pacific zone the maximum uranium content is found in Jurassic and Triassic deposits, and to some extent in Cretaceous deposits.

7. The problem least solved is that of the conditions of accumulation of uranium in the sedimentary covering of platforms. But the presence of uranium concentrations, which are large when viewed from the aspect of reserves (although having low contents), in the shales of Sweden and the black shales of the USA indicates the possibility of the discovery of uranium deposits in the sedimentary covering of platforms. In general, those parts of the platform in which the following factors are present are the most promising; 1) the sedimentary blanket was laid down on the uranium-bearing zones of the foundation; 2) during the process of formation of the covering the foundation retained a certain mobility, which led to considerable differentiation of the superincumbent sedimentary rocks.

## Field Criteria Based on a Regional Scale (B)

For a general positive assessment of the prospects of finding uranium in a large region extending for hundreds or even thousands of kilometers it is necessary, of course, to employ more immediately practical criteria which would make it possible to distinguish in

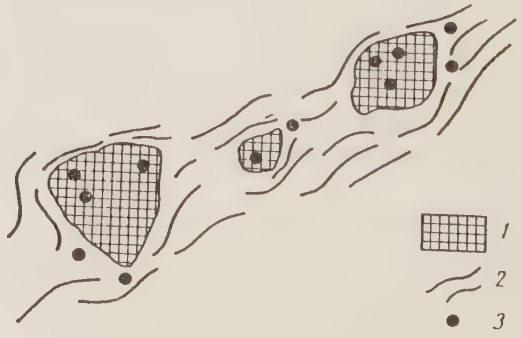


Fig. 2. Diagram of the correlation of uranium mineralization with rigid massifs in a folded region: 1) rigid massifs; 2) fold axes; 3) uranium deposits.

these vast areas regions where the occurrence of uranium mineralization is most probable.

The following geological factors may be such criteria:

1. Regions with a relatively lesser degree of metamorphism of the sedimentary rocks are favorable for the prospecting of sedimentary-metamorphic (stratiform) uranium deposits in ore regions of Precambrian shields. Areas with more intense metamorphism, the development of fissure tectonics, the occurrence of granitization and the younger intrusive activity in the shield are favorable for prospecting deposits of the vein type.

2. Median rigid massifs with a Precambrian base and their surrounding folded terrains (Fig. 3) are favorable for prospecting uranium deposits in folded zones. A spatial association is often noted between uranium ore fields and regions of development of granitoid massifs, primarily of acid or medium composition, normal biotite granites and small intrusions of the type of quartz monzonites, trachytes, trachyliparites and quartz porphyries.

3. A more intense occurrence of young volcanism, together with uranium mineralization, is noted in areas of discordant superposition of young folding on older folding (for example, Laramie folding on Variscian in North America, the Cordilleras and Andes).

4. In intermontane depressions uranium is most frequently found in depressions characterized by the alternation of deposits typical of arid conditions (including haloid deposits) and beds rich in organic matter, formed in a hot moist climate, with an increased uranium content in dispersed or concentrated form in rocks of folded structures surrounding the depression (region of removal) and also characterized by the presence (frequently, but not always) of acid effusives with an increased uranium content at the periphery of the depression or in the series of its sedimentary deposits.


Fig. 3. Diagram of the location of uranium mineralization on the Colorado Plateau and in its surrounding terrain: 1) boundary of the Colorado Plateau; 2) effusive coverings; 3) region of development of sedimentary uranium deposits; 4) hydrothermal deposits and ore occurrences of uranium.

5. In foothill troughs and large intermontane depressions, the most promising regions are those adjoining the most mobile areas of the folded zones, where orogenic activity was still taking place recently. By affecting the adjacent region of the trough, this recent movement causes a change in the hydrodynamic conditions and intensified filtration of underground water through the series of terrigenous rocks, which may lead to migration of uranium and its concentration in beds impregnated with organic matter.

6. The littoral facies of marine paleobasins, consisting of shallow-water deposits: carbonaceous-argillaceous shales, phosphorite-bearing deposits, limestones and sandstones containing organic matter, and also quartz-pebble conglomerates containing organic matter and bearing traces of mineralization (pyritization, the presence of gold, etc.) are favorable for prospecting sedimentary deposits.

7. Basins located in a region of extensive occurrence of eruptive and metamorphic rocks are favorable for prospecting uranium deposits in coal, particularly if the clarke of uranium in the sedimentary rocks is high. In this connection, the most promising areas are young coalfields with a high degree of metamorphism of the coal (lignites, brown coals, metamorphosed hard coals) [4].

8. The conjunction of sedimentary and hydrothermal deposits is a general rule for all uranium-bearing provinces of ancient and young folded regions. The discovery of hydrothermal deposits may, therefore, indicate the presence of deposits of the sedimentary type. On the other hand, the presence of sedimentary formations may be used as a criterion for the occurrence of hydrothermal deposits in those areas where these formations are subjected to metamorphism, granitization, etc.

9. A. P. Vinogradov [5] has recently drawn attention to the possibility of using specific ratios of isotopes of lead, sulfur and other elements as a geochemical criterion. This idea was developed for uranium deposits in [6], in which it was shown, that the presence of increased amounts of radiogenic lead in nonradioactive minerals can be considered as a criterion of the probability of the existence of uranium deposits in a region.

10. An appreciable enrichment of water with uranium over considerable areas is one of the important

prospecting criteria for uranium fields [7, 8]. But the use of radiohydrochemical indicators meets with a number of difficulties and can only be effective if the geological, climatic, and other factors influencing the formation of underground water are fully taken into account. Thus, it is found that a hydrogeochemical background must be established both for each region separately and for each season of the year and each type of rock. It must also be taken into consideration whether the hydrochemical conditions in which the water-bearing rocks are located assists or impedes the solution and migration of uranium.

In the majority of uranium regions, the uranium content in the surface water varies between $1 \cdot 10^{-6}$ to $10 \cdot 10^{-6}$ g/liter, but in acid underground water it may reach $n \cdot 10^{-5}$ g/liter. Large rivers, with the exception of those flowing directly beneath uranium-bearing regions, generally scarcely differ in radioactivity from the background of the given region.

Contents generally 3-10-fold higher than normal, depending on the geological and chemical factors, are taken as anomalous contents which can be considered as a prospecting indicator.

11. An increased radioactivity of granitoids, with which a uranium mineralization may be genetically established, was considered by certain investigators as a positive criterion for prospecting uranium-bearing ore fields. But practice showed that this criterion is not acceptable for all uranium provinces. W. Gross [9] considers that the presence of local zones of increased radioactivity in granite intrusions may indicate the probability of the occurrence of uranium ores in the adjacent structures and that if high and local concentrations of radioactivity are not found in these in-

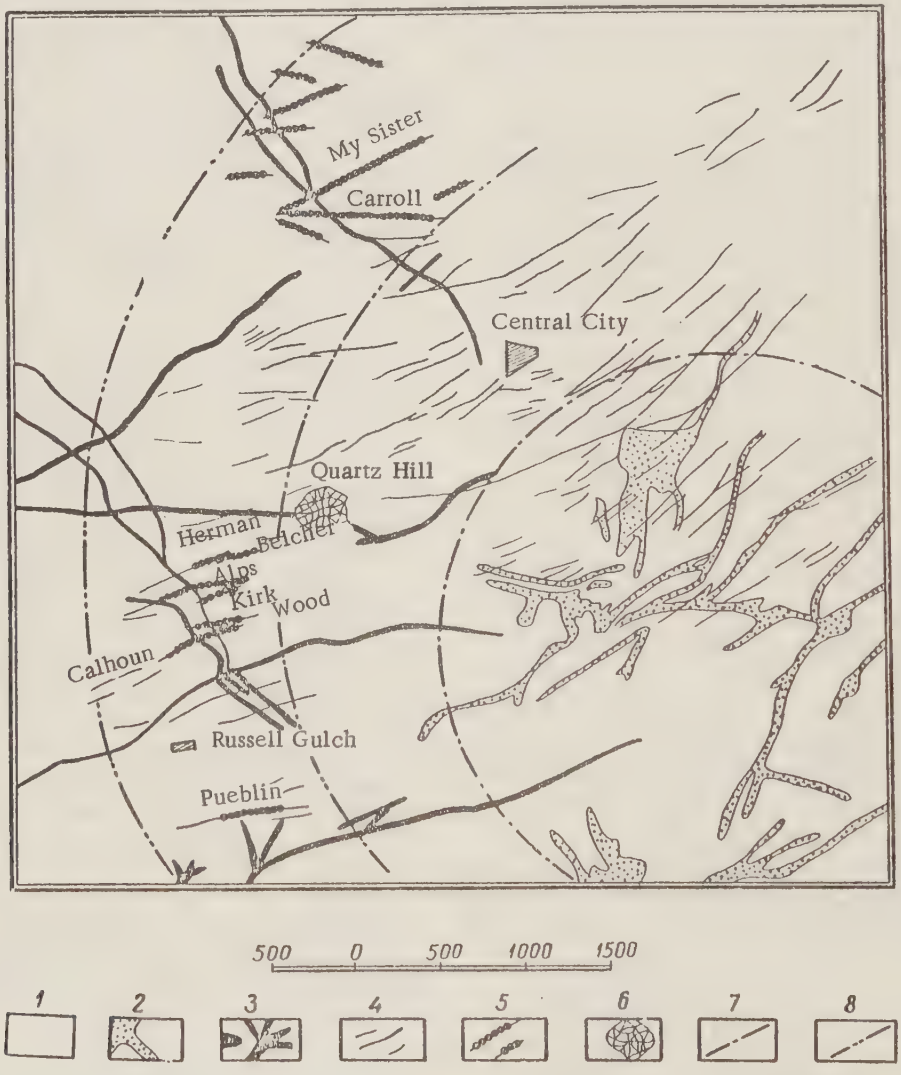


Fig. 4. Diagram of the location of ore zones of the Central City, Colorado region: 1) Precambrian; 2) quartz-monzonite; 3) bostonite; 4) ore veins; 5)uranium-bearing veins; 6) ore breccia; 7) boundary of the area of the quartz-monzonite outcrop; 8) boundary of the ore zones. [A) gold-pyrite zone; B) uranium zone; C) polymetallic zone].

trusions the latter may be excluded from detailed prospecting operations.

12. The γ-anomalies recorded in an aerial survey, associated with geologic features of the region – specific formations of rocks, tectonic zones, etc. – which are favorable for the occurrence of uranium ores may be a more specific criterion. The γ-anomalies can be divided as a first approximation into three groups, according to whether they were determined in an airplane, on the ground or in underground workings; the aero-γ-anomalies correspond to the above-described category of regional-prospecting criteria (B), the surface anomalies to local-prospecting characteristics (C), and the underground anomalies to prospecting-surveying characteristics (D).

## Local-Prospecting Criteria (C)

When the presence of uranium in a region has been established by general geological premises, direct prospecting characteristics, radioactive anomalies, the occurrence of uranium minerals, individual ore occurrences of uranium, etc., the main problem is the discovery of industrial uranium deposits. It should be noted that this problem can also be solved in the earlier stages of the investigation of the region, commencing with the reconnaissance of the latter, a geologic survey on various scales, etc. The following very important prospecting indications can be used for prospecting workable deposits:

1. A structural check of the mineralization is of great importance of endogenic uranium deposits. During the prospecting of such deposits, the following are of primary interest: large fault zones with a developed system of feather joints and, in between them, zones transverse to the general direction of folding; zones located in regions of intense bending of the folding, and most important, deep-lying zones overlying a Precambrian base.

2. Stocks, stockworks, and laccoliths of the acid varieties of granitoids and adjoining regions of the intruded rocks are favorable for prospecting uranium deposits in young folded regions which are characterized by the development of small intrusions. The uranium mineralization is sometimes correlated with a specific ore zone around the intrusion (Fig. 4).

3. The neighborhoods of dikes of basic rocks near the contact face are often favorable for the concentration of an endogenic uranium mineralization and, therefore, for prospecting.

4. For individual uranium-bearing provinces there are specific "families" of deposits of various metals, including uranium deposits. Thus, in the Variscan folded region of Europe uranium deposits are found in many cases in the same ore zones as tungsten-tin deposits. They are located in different fissures and belong to different stages of the mineralization but are characterized by a consistent spatial relation. For such regions the presence of a tungsten-tin mineralization may be considered as a criterion for the possible occurrence of uranium ores, too, in the same ore field. Other "families" of deposits and different prospecting criteria can be established for other provinces.

5. Uranium is an "omnipresent" element, giving workable concentrations in various mineralogical formations.

But the number of uranium-bearing mineralogical formations in individual provinces, particularly those correlated with Precambrian shields, is evidently limited. Thus, in the Canadian ore zone, where there are numerous deposits and ore occurrences of uranium of various scales, two types of mineralization are consistently present: the so-called "five-element" formation (principally in the north) and carbonate-pitchblende ores of simple composition. Three types of uranium mineralization are noted in the European uranium zone: the same "five-element" formation, the uranium-fluorite and the true uranium type.

In Alpine folded regions, uranium is found in various mineralogical formations. But here, too, as experience is accumulated it may be possible to distinguish formations in which it is most frequently found.

In a number of cases it is possible to establish certain minerals which are indicators of uranium mineralization. Thus, in the case of the European ore zone and the Cordilleras of the USA, purple fluorite, nearly black in color, is considered as an indicator of the possible presence of uranium mineralization.

Thus, although it is impossible to distinguish specific mineralogical formations or mineral-indicators, which could be employed universally as prospecting indications for uranium, they can be established within the limits of the same metallogenic provinces and used successfully for prospecting work.

6. Modifications of adjacent rocks in the neighborhood of hydrothermal veins are one of the prospecting criteria used in a number of regions.

Hematitization (reddening) of the adjoining rocks is found most frequently. In a number of cases the following and investigation of a reddening zone made it possible to discover workable uranium ores, although regions exist where such zones are not associated with uranium mineralization.

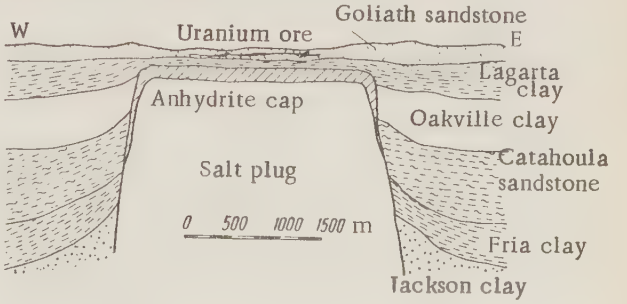


Fig.5. Diagram of the position of uranium mineralization in the petroleum structure in the Panhandle, Texas.

Zones of bleaching (Marysvale region, Utah, etc.), the formation of which is due to sericitization and kaolinization of the adjoining rocks, are also used for prospecting uranium deposits. In certain regions a close association is noted between uranium mineralization and fluoritization, in other regions chloritization zones are a characteristic feature [10]. In a number of deposits an association is established between uranium mineralization and zones of development of sodium metasomatism (albitization).

Modifications of the adjoining rocks of uranium deposits near veins may, therefore, be used as a prospecting indication within the limits of individual provinces, where a typical type of modification of the adjoining rocks has already been established for these deposits.

7. Areas with relatively calm hydrodynamic conditions are the most favorable for the accumulation of uranium in deposits of the littoral zone of marine paleobasins. Such paleogeographic elements as bays and areas cut off from the open sea by a submarine terrace or lip are, therefore, one of the important prospecting criteria for uranium.

Individual sedimentary deposits are correlated with the sediments of ancient estuaries, deltas and sounds; certain investigators explain this by the precipitation of uranium in the zone where waters of markedly different chemical composition mix.

8. Concentrations of organic matter in sedimentary rocks are a very important prospecting indication. When uranium-bearing solutions circulate through beds enriched with organic matter, if conditions are favorable the latter can act as a precipitating agent for the uranium, both during the process of sedimentation and epigenesis. For this reason, on the Colorado Plateau the courses of ancient paleocurrents enriched with plant residue are one of the most important prospecting criteria.

Ancient petroleum structures with a deposit of residual petroleum products of the asphaltite type, which can be collectors of uranium mineralization (Fig. 5), are of substantial importance in regions where uranium is found in sedimentary rocks.

9. In uranium-bearing coal basins, ore beds of the infiltration type must be sought in the areas located near granite massifs or covered by tuffaceous or sedimentary rocks containing a large amount of pyroclastic material [4].

10. Lithologic criteria in the form of series, formations and facies zones favorable for uranium mineralization are a great help in prospecting uranium deposits in a number of provinces. On the Colorado Plateau, for example, sandstones of fluvial origin are the most favorable for the localization of uranium, whereas sandstones of marine or eolian origin are generally unmineralized. The majority of deposits in the Morrison formation were accumulated by facies transitional between massive sandstones and argillites in areas where there is a fine laminar alternation of these rocks. The distinguishing of zones of development of favorable facies or formations, extending for hundreds of kilometers and having a width of tens of kilometers, was an effective help in prospecting uranium deposits within such zones.

The presence of rocks with optimum porosity, enclosed in less permeable deposits, or, as already noted, the presence of organic matter: coal, lignites, asphaltites and other deposits is favorable for infiltration deposits.

11. The different dispersion (including diffusion) aureoles formed around a deposit are of particular importance in the prospecting criteria used for the discovery of deposits. These include aureoles of secondary minerals (salt aureoles) and in certain (rare) cases aureoles of primary minerals, hydrochemical, botanical and radiogenic aureoles.

Secondary minerals of uranium formed in the outcrops of ore bodies and giving rise to aureoles around them show a definite tendency to zonal location.

The distinct aureoles near the outcrops of uranium ores form uranium minerals of micaceous habit (uranium phosphates, arsenates and vanadates), which are good prospecting indicators. The laws of the distribution of uranium micas near uranium ore bodies disintegrating in the supergene zone have been investigated and described by V. G. Melkov [7].

Uranium-bearing secondary minerals: opal, chalcedony calcite, and limonite, developed in the oxidation zone of uranium deposits, are also good prospecting indicators, forming aureoles around the outcrops of ore bodies.

12. Dispersion aureoles of primary uranium minerals are not characteristic of uranium deposits; this is due to the poor stability of uraninite and pitchblende in the supergene zone. But in certain cases, fine grains of these minerals, enclosed in a firm en-

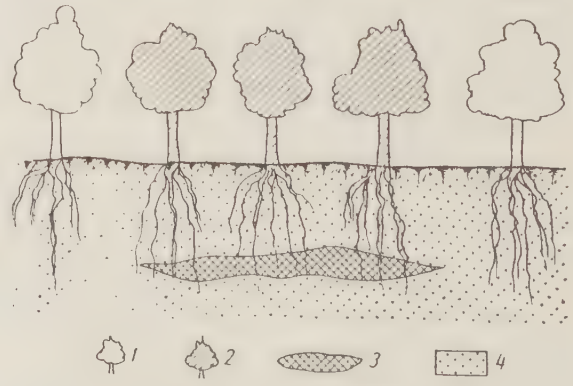


Fig. 6. Connection between the radioactivity of plants and a uranium deposit : 1) plants with normal (background) uranium content; 2) plants with abnormal uranium content; 3) uranium layer; 4) sandstone.

velope of vein quartz or quartzite, can be transported together with these for considerable distances. The preservation of uraninite is sometimes assisted by organic matter investing the grains of the mineral. As regards brannerite and davidite, which in a number of deposits are the principal uranium minerals, they can evidently give considerable dispersion aureoles.

13. In a number of regions the accumulation of uranium by plants can serve as a prospecting characteristic. Plant ash generally contains 0.2-1.0 g/t of uranium. But in plants whose roots are located in rocks enriched with uranium the uranium content of the ash may sometimes reach 100 g/t. Different plant species accumulate uranium in different ways. Experiments showed that the plants which tend to accumulate uranium most readily are those with the strongest tendency to absorb large amounts of sodium, sulfur, selenium, calcium and small amounts of potassium. Conifers and steppe shrubs of the family Compositae are, in particular, examples of such plants (Fig. 6).

The depth at which the ore can be detected by means of plant analysis depends on the nature of the plant roots and their access to water. In the uranium-bearing desert regions of the Colorado Plateau the depth of penetration of the root system of a shrub or tree is generally 15-25 m.

The mineralized areas of a coal seam in the La Ventana Plateau (New Mexico) were successfully distinguished by the analysis of pines and junipers, the roots of which penetrate through a 25 m layer of sandstone.

It is considered, however, that prospecting of ores lying at a depth of more than 20 m by the plant analysis method is evidently not very effective [11].

14. Plant-indicators are used as a prospecting characteristic for uranium in the region of the Colorado Plateau, the Katanga copper belt of North Rhodesia and in other regions.

In the Colorado Plateau region, the most characteristic plant-indicators are astragalus (Astragalus pattersoni A. Gray), belonging to the vetch family.

In addition to Astragalus, selenium indicators, which can also serve as uranium ore indicators if the selenium content in the ore is less than 2 g/t, are Aster venustus M. E. Jones, Gindelia spp., Oryzopsis Rimonoides and Stanleya spp.

In the copper-uranium belt of Katanga, North Rhodesia, where the uranium concentration is associated with copper and cobalt deposits, plant-indicators of copper and cobalt can be used as an indirect prospecting indicator for uranium.

15. Radiohydrochemical anomalies can be used not only for detecting uranium-bearing areas but also in prospecting for uranium deposits. The underground water circulating in the ore regions may be enriched with uranium and also with radium and radon, and create hydrochemical aureoles with anomalous contents of these elements around the deposit. In a number of cases an increased uranium content in underground water has been recorded at distances up to 1-5 km from the deposit (Fig. 7).

In some cases an appreciable enrichment with radon (tens to a few hundred emanations) is observed at distances of several hundred meters from the uranium mineralization. Abnormally high radon contents (up to several thousand emanations) are generally clearly traced at distances of several dozen meters from the ore body.

An increased radium content in water also indicates the presence of uranium mineralization in the immediate neighborhood.

16. In practice, the most important prospecting criteria for uranium deposits are $\gamma$-anomalies established by $\gamma$-surveying on the surface. The degree of reliability of $\gamma$-anomalies as prospecting criteria is different and depends on the type of $\gamma$-surveying (by automobile, on foot) and its degree of detail. This problem has been examined in special handbooks [7].

17. During the process of radioactive decay there is continual emanation of radium (radon), thorium (thoron) and actinium (actinon). Thoron with $T_{\frac{1}{2}}$ = 54.6 sec, and actinon $T_{\frac{1}{2}}$ = 3.92 sec occur not more than 10-20 cm and 2-3 cm, respectively, from the source (ore body). Radon with $T_{\frac{1}{2}}$ = 3.82 days penetrates 4-5 m from the ore body, and a still further distance if secondary dispersion aureoles are present in its vicinity. Being accumulated in ground water, radon creates characteristic aureoles of developed gas around uranium-bearing ore bodies, which are one of the most important prospecting characteristics of uranium deposits. They are distinguished by means of emanation surveying.

## Prospecting-Surveying Criteria (D)

This group combines criteria which can be used for prospecting uranium ore bodies (including blind bodies) in already known uranium deposits and in ore fields with nonuranium mineralization, and also for the assessment of deposits from outcrops.

The majority of these criteria are of a local character and since they are only effective for individual deposits and regions, cannot be of value for other deposits.

The following may be mentioned as prospecting criteria of relatively high importance:

1. In many uranium ore fields bands or individual rock beds particularly favorable for the localization of uranium ores are distinguished (Fig. 8). More than 80% of all the uranium reserves of a given ore field or deposit are often included in such "uranium-loving rocks." These rocks are generally characterized by the presence of mineral-precipitants of uranium (amphiboles, pyroxenes, pyrite, etc.), and also by physical properties

favorable to the precipitation of uranium (optimum porosity, fissuration, etc.). The distinguishing of such uranium-loving rocks and their use as prospecting criteria increases markedly the efficiency of prospecting operations for uranium ore bodies in a given ore field or region.

2. In some deposits reddening (hematitization) of the adjoining rocks gives such distinct local aureoles in the immediate vicinity of the uranium-bearing areas that they can be used as prospecting criteria for uranium ore chutes. The Sunshine deposit in the USA and the Ace-Fay and other deposits in the Lake Athabaska region of Canada may serve as examples. At the Lake Contact deposit, by the reddening of the adjoining rock it was not only possible to establish the proximity of the uranium ore but also to judge the richness of the ore from the intensity of reddening.

3. Structural prospecting criteria are of primary importance for the discovery of regions with industrial uranium ores.

In many deposits some particular system of fissures is a structure favoring ore localization. In this connection it is noted that the ore is more often found in conjugated fissures of the second and third order, not in fissure structure of the first order. Sometimes, when fissures of the first order are slightly opened the uranium ore may also be localized in the main fissures in the latter stage of the ore process.

In some deposits accumulations of uranium ore were recorded in the interstitial conjugated fissures of different direction or in areas where there was a sudden (angular) change in their strike. Such prospecting criteria must be established and used for specific deposits.

4. In infiltration deposits of the type with shifting current bedding maximum concentration of uranium is found at intervals characterized by a marked change in the hydrodynamics of the current – in bottom depressions, bends of the bed, transverse washouts, etc. Areas of enrichment with organic matter are a general feature of the accumulation of uranium in infiltration and sedimentary-syngenetic deposits.

5. Gamma-anomalies recorded by means of underground $\gamma$-surveying are widely used for prospecting uranium ore chutes, particularly when deposits of other mineral products are examined for the presence of uranium. The type of the oxidation zone to which a discovered uranium ore occurrence belongs may be a criterion for the assessment of a deep-lying uranium-bearing ore body and for deciding whether surveying is worthwhile. Six mineralogical types of oxidation zones, depending on the characteristic associations of the uranium minerals, are quite clearly distinguished [12].

A general assessment of the type of primary ores of an ore body from its surface outcrop may be accompanied by a certain forecast of its behavior at depth,

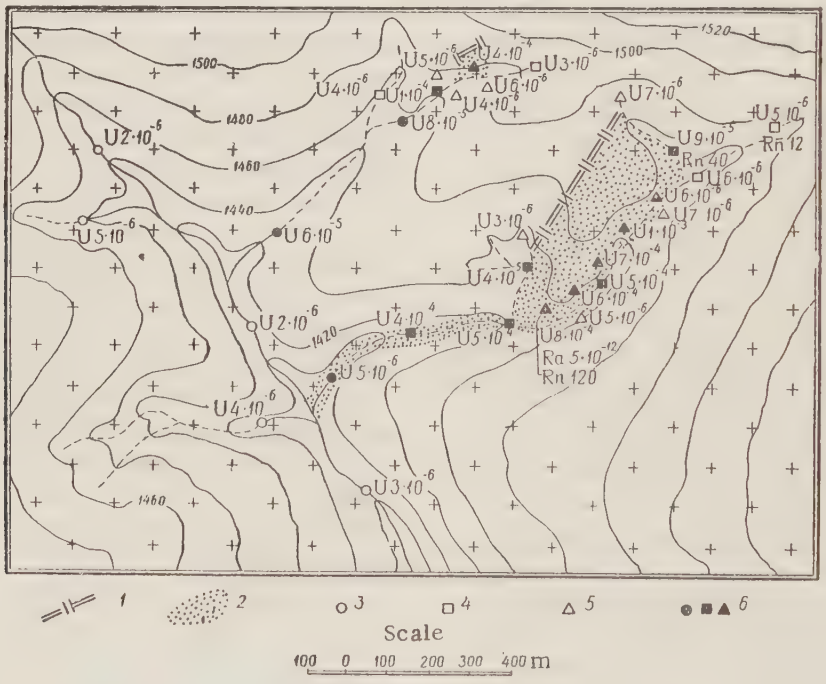


Fig. 7. Map of radiohydrogeological testing of different activities: 1) ore-bearing structure; 2) aureoles of anomalous waters of different concentration; 3) sites at which samples were taken from various springs and water courses; 4) boreholes sunk in the first stage of prospecting-surveying operations; 5) boreholes sunk in the second state of prospecting-surveying operations; 6) anomalous springs (the figures indicate anomalous contents of uranium and radium (g / liter) and radon (emanations).


Fig. 8. Influence of the adjoining rock on the localization of uranium mineralization: 1) rocks unfavorable for uranium mineralization; 2) uranium-loving rocks; 3) main (oreless) fault zones; 4) oreless quartz-carbonate veins; 5) uranium-bearing veins.

because in the distribution of secondary uranium minerals in the oxidation zone it is possible in a number of cases to distinguish a specific secondary zonality, which is different for true uranium and sulfide-uranium deposits.

6. Criteria for prospecting blind ore bodies are still in the early stage of development. In a number of cases, primary dispersion aureoles of metals accompanying uranium mineralization may be a fairly effective criterion. Thus, according to A. D. Kablukov and G. I. Vertepov (1959), in certain deposits where lead and molybdenum are present together with uranium minerals, the former create an aureole in the adjoining rock, extending 100-200 m above the upper end of the blind ore body, whereas the uranium aureole terminates much lower down (Fig. 9). In ore fields with this type of primary aureole, prospecting of blind uranium ore bodies can be carried out by the detection of areas of increased galena concentration found on the surface.

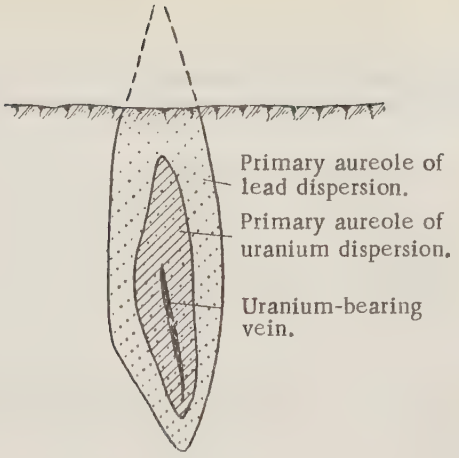


Fig. 9. Location of primary dispersions aureoles around a uranium ore body (cross section) (according to A. D. Kablukov and G. I. Vertepov).

## LITERATURE CITED

1. V. I. Smirnov, Geologic Bases for Prospecting Deposits of Mineral Products [in Russian](Izd. MGU, 1954).
2. F. Ippolito, Documents of the Second International Conference on the Peaceful Uses of Atomic Energy (Geneva, 1958). Selected Reports of Foreign Scientists [Russian translation] (Atomizdat, Moscow, 1959) Vol. 8, p. 298.
3. N. Katayama, Documents of the Second International Conference on the Peaceful Uses of Atomic Energy (Geneva, 1958). Selected Reports of Foreign Scientists [Russian translation] (Atomizdat, Moscow, 1959) Vol. 8, p. 271.
4. Z. A. Nekrasova, Problems of Uranium Geology. Appendix No. 6 to the journal Atomnaya Énergiya [in Russian] (Atomizdat, Moscow, 1957) p. 37.
5. A. P. Vinogradov, Atomnaya Énerg. 4, 5, 409 (1958). (1958).†
6. R. Cannon, L. Stieff, and T. Stern, Documents of the Second International Conference on the Peaceful Uses of Atomic Energy (Geneva, 1958). Selected Reports of Foreign Scientists [Russian translation]. The Geology of Atomic Raw Material (Atomizdat, Moscow, 1959) Vol. 8, p. 31.
7. V. G. Melkov and L. Ch. Pukhal'skii, Prospecting of Uranium Deposits [in Russian] (Gosgeoltekhizdat, Moscow, 1957).
8. A. N. Tokarev and A. V. Shcherbakov, Radiohydrogeology [in Russian] (Gosgeoltekhizdat, Moscow, 1956).
9. W. Gross, Radioactivity as an Ore Indicator. Symp. Geochemical Prospecting Methods [Russian translation] (IL, Moscow, 1954).
10. P. Kerr, Documents of the International Conference on the Peaceful Uses of Atomic Energy (Geneva, 1955) (Gosgeoltekhizdat, Moscow, 1958) Vol. 6, p. 795.
11. H. Cannon and F. Kleinhampl, Documents of the International Conference on the Peaceful Uses of Atomic Energy (Geneva, 1955) (Gosgeoltekhizdat, Moscow, 1958) Vol. 6, p. 937.
12. G. S. Gritsaenko and R. V. Getseva, Documents of the Sceond International Conference on the Peaceful Uses of Atomic Energy (Geneva, 1958). Reports of Foreign Scientists [Russian translation], Nuclear Fuel and Reactor Metals (Atomizdat, Moscow, 1959) Vol. 3, p. 69.

†Original Russian pagination. See C. B. translation.

# DOSIMETRY OF INTERMEDIATE-ENERGY NEUTRONS

A. G. Istomina and I. B. Keirim-Markus

Translated from Atomnaya Énergiya, Vol. 8, No. 3, pp. 239-247,
March, 1960
Original article submitted March 31, 1959

The maximum and average-tissue doses of neutrons absorbed in the human organism is calculated from data in the literature for the energy range from the thermal region to 1 Mev. The results are averaged for a typical spectrum ~1/E and different conditions of irradiation. The maximum permissible flux of intermediate neutrons is equal to 680 neutrons/$cm^2$ sec.

The known methods of recording neutrons are considered from the viewpoint of their applicability to the dosimetry of intermediate neutrons, and it is shown that for this purpose it is convenient, with certain restrictions, to shield the detectors from thermal neutrons.

By intermediate-neutron energies we understand neutron energies in the interval from 0.2-1 ev to 0.5-1 Mev.

From the standpoint of dosimetry, intermediate neutrons have a number of special properties:

1. They constitute an important part of the absorbed dose of neutrons slowed down in the human body. Thus, at a neutron energy of 0.5 Mev, more than 10% of the average-tissue absorbed dose (in rems) is produced by neutrons slowed down to thermal energies [1]. If the same dose is expressed in rads, then the fraction of gamma rays from the capture of slowed-down neutrons comes to more than 50% of the absorbed dose [2]. For neutrons of energy below 0.5 Mev, this contribution in the absorbed dose due to the slowed-down neutrons is still higher.

2. Owing to the important role of the $\gamma$ component, the relative biological effectiveness (RBE) of intermediate neutrons, in contrast to the RBE of faster neutrons, sharply varies over the volume of the body and decreases with depth [3]

3. In the interaction with tissue, the ionization due to recoil nuclei plays a less important role than the ionization due to recoil nuclei from fast neutrons. Thus, for neutrons of energy below 1 Mev, all recoil nuclei, apart from the protons, gradually cease to participate in the ionization of the tissue [4]. Hence, one of the processes of energy transfer to the tissue, the most effective biologically, is eliminated. Below 20 kev, recoil protons, as a result of electron capture, also gradually cease to ionize the medium [4, 5]. The energy of such protons is partially expended in the collisions on the rearrangement of the molecules of the medium – a process whose mechanism, relative contribution, and RBE are not yet known. It may, however, be assumed that the role of this process in the over-all effect of neutrons on the organism is not large, since a neutron of energy below 20 kev spends practically its entire lifetime inside the organism as a thermal neutron, and the energy released upon its capture is, in many cases, several times as great as the kinetic energy of an intermediate neutron.

4. Intermediate neutrons, as a rule, are obtained from the slowing down of fast neutrons, owing to which, in weakly absorbing media, the intermediate neutrons have a characteristic spectra $\varphi(E)dE \sim dE/E$, where $\varphi(E)$ is the neutron flux of energy E.

5. Finally, an important, but not the principal, property of intermediate neutrons is the complexity of their registration. This is one of the reasons why up to the present time intermediate neutrons have not been taken into account in dosimetry practice, despite the fact that they frequently compose an important part of the total neutron flux. Thus, in beams of radiation brought out from the active zone of a thermal nuclear reactor, the intermediate neutron flux is of the same order as the thermal neutron flux [6].

Intermediate neutrons compose about 40% of the total flux in neutron radiators [7]. In nuclear air showers, the intermediate-neutron flux reaching the earth turns out to be an order of magnitude greater than that of fast neutrons, since the fission neutrons are slowed down in the charged layer and in air, while the thermal neutrons are absorbed by the nitrogen of the air [8].

Thus, intermediate neutrons make a greater contribution to the absorbed dose, since the effect of an intermediate-neutron flux on the organism is stronger than an equal flux of thermal neutrons.

In [1-3], the distribution of the absorbed doses of secondary radiation in a flat tissue-equivalent layer 30 cm thick was calculated. These data are shown in recalculated form in Fig. 1. In calculating the absorbed

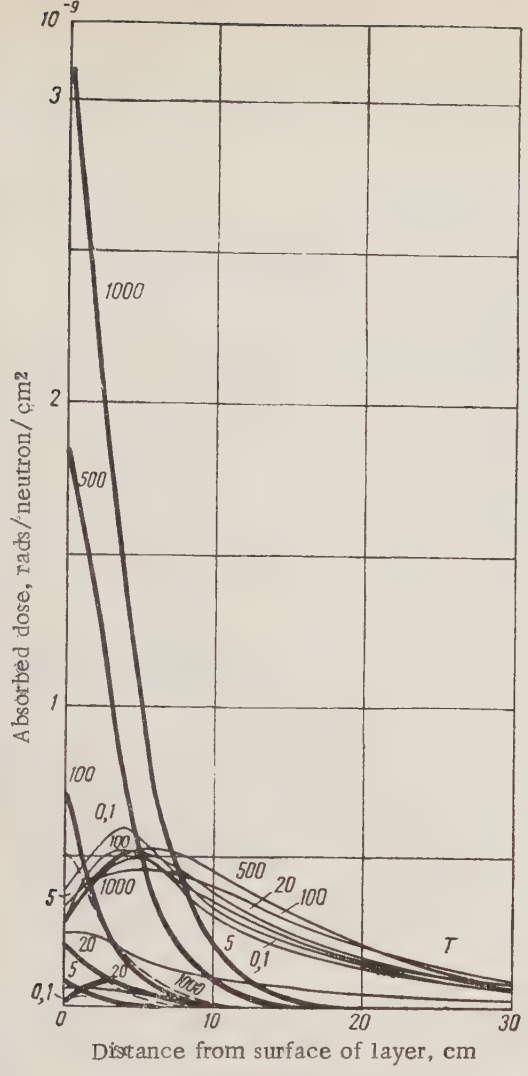


Fig. 1. Absorbed dose of a unit flux of neutrons incident perpendicularly on a tissue layer of thickness 30 cm [2]. The numbers on the curves represent the neutron energy in kiloelectron-volts; ▬▬ recoil protons and protons from the reaction N(n, p); ——— γ rays from the reaction H(n, γ)D; — — — heavy recoil nuclei.

doses in rems, the authors of [1-3] started from the largest values of the RBE: 10 for protons and 20 for heavy recoil nuclei. The latter value is overstated for the considered neutron energy region, but this does not strongly affect the end result.

In 1956, P. A. Yampol'skii, L. A. Chudov, G. G. Petrov, and A. M. Kogan of the Chemical Physics Institute (CPI) of the Academy of Sciences, USSR carried out similar calculations for neutron fluxes incident on a semispace filled with paraffin. The contribution of heavy recoil nuclei to the absorbed dose was not taken into account in this work. The maximum absorbed dose was calculated with proton RBE values of 2, 4.5, and 10. The recalculated results are shown in Fig. 2.

The maximum absorbed dose, however, does not always determine the biological effect of the radiation. The RBE of the radiation is also not the same for different conditions of irradiation, and depends on the reaction of the organism. We shall give a number of examples.

1. For work under conditions of occupational hazard, the total chronic irradiation of the organism by small doses and the after-effects of the irradiation is usually characteristic. In this case, the RBE of protons of mean energy is close to 10 and the biological effect of the radiation is determined by the absorbed dose and the critical organ, or, in a first approximation, by the maximum absorbed dose. This corresponds to curve 10 of Fig. 2, which, of course, should be used for the calculation of the maximum permissible level of the radiation and in dosimetric controls of the working conditions.

2. In the investigation of the depth distribution of the absorbed dose, it is important to know the absorbed dose from the first collision for the real spectra neutrons and secondary γ rays over a given volume element.

3. In experiments devoted to determining the RBE of radiation, it is necessary to know the average tissue (or maximum) absorbed dose expressed in rads (curve 1, Fig. 2).

4. In the use of neutron fluxes for therapy and also in the case of accident and exposure from nuclear weapons, there may occur a short-lasting exposure to large doses. Then the average-tissue absorbed dose is important, the value of the proton RBE for sharp reactions of the organism evidently lying between 2 and 4.5.

We carried out calculations of the average-tissue absorbed dose for a tissue layer of thickness 30 cm based on various values of the proton RBE (the data shown in Fig. 1 [2] was used). The results are given in Table 1 and are shown in Fig. 3.

The shape of the curve of the absorbed dose versus the neutron energy is different for all curves of Figs. 2 and 3. From this it follows, among other things, that the attempts by a number of authors [9, 10] to find the best tissue-equivalent detector for dosimeters are not always warranted.

Using the data of Figs. 2 and 3, we can determine the mean absorbed dose for a unit flux of intermediate neutrons with any energy spectrum:

$$\overline{D} = \frac{\int_{E_1}^{E_2} D(E)\,\varphi(E)\,dE}{\int_{E_1}^{E_2} \varphi(E)\,dE}.$$

Here D(E) is the absorbed dose per unit neutron flux of energy E; $\varphi(E)dE$ is the neutron energy flux between E and E+dE; $E_1$ and $E_2$ are the limits of the intermediate-neutron spectrum.

TABLE 1

Average-Tissue Absorbed Dose (in millimicroreps per 1 neutron/cm$^2$) for a Tissue Layer of Thickness 30 cm [2]

| | RBE | | Neutron energy | | | | | | |
|---|---|---|---|---|---|---|---|---|---|
| | protons $\eta$ | heavy nuclei | thermal | 100 ev | 5 kev | 20 kev | 100 kev | 500 kev | 1 Mev |
| Gamma-ray from capture | — | — | 0,091 | 0,20 | 0,24 | 0,25 | 0,28 | 0,30 | 0,28 |
| Recoil protons | 1 | — | 0,0052 | 0,015 | 0,018 | 0,024 | 0,065 | 0,25 | 0,44 |
| Heavy recoil nuclei | — | 1 | — | — | — | — | — | 0,019 | 0,063 |
| Total dose . . . | 1 | 1 | 0,096 | 0,215 | 0,25 | 0,27 | 0,345 | 0,57 | 0,78 |
| " . . . | 2 | 5 | 0,105 | 0,23 | 0,27 | 0,30 | 0,41 | 0,90 | 1,48 |
| " . . . | 4,5 | 10 | 0,114 | 0,28 | 0,32 | 0,36 | 0,57 | 1,62 | 2,90 |
| " . . . | 10 | 20 | 0,143 | 0,35 | 0,42 | 0,49 | 0,93 | 3,18 | 5,95 |

From this formula, taking $E_1$ = 0.4 ev, $E_2$ = 0.5 Mev, we calculated the mean absorbed dose per unit intermediate-neutron flux with the spectrum ~1/E (Table 2 and Fig. 4). The mean value of the absorbed dose practically does not change if the lower limit of integration is taken within the limits of 0.2-1 ev. There is no strong effect from the deviation of the intermediate-neutron spectrum from the law ~1/E arising at low neutron energies owing to their absorption by atoms of nitrogen or hydrogen in the usual moderating media. Therefore the obtained results can have a rather wide application.

The choice of the upper limit of integration depends on two factors: first, in the energy region above 0.5 Mev the intermediate-neutron spectrum considerably overlaps the spectrum of the primary fission neutrons, and the 1/E law proves to be invalid; second, neutrons of energy above 0.5 Mev can be recorded by fast neutron

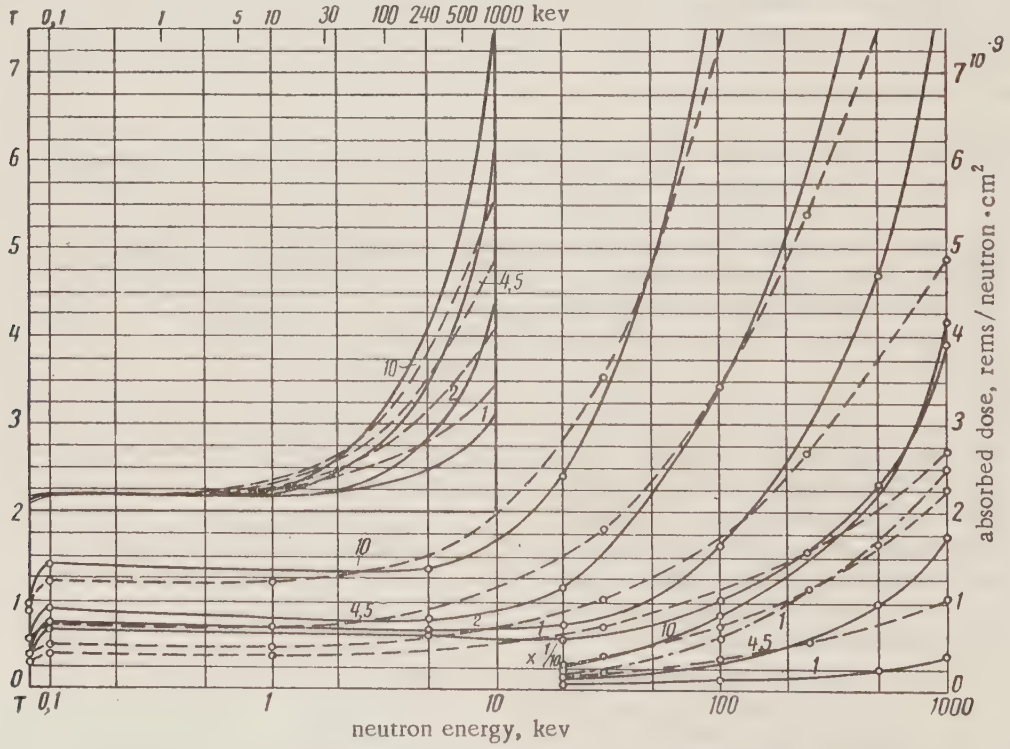


Fig. 2. Maximum absorbed dose for tissue layer irradiated by a unit neutron flux. The numbers on the curves indicate the values taken for the RBE of protons; ▬▬ — data of [2];— – – – data of the CPI, Acad. Sci. USSR. The upper set of curves are normalized to the value of 1 kev.

TABLE 2

Absorbed Dose D(in millimicroreps per 1 neutron/cm$^2$ ) Averaged over the Spectrum ~1/E from 0.4ev to 0.5 Mev (or from 0.4ev to 1 Mev)

| | Proton RBE $\eta$ | | | | | | | | | | | |
|---|---|---|---|---|---|---|---|---|---|---|---|---|
| | $\eta$=1 | | | $\eta$=2 | | | $\eta$=4,5 | | | $\eta$=10 | | |
| | average tissue | maximum | | average tissue | maximum | | average tissue | maximum | | average tissue | maximum | |
| | | data of [2] | CPI data | | data of [2] | CPI data | | data of [2] | CPI data | | data of [2] | CPI data |
| For thermal neutrons | | | | | | | | | | | | |
| dose ($D_T$) | 0,096 | 0,32 | 0,30 | 0,10$_5$ | 0,39 | 0,37 | 0,11$_5$ | 0,54 | 0,55 | 0,14 | 0,90 | 0,94 |
| RBE | 1 | 1 | 1 | 1,1 | 1,2 | 1,2 | 1,2 | 1,7 | 1,8 | 1,5 | 2,8 | 3,1 |
| For intermediate neutrons to 0.5 Mev | | | | | | | | | | | | |
| dose ($D_I$) | 0,23 | 0,70 | 0,57 | 0,26 | 0,97 | 0,87 | 0,34 | 1,6 | 1,5 | 0,48 | 3,4 | 2,9 |
| RBE | 1 | 1 | 1 | 1,1 | 1,4 | 1,5 | 1,5 | 2,3 | 2,6 | 2,1 | 4,7 | 5,0 |
| For intermediate neutrons to 1 Mev | | | | | | | | | | | | |
| dose ($D_I$) | 0,25 | 0,91 | 0,63 | 0,31 | 1,2 | 1,0 | 0,43 | 2,1 | 1,8 | 0,67 | 4,6 | 3,6 |
| RBE | 1 | 1 | 1 | 1,2 | 1,3 | 1,6 | 1,7 | 2,3 | 2,9 | 2,7 | 5,0 | 5,8 |
| For fast neutrons to 1 Mev | | | | | | | | | | | | |
| dose ($D_F$) | 0,78 | 3,6 | 2,7 | 1,5 | 8,4 | 4,9 | 2,9 | 17,0 | 10,3 | 6,0 | 38,0 | 22,0 |
| RBE | 1 | 1 | 1 | 1,9 | 2,3 | 1,9 | 3,7 | 4,7 | 3,8 | 7,6 | 10 | 8,3 |
| $D_I/D_T$ | 2,4 | 2,2 | 1,9 | 2,5 | 2,5 | 2,4 | 3 | 2,9 | 2,7 | 3,4 | 3,7 | 3 |
| $D_F/D_I$ | 3,4 | 5,2 | 4,7 | 5,7 | 8,7 | 5,6 | 8,5 | 11 | 7,6 | 13 | 11,3 | 7,9 |

dosimeters [9]. If we take 1 Mev as the upper energy limit, the change in the value of the mean absorbed dose for intermediate neutrons proves to be sufficiently small for many practical applications.

Table 2 also shows data on the absorbed dose and RBE for thermal neutrons and for 1 Mev neutrons. It is seen that the intermediate neutrons actually have intermediate characteristics. The mean absorbed dose from the intermediate neutrons is two to four times as great as the dose from thermal neutrons. The maximum permissible intermediate-neutron flux during a six-hour working day is 680 neutrons/cm$^2$·sec,* while for thermal neutrons this flux is equal to 2600 neutrons/cm$^2$·sec (according to other data [11], 1650 neutrons/cm$^2$·sec). From this it follows that the control of intermediate-neutron fluxes is of great importance.

The efficiency of the dosimeter in the intermediate-neutron region should correspond to the curves of Figs. 2 or 3, which correspond to the use of the dosimeter (medical, military, for shielding control, etc) and in the fast-neutron region it should correspond to the prolongation of the dose curve or sharply decrease. At the present time there are no such dosimeters. That is why it is sometimes convenient to split up the over-all neutron spectrum into three regions with known energy distributions: thermal – with a Maxwellian distribution; intermediate – with a ~1/E spectrum; fast – with a fission-neutron spectrum. By measuring the absorbed dose from the neutron fluxes corresponding to some part of the spectrum, where these partial spectra are known not to overlap, one can recalculate the obtained values for the total neutron flux in the limits of each of the partial spectra and obtain a quite reliable idea of the absorbed dose from the over-all neutron spectrum.

We shall consider the methods of recording thermal and fast neutrons known at the present time from the standpoint of their suitability in the intermediate-energy region.

The activation method can be used to record both slow and fast neutrons. In the measurement of thermal neutrons the intermediate neutrons are usually separated by the cadmium ratio method. A layer of cadmium 0.5 mm thick absorbs practically all neutrons of energy below 0.4 ev [6].

By determining the cadmium ratio $R_{Cd}$ [6], one can obtain the ratio of intermediate ($\Phi_I$) to thermal ($\Phi_T$) neutrons:

$$\frac{\Phi_I}{\Phi_T} = \frac{13{,}9\sigma_T}{(R_{Cd}-1)\int\limits_{0{,}4}^{5\cdot 10^5}\frac{\sigma\,dE}{E}}. \qquad (2)$$

* The data obtained by the authors for the maximum permissible intermediate-neutron flux has not been officially established by the standards. (Note by editor).

Here $\sigma_T$ is the activation cross section for thermal neutrons; $\int$ is the resonance integral of activation.

As an example we shall consider the case of the chronic effect of small doses of neutrons. Then for the characteristic of the effect one should take the maximum absorbed dose for a proton RBE of 10. The ratio of the absorbed dose of intermediate ($D_I$) to thermal ($D_T$) neutrons in this case has the form (see Table 2)

$$\frac{D_I}{D_T} = \frac{3{,}7\Phi_I}{\Phi_T}.$$

Then

$$\frac{D_I}{D_T} = \frac{51\sigma_T}{(R_{Cd}-1)\int\limits_{0{,}4}^{0{,}5\cdot 10^6}\frac{\sigma\, dE}{E}}. \qquad (3)$$

Equal absorbed doses of intermediate and thermal neutrons produce equal effects ($R_{Cd}$ = 2) in a detector for which the ratio

$$\frac{\int\limits_{0{,}4}^{0{,}5\cdot 10^6}\frac{\sigma dE}{E}}{\sigma_T} \simeq 50. \qquad (4)$$

In this case the induced activity is proportional to the absorbed mixed dose of thermal and intermediate neutrons. The isotope $Sb^{123}$ is such a detector [12]. Unfortunately, $Sb^{123}$ produces some isomers with different half-lives as a result of neutron capture. Moreover, in natural antimony the $Sb^{121}$ isotope is also activated with a cross section ratio of 21.6 [13]. No other isotopes with the ratio (4) close to 50 have been observed.

The activation method gives the value of the absorbed dose averaged over the activation time. For accurate measurements it is necessary that the activation time be one-third to one-fifth of the half-life period of the induced activation. For daily dosimetric control it is convenient to use gold foil ($T_{\frac{1}{2}}$ = 2.7 days, $\sigma_T$ = 98 barns, $\int$ = 1558 barns [13]; here

$$\frac{\Phi_I}{\Phi_T} = \frac{0{,}87}{R_{Cd}-1}; \quad \frac{D_I}{D_T} = \frac{3{,}2}{R_{Cd}-1};$$

$$D = D_T + D_I = D_T\left(1 + \frac{3{,}2}{R_{Cd}-1}\right).$$

Thus, the sensitivity of the gold detector to the intermediate and thermal neutron fluxes is practically the same. The same relation is approximately valid for an indium detector.

One can measure the maximum permissible neutron dose with the aid of gold foils; in 100 mg of gold an activity of about 0.5 μC is induced in 6 hours.

Relations (2) and (3) are also convenient for the measurement of the absorbed dose rate or flux. In the thermal energy region use is made of the exothermal nuclear reactions in $B^{10}$, $Li^6$, and $N^{14}$, whose cross sec-

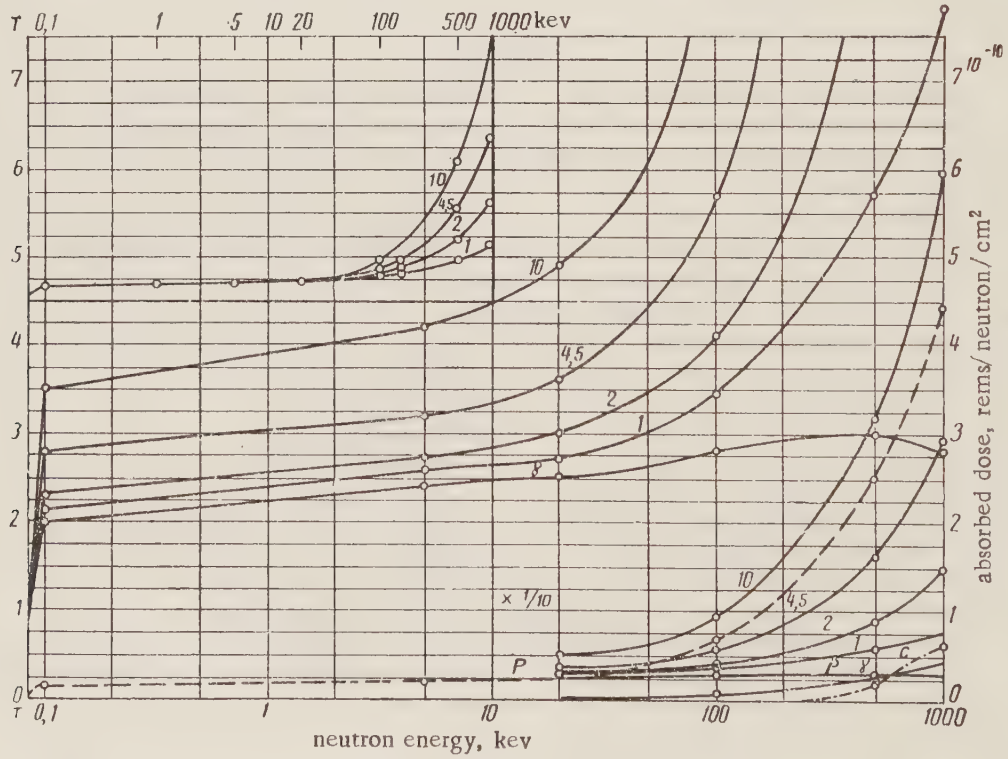


Fig. 3. Average-tissue absorbed dose for tissue layer irradiated by a unit neutron flux. The numbers on the curves represent the RBE values taken for protons. The absorbed dose of the individual components of secondary radiation is expressed in rads; γ – gamma radiation; p – protons; c – heavy recoil nuclei. The upper set of curves is normalized to the value at 1 kev.

tions are inversely proportional to the neutron velocity v.

For detectors of the 1/v type, the ratio (4) is equal to 0.5 [6]; therefore

$$\frac{\Phi_I}{\Phi_T} = \frac{27{,}8}{R_{Cd} - 1}; \quad \frac{D_I}{D_T} = \frac{100}{R_{Cd} - 1}.$$

In other words, the dose sensitivity of detectors with $\sigma \sim 1/v$ for the intermediate neutrons is one-hundredth of that for thermal neutrons.

The efficiency of ionization chambers or of those counters filled with $BF_3$ for thermal neutrons is a few percent [4, 14]. Thus a $BF_3$ counter carefully covered by a cadmium layer 0.5-1 mm thick can be used for the dosimetry of small fluxes of intermediate neutrons. The ordinary $BF_3$ counter records about 200 cpm at the maximum permissible intermediate-neutron flux.

The efficiency of scintillation counters with a ZnS–Ag, B luminescent screen attains several percent for thermal neutrons [15, 16]. A sealed cadmium counter with a screen area of 6 $cm^2$ records about 100 cpm at the maximum permissible intermediate-neutron flux.

The existing methods of personal dosimetric control of thermal neutrons [17-20] cannot be adapted to intermediate-neutron dosimetry.

Fission chambers can also be used for the recording of intermediate neutrons. For example, for $U^{235}$ ($\sigma_T$ = 549 barns, $\int$ = 400 barns [21])

$$\frac{\Phi_I}{\Phi_T} = \frac{18{,}7}{R_{Cd} - 1}; \quad \frac{D_I}{D_T} = \frac{70}{R_{Cd} - 1}.$$

As in the case of $BF_3$ counters, it is advantageous to have two chambers with different amounts of $U^{235}$ for thermal and intermediate neutrons [22].

In the fission chambers a layer of uranium of thickness up to 10 mg/$cm^2$ is used [14, 23]. The maximum permissible intermediate-neutron flux produces up to 20 fissions in 1 min for 1 $cm^2$ of the uranium layer. The fission-chamber sensitivity to fast neutrons is much lower. Chambers with $U^{233}$ or $Pu^{239}$ have similar characteristics.

Detectors with thresholds above 0.5 Mev ($U^{238}$, sulfur, etc. [24]) are, of course, unsuitable for intermediate neutrons.

We shall consider the operation of detectors recording neutrons by means of the recoil protons such as ionization chambers and proportional counters with tissue-equivalent walls and filling mixtures [9]. Let a proportional counter be connected to a discriminator which passes pulses corresponding to an energy greater than B. The ionization current due to the recoil protons [4, 25] is

$$i(E) = n\varphi(E)\sigma(E)(E - B)K(E, B) \simeq E^{1/2}\left(1 - \frac{B}{E}\right)K(E, B), \qquad (5)$$

where E is the neutron energy; n is the number of hydrogen atoms in the counter volume; $\varphi$ is the neutron flux; $\sigma$ is the scattering cross section on protons; K is a coefficient taking into account the sub-threshold ionization loss [26] (K usually has the value 0.7-0.9, which slowly decreases with an increase in E).

With an increase in E the ionization current increases rapidly at first and then somewhat more slowly than $\sqrt{E}$. The counter is not sensitive to neutrons of energy lower than B, since its average efficiency for intermediate neutrons is much lower than for fast neutrons. The measurement of intermediate neutrons in the presence of fast neutrons proves to be difficult.

The ionization chamber is similar to a proportional counter with a low threshold of discrimination (B ~20 kev). With a decrease of this threshold the efficiency for intermediate neutrons increases in comparison with the efficiency for fast neutrons. But since the threshold for $\gamma$ rays is practically zero, the ionization chamber simultaneously measures the accompanying $\gamma$ rays, i.e., it has poorer selectivity, which makes the ionization chamber unsuitable for practical use.

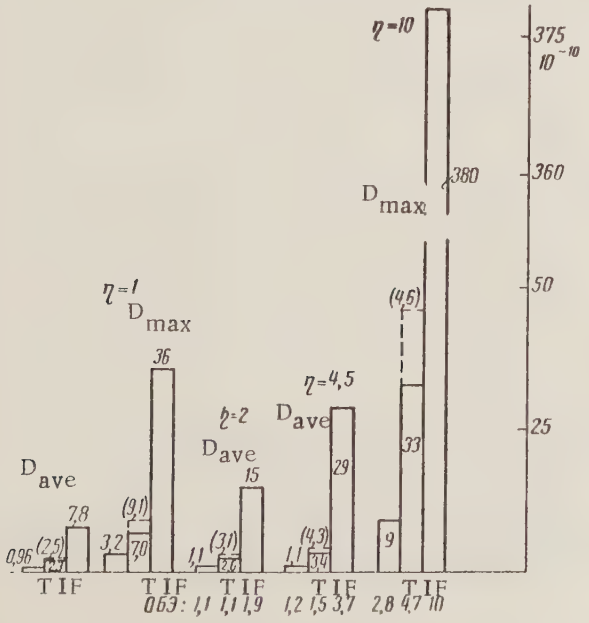


Fig. 4. Absorbed dose per unit neutron flux for different values of the proton RBE $\eta$ [2]. $D_{ave}$ is the average-tissue and $D_{max}$ is maximum absorbed dose for thermal neutrons (T); for the intermediate-neutron spectrum ~1/E (I) and for fast neutrons (F) of energy 1 Mev. The value of the RBE for neutrons is shown below. The dotted lines give the intermediate-neutron spectrum to 1 Mev.

A higher selectivity with respect to fast neutrons can be achieved if they are counted by means of a proportional counter. The efficiency of the counter [25]

$$\varepsilon(E) \sim E^{-1/2}\left(1 - \frac{B}{E}\right) K(E, B)$$

increases sharply from the threshold, attains a maximum at E ≃ 3B, then smoothly decreases with an increase in E. The average efficiency for an intermediate-neutron flux with a spectrum of the ~1/E type is, however, a bare fraction of the efficiency for fast neutrons of energy 1-2 Mev (at B ~ 0.1 Mev).

The characteristics of counters with solid-state radiation are even less favorable for the measurement of intermediate neutrons; they tend to act differently, which is frequently inconvenient.

Thus, of all the types of detectors considered for the recording of intermediate neutrons the acceptable detectors are those of the thermal-neutron type which use gold, $B^{10}$, or $U^{235}$ shielded by a layer of cadmium (or borium).

No acceptable true neutron dosimeter applicable over the entire spectral region of practical importance has been produced as yet. An exception, perhaps, is the use of devices similar to the long counter [4, 22, 25, 27]. It might be possible to obtain the variation of the efficiency with energy shown in Figs. 2 and 3 by some choice of the configuration of the moderator and absorbers.

## LITERATURE CITED


1. W. Snyder and J. Neufeld, Brit. J. Radiology 28, 330, 342 (1955).
2. W. Snyder and J. Neufeld, ORNL-LR-DW 11192-11205.
3. W. Snyder and J. Neufeld, ORNL-LR-DW 11546; 19164.
4. H. Rossi, Radiation Dosimetry, edited by G. Hine, and G. Browell [Russian translation], (IL, Moscow, 1958) p. 549.
5. H. Bethe and J. Ashkin, Experimental Nuclear Physics, edited by E. Segre [Russian translation] (IL, Moscow, 1955), Vol. 1, p. 143.
6. D. Hughes, Neutron Pile Research [Russian translation] (IL, Moscow, 1954).
7. A. G. Istomina and I. B. Keirim-Markus, Meditsinskaya Radiologiya, 4, 69 (1958).
8. Collection: Effect of Atomic Weapons [Russian translation] (Moscow, IL, 1954).
9. G. S. Hurst, R. H. Ritchie, and W. A. Mills, Proceedings of the International Conference on the Peaceful Uses of Atomic Energy [Russian translation] (Fizmatgiz, Moscow, 1958), Vol. 14, p. 265.
10. B. Brown, and E. Hopper, Nucleonics 16, No. 4, 96 (1958); H. Rossi and G. Failla, Nucleonics 14, No. 2, 32 (1956).
11. A. G. Istomina and I. B. Keirim-Markus, Proceedings of the Second International Conference on the Peaceful Uses of Atomic Energy, Geneva, 1958, Report by Soviet Scientists, Radiobiology and Radiation Medicine [in Russian], (Atomizdat, Moscow, 1959) Vol. 5, p. 196.
12. S. Harris, C. Muehlhause, and G. Thomas, Phys. Rev. 79, 1, 11 (1950).
13. M. Davis, and D. Hauser, Nucleonics 16, 3, 87
14. (1958).
14. B. Rossi and H. Staub, Ionization Chambers and Counters [Russian translation] (IL, Moscow, 1951).
15. T. V. Timofeeva, Atomanya Énerg. 3, 8, 156 (1957).†
16. Jan Urbanec, Proceedings of the International Conference on the Peaceful Uses of Atomic Energy (Geneva, 1955) [Russian translation] (Fizmatgiz, Mosc Moscow, 1958) Vol. 14, p. 283.
17. V. V. Antonov-Romanovskii, I. B. Keirim-Markus, M. S. Poroshina, Z. A. Trapeznikova, Meeting of the Acad. Sci. USSR on the Peaceful Uses of Atomic Energy (Session of the Section of Physical and Mathematical Sciences) [in Russian] (Izd. AN SSSR, Moscow, 1955) p. 342.
18. I. P. Belov, K. S. Kalugin, I. B. Keirim-Markus, V. I. Nikiforov, and M. S. Proshin, Pribor. i Tekh. Éksp.,4, 74 (1959).
19. F. Kalil, Nucleonics 13, 11, 91 (1955).
20. I. B. Keirim-Markus and A. P. Pesotskaya, Collection on Dosimetric and Radiometric Methods [in Russian] (Medgiz, Moscow, 1959).
21. S. Ya. Nikitin, S. I. Sukhoruchkin, K. G. Ignat'ev, and N. D. Galanina, Meeting of the Acad. Sci. USSR on the Peaceful Uses of Atomic Energy (Session of the Section of Physical and Mathematical Sciences) [in Russian] (Izd. AN SSSR, Moscow, 1955) p. 87.
22. R. Nobles and A. Smith, Nucleonics 14, 1, 60 (1956).
23. B. Diven, Proceedings the International Conference on the Peaceful Uses of Atomic Energy (Geneva, 1955), [Russian translation] (Izd. AN SSSR, Moscow, 1958) Vol. 4, p. 296.
24. F. Cowan and J. O'brien, Proceedings of the International Conference on the Peaceful Uses of Atomic Energy (Geneva, 1955) [Russian translation] (Izd. AN SSSR, Moscow, 1958) Vol. 4, p. 231.
25. B. Feld, Experimental Nuclear Physics, edited by E. Segre [Russian translation] (IL, Moscow, 1955) Vol. 2, p. 181.
26. Yu. I. Petrov, Atomnaya Énerg. 3, 10, 326 (1957).†
27. I. B. Keirim-Markus, A. M. Lushchikhin, V. V. Markelov, and L. N. Uspenskii, Pribor. i Tekh. Éksp., No. 4 (1960) (in press).


†Original Russian pagination. See C. B. translation.

# THE NEUTRON- DEFICIENT ISOTOPE $Ho^{155}$

B. Dalkhsuren, I. Yu. Levenberg, Yu. V. Norseev,
V. N. Pokrovskii and S. S. Khainatskii

Translated from Atomnaya Énergiya, Vol. 8, No. 3, p. 248
March, 1960
Original article submitted July 14, 1959

The existence of a short-lived isotope $Ho^{155}$ as a parent nucleus was suggested to account for the production of the isotopes $Dy^{155}$ and $Tb^{155}$ observed in a number of cases [1, 2]. Moreover, a holmium isotope (emitting a 2.1 Mev positron) with a half-life period of ~50 min, which, according to Levy's scheme [4], can have a mass number of 155 or 158 was observed in [3].

We studied on a scintillation $\gamma$ spectrometer the $\gamma$ spectrum of fractions of holmium obtained as a result of a deep-spitting reaction under the bombardment of tantalum by 660 Mev protons from the synchrocyclotron of the Joint Institute of Nuclear Studies and we also carried out multiple chromatographic separation of the daughter element (dysprosium). The gamma spectrum of holmium turned out to be quite complex; the 140 kev $\gamma$ ray, whose intensity decayed with a half-life of ~45-50 min, was the most intense.

Triple separation of the daughter element (dysprosium) with intervals of ~1 hour indicated that only the isotope $Dy^{155}$, identified by the $\gamma$ spectrum and half-life period, was present in all three fractions. The mass number of $Dy^{155}$ was unequivocally established earlier [5] by means of a mass spectrometer. The amount of $Dy^{155}$ in the subsequent fractions, proportional to the activity of the parent substance $Ho^{155}$ varied in accordance with the half-life period of ~46 min.

Thus, we finally established the existence of the holmium isotope with a mass number 155 and half-life period of 46 ± 3 min. The gamma spectrum of this isotope probably contains the line ~140 kev. We note that the 138 kev $\gamma$ line observed in [1] with a half-life of ~1 hour was attributed to $Ho^{156}$. The authors themselves note, however, that the determination of the mass number was not sufficiently substantiated.

LITERATURE CITED

1. J. Mihelich, B. Harmatz, and T. Handley, Phys. Rev. 108, 989 (1957).
2. T. Ward, K. Jacob, J. Mihelich, B. Harmatz, and T. Handley, Bull. Amer. Phys. Soc., Ser. II 2, 259 (1957).
3. A. V. Kalyamin, I. Yu. Levenberg, and V. A. Yakovlev, Atomnaya Énerg. 6, 5, 582 (1959).*
4. Y. Riddel, A Table of Levy's Empirical Atomic Masses (Chalk River, Ontario, 1956).
5. A. N. Dobronravova, L. M. Krizhanskii, A. N. Murin, and V. N. Pokrovskii, Izvest. Acad. Nauk SSSR, Ser. Fiz. 22, 815 (1958).

*Original Russian pagination. See C. B. translation.

* * *

# DETERMINATION OF THE DAMPNESS OF DRY GRANULAR SUBSTANCES, BY MEANS OF NEUTRON MODERATION

A. K. Val'ter and M. L. Gol'bin

Translated from Atomnaya Énergiya, Vol. 8, No. 3, pp. 248-250, March, 1960
Original article submitted May 25, 1959

Among the known methods of measuring the dampness of dry granular substances, are those based upon weight, chemical, and electrical properties. However, each of these has certain disadvantages and therefore, industry does not, up to the present time, have a rapid and successful method of measuring the dampness of dry granular substances.

The use of nuclear radiation, and, in particular, of neutrons, provides us with a more effective means of reaching this goal. However, it should be noted that the use of low-energy $\gamma$ rays is difficult, especially in the measurement of the dampness of granular dry substances, i.e., concentrates or charges, or mineralogical compounds of varying chemical composition.

We used plastic soil as our test material. We also made use of the conclusions reached in [1], where it was noted that the results of the measurements were independent of the presence of other elements with a $Z > 5$ (except for strong neutron absorbers), and also of the density of mass of the absorber. In connection with this, the results of the investigation obtained for plastic soil are entirely applicable to other granular dry substances provided a correction is made for the hydrogen content.

The method used in measuring dampness consisted in measuring the slow neutron flux, which is a function of the dampness of the material that is being investigated, and registering the measurment by means of a scintillation detector. The fast neutron source Po–Be contained 1 C of $Po^{210}$ ($2.5 \cdot 10^6$ neutrons/sec).

We determined experimentally* that for the same degree of dampness it was more profitable to completely surround the source and the detector with the material being investigated than to merely place the plastic soil between the source and the detector.

The diagram shows the experimental set-up. The current from the photoelectronic multiplier (FÉU-19) 1 is fed to the amplifier 3, amplitude discriminator 5 and counter 6. The source Po–Be 8 is attached to the body of the slow neutron detector 9 of cylindrical form [2]. The FÉU-19 and the amplifier are fed from 2 and 4, respectively. The plastic soil 7 is placed between the surface of two steel cylinders. Investigations have shown that for a constant degree of dampness, the counting speed increases as the thickness of the plastic soil layer increases up to 10 cm, where it then remains constant. This completely confirms the conclusions reached in [1].

Plastic soil, dried in a drying closet at a temperature not above 125°C and weighing 16 kg, was placed in the space between the two cylinders. The counting speed with soil of 0% dampness did not differ from the speed for the case where an empty measuring volume was used, i.e., it was equal to the background value. Then water was added, the amount of water used corresponding to a dampness W = 3% by weight and was determined by not less than 3 indications of the counting speed. Analogous experiments were carried out for dampness of 6, 9, and 12% by weight. At the conclusion of the measurements, a control measurement of the dampness was made by choosing from various parts of the measuring volume not less than 3 to 5 samples (by weight). The error in the dampness measurement did not, as a rule, exceed 0.5% in weight. Special attention was paid, during the addition of water to the plastic soil, to the uniformity of its distribution, and this was obtained through practice, by careful mixing.

The table presents the results of three series of experiments.

Analysis of the results obtained shows the great sensitivity of this method. For example, for a change in dampness of 1%, the counting speed for the range W = 3 to 6% in weight was 63 impulses/min, in the range W = 6-9% in weight, 94 impulses/min, and finally in the range W = 9-12% in weight, 220 impulses/min. The high sensitivity in the latter case has great significance since in industry dampness is measured within the limits of 8-12% of the weight.

Application of the interpolation formula [3] to the data permits us to determine the empirical dependence of the counting speed upon the dampness:

$$I = 1225 + 4W + 1219W^2 - 1.53W^3 + .01\ W^4.$$

This paper has confirmed the possibility of measuring the dampness of granular dry substances by means of

* The experiments were carried out by A. P. Krivchikov and N. V. Pavlenko.

Dependence of the Counting Speed I upon the Dampness W

| W, weight % | 0 | 3 | 6 | 9 | 12 |
|---|---|---|---|---|---|
| $I_1$, imp/min | 1211±10 | 1316±6 | 1468±27 | 1821±33 | 2445±100 |
| $I_2$, imp/min | 1232±12 | 1312±9 | 1529±27 | 1751±20 | 2425±70 |
| $I_3$, imp/min | 1223±10 | 1307±7 | 1457±36 | 1784±34 | 2487±119 |

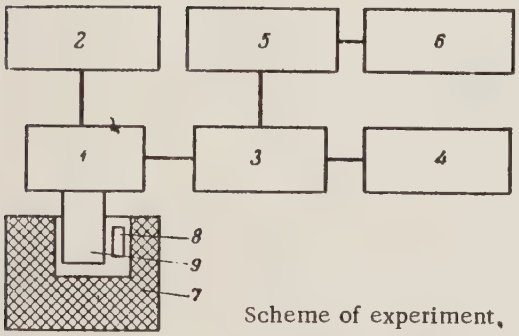


Scheme of experiment.

neutron irradiation provided that both the source and the detector are completely surrounded by the material under test. This will permit us in the near future to design a set-up of such high sensitivity that it may be used in industry.

In conclusion, the authors wish to take this opportunity of expressing their gratitude to Candidate of Tech. Sciences, T. V. Timofeeva, for her valuable advice as to the methods to be used in carrying out the experiments.

LITERATURE CITED

1. Putman, Materials of the International Conference on the Peaceful Uses of Atomic Energy (Geneva, 1955) [in Russian] (Mashgiz, Moscow, 1957) Vol. 15, p. 151.
2. T. V. Timofeeva, Atomnaya Énergiya 3, 8, 156 (1957).†
3. K P. Yakovlev, Mathematical Processing of Experimental Results, [in Russian] (Gostekhizdat, Moscow, 1953).

† Original Russian pagination. See C. B. translation.

* * *

# LOCAL AND MEAN HEAT-TRANSFER FOR A TURBULENT FLOW OF NONBOILING WATER IN A TUBE WITH HIGH HEAT LOADS

V. V. Yakovlev

Translated from Atomnaya Énergiya, Vol. 8, No. 3, pp. 250-252, March, 1960
Original article submitted December 2, 1959

The experimental method used in the work, and some preliminary results have already been published in [1].

The results given below were obtained after a change in the lead carrying the heating current to the input end of the operating tube. This change consisted of decreasing the thickness of the bus bar carrying the current to 3 mm.

The operating part of the apparatus was made of copper tubing ($d \simeq 6.7$ mm, $l \simeq 540$ mm), which was heated by an alternating current. The wall temperature of this tube was measured by 15 copper-constantan thermocouples which were tin-soldered to the internal surface of the tube.

Examples of wall temperature measurements are given in Fig. 1. The preheating of the water in the

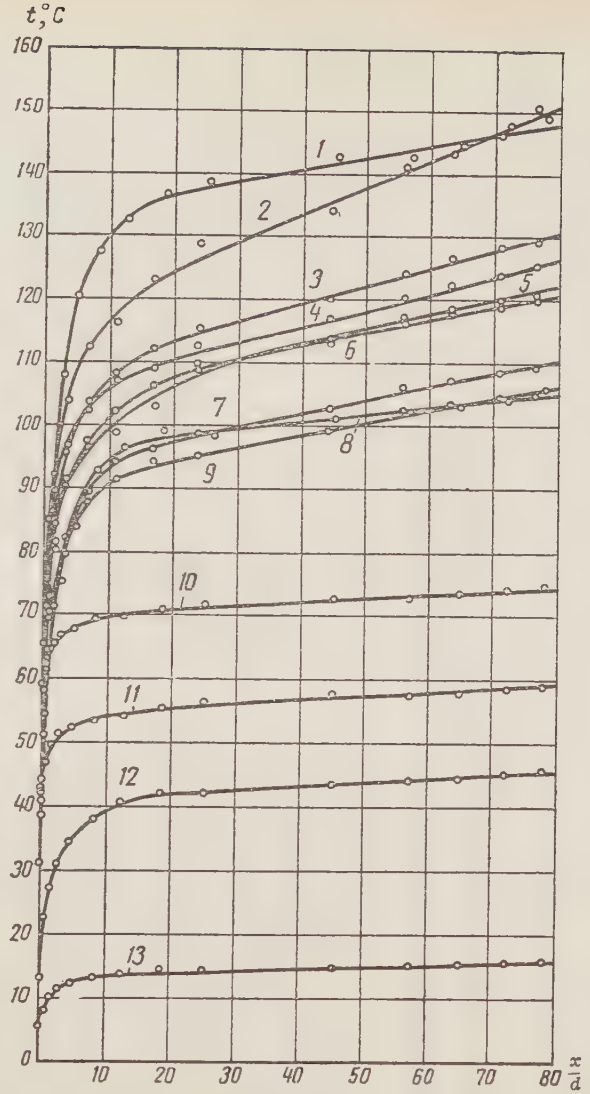


Fig. 1. Distribution of wall temperature in the tube (q in kcal/m² · hr):

1—$q=3{,}3\cdot10^6$, $Re=60\,200$; 2—$q=2{,}29\cdot10^6$, $Re=55\,600$;
3—$q=2{,}3\cdot10^6$, $Re=61\,000$; 4—$q=1{,}883\cdot10^6$, $Re=99\,600$;
5—$q=2{,}355\cdot10^6$, $Re=66\,100$; 6—$q=2{,}327\cdot10^6$, $Re=65\,940$;
7—$q=1{,}907\cdot10^6$, $Re=59\,600$; 8—$q=1{,}764\cdot10^6$, $Re=39\,800$;
9—$q=1{,}92\cdot10^6$, $Re=61\,900$; 10—$q=4{,}58\cdot10^5$, $Re=89\,800$;
11—$q=4{,}66\cdot10^5$, $Re=66\,700$; 12—$q=5{,}05\cdot10^5$, $Re=22\,900$;
13—$q=1{,}42\cdot10^5$, $Re=39\,800$.

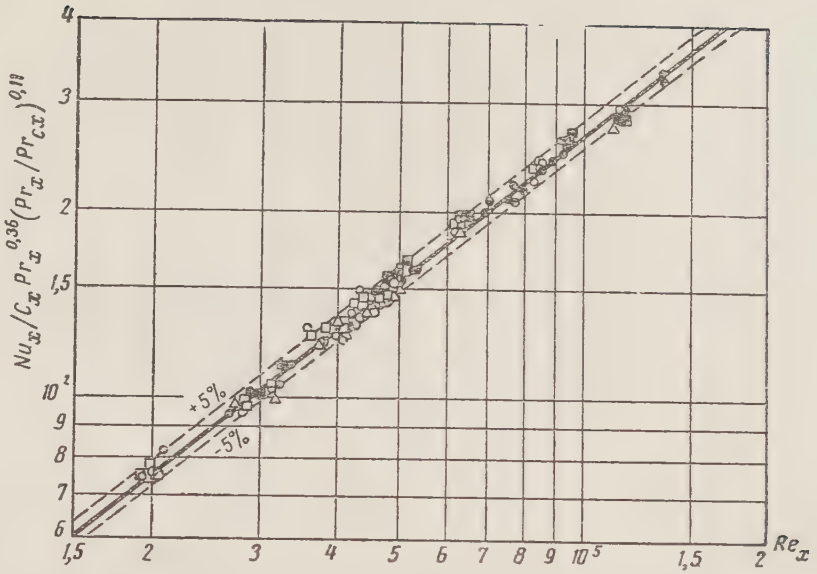


Fig. 2. Generalized dependence of the values of the local heat-transfer coefficient in $Re_x$. The experimental points are characterized by the following values of the ratio x/d: ○) 0.45; □) 1.0; △) 2.25; ◑) 3.75; ■ 7.5; ●) 15-80.

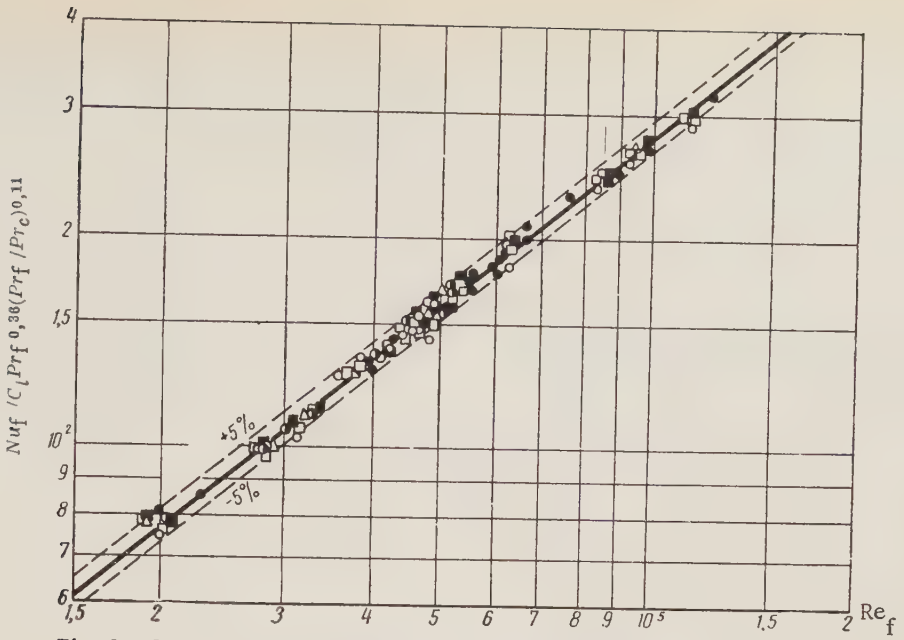


Fig. 3. Generalized dependence of the mean values of the heat-transfer coefficient on $Re_f$. The experimental points are characterized by the following values of the ratio $l/d$: ○) 1.5; □) 3.0; △) 7.5; ◑) 15; ■) 22.5; ●) 80.

tube was determined by using a differential thermocouple.

The values of the local heat-transfer coefficient $\alpha_x$ and the mean heat-transfer coefficient along the length of the tube $\alpha_l$ were obtained from the formulas

$$\alpha_x = \frac{q_x}{t_{cx} - t_x} \text{ and } \bar{\alpha}_l = \frac{q_l}{t_c - t_f}, \qquad (1)$$

where $q_x$, $t_{cx}$ and $t_x$ are, respectively, the local density of heat flow, the temperature of the internal surface of the tube, and the temperature of the liquid at the section of the tube at a distance $x$ from the input, while $q_l$, $t_c$, and $t_f$ are, respectively, the density of heat flow, the mean-integral value of the temperature of the internal surface of the tube, and the mean temperature of the fluid along the length $l$ of the tube.

Figure 2 shows the results of measurement of the local heat-transfer coefficient in the tube with coordinates $Nu_x/C_x Pr_x^{0.36} \times (Pr_x/Pr_{cx})^{0.11}$ and $Re_x$. It is evident from the diagram that the experimental results are described by the equation

$$Nu_x = 0{,}0274 C_x Re_x^{0,8} Pr_x^{0,36} \left(\frac{Pr_x}{Pr_{cx}}\right)^{0,11}. \qquad (2)$$

with an error of less than ±5%. Here

$$C_x = 1 + (2{,}76 - 0{,}44 \lg Re_x)\left[\left(\frac{d}{x}\right)^{0,6} - \left(\frac{1}{15}\right)^{0,6}\right]$$

with

$$0{,}45 \leqslant \frac{x}{d} \leqslant 15,$$

$$Re_x = \frac{Gd}{F\mu_x g\, 3600}.$$

Equation (2) was obtained for the calculation of the local coefficient of heat-transfer in heating a turbulent current of nonboiling water in the following range of variation of the parameters:

$$2 \cdot 10^4 \leqslant Re_x \leqslant 1{,}3 \cdot 10^5;\ 2 \leqslant Pr_x \leqslant 12;\ 1 \leqslant \frac{Pr_x}{Pr_{cx}} \leqslant 6{,}5;$$

$$0{,}45 \leqslant \frac{x}{d} \leqslant 80 \text{ and } q_x \leqslant 3{,}3 \cdot 10^6 \text{ kcal/m}^2 \cdot \text{hr}.$$

The coordinates (Fig. 3)

$$Nu_f/C_l Pr_f^{0,36}\left(\frac{Pr_f}{Pr_c}\right)^{0,11} \text{ and } Re_f$$

are used to show the results of measuring the mean (along the length of the tube) of the heat-transfer coefficient. It can be seen from the diagram that the experimental results can be expressed with an error of not more than 5% by the equation

$$Nu_f = 0{,}0277 C_l Re_f^{0,8} Pr_f^{0,36}\left(\frac{Pr_f}{Pr_c}\right)^{0,11}. \qquad (3)$$

Here

$$C_l = 1 + (3{,}62 - 0{,}54 \lg Re_f)\left[\left(\frac{d}{l}\right)^{0,65} - \left(\frac{1}{50}\right)^{0,65}\right]$$

for $1{,}5 \leqslant \frac{l}{d} \leqslant 50$,

$$Re_f = \frac{Gd}{F\mu_f g 3600}.$$

Equation (3) was obtained for the calculation of the mean (along the tube) of the heat-transfer coefficient,

in the heating of a turbulent current of nonboiling water in the following range of variation of the parameters:

$$2\cdot10^4 \leqslant Re_f \leqslant 1{,}3\cdot10^5; \quad 2 \leqslant Pr_f \leqslant 12;$$

$$1 \leqslant \frac{Pr_f}{Pr_c} \leqslant 6;$$

$$1{,}5 \leqslant \frac{l}{d} \leqslant 80 \text{ and } q_l \leqslant 3{,}3\cdot10^6 \text{ kcal/m}^2\cdot\text{hr}.$$

It should be noted in conclusion that the possibility of applying formulas (2) and (3) for the calculation of heat-transfer requires special verification for liquids with values of Pr lying outside the range we have permitted. The equation given previously by M. A. Mikheev in [2], obtained for $q \leq 0.5 \cdot 10^6$ kcal/m$^2$ · hr, is therefore still of value as a general formula, applicable for a wide range of variation of Pr and Re.

LITERATURE CITED


1. V. V. Yakovlev, Atomnaya Énerg. 11, No. 2 (1957).*
2. M. A. Mikheev, Izvest. Akad. Nauk SSSR, Otd. Tekh. Nauk, 10, 1448 (1952).


*Original Russian pagination. See C. B. translation.

* * *

# ON THE QUESTION OF THE CHOICE OF HEAT CARRIERS FOR NUCLEAR REACTORS


E. I. Siborov



Translated from Atomnaya Énergiya, Vol. 8, No. 3, pp. 252-253, March, 1960
Original article submitted December 18, 1958


The diversity of heat carriers used in nuclear reactors is associated with the search for the most effective heat carrier. An analysis of the various heat carriers from the point of view of the coefficient of heat transfer and energy usage during the passage of the heat carrier. The influence of these factors is seen in the magnitudes of the usual (customary) economic coefficients of heat transfer.

The dimensionless economic coefficient of heat transfer represents the ratio of conductable thermal energy received by a heat carrier to the mechanical energy required for the passage of the heat carrier through the pipes. The available data with regard to the problem [1] is approximate, more accurate and voluminous data and data which takes account of the results of new investigations [2, 3] are required.

Heat carriers can be divided into two classes according to their thermophysical properties: 1) liquids and gases characterized by the value of the dimensionless Prandtl number Pr $\simeq$ 1 or >1; 2) liquid metal (Pr = $= 10^{-2}$-$10^{-4}$).

For substances belonging to the first class the coefficient of heat transfer during the stabilized turbulent flow of these substances is characterized by a dependence of the form [4]

$$\alpha = 0{,}023C\lambda Pr^{0,4}\nu^{-0,8}, \qquad (1)$$

where the factor $C = \nu^{0.8}d^{-0.2}$ is determined by the construction of the heat exchange mechanism and the speed of passage of the heat carriers (d is the inner diameter of the pipe along which the heat carriers move, v is the mean velocity of motion of the heat carrier); $\lambda$ and $\nu$ are the coefficients of thermal conductivity and kinetic viscosity of the heat carriers, respectively.

When thermal carriers of the second class are used the heat exchange is given by the formula [2]

$$\alpha = 4{,}5\frac{\lambda}{d} + 0{,}014C\lambda Pr^{0,8}\nu^{-0,8}. \qquad (2)$$

In our analysis, formula (2) is mostly used in practice in the region of the Peclet number: Pe = (vd/$\nu$)Pr = $= 10^3$–$10^4$ and it is more convenient to use the approximate formula

$$\alpha = 0{,}025C\lambda Pr^{0,8}\nu^{-0,8}. \qquad (3)$$

The average error resulting from the use of such an approximation in the indicated range of Pe numbers is about 20% and lies within the limits of accuracy of the thermophysical properties of a series of liquid metals.

The use of formulas (1) and (3) permits us to omit the examination of the value of C, characterizing the heat-exchange of the set-up and the circulating speed of the heat carriers, and to express in "pure form" the influence of the physical properties of the various heat carriers.

In Table 1 we present the results of the calculations giving the changes in the relative coefficient of heat

TABLE 1

Coefficients of Heat Transmission for Various Heat Carriers

| Heat carrier | Coefficients of heat transmission (based upon 2.8 kcal · $sec^{0.8}$/ / $m^{2.6}$ hr · degree as the unit point) | | | | |
|---|---|---|---|---|---|
| | 100 | 200 | 300 | 400 | 500 |
| Air (p = 1 atm) | 1,0 | 0,9 | 0,8 | 0,7 | 0,7 |
| Carbonic acid (p = 1 atm) | 1,2 | 1,1 | 1,1 | 1,0 | 1,0 |
| Steam (at the saturation point) | 1,0 | 10 | 70 | — | — |
| Water (at the saturation point) | $1,0 \cdot 10^3$ | $1,2 \cdot 10^3$ | $1,2 \cdot 10^3$ | — | — |
| Dowtherm (liquid diphenol mixture) | — | $1,6 \cdot 10^2$ | $2,2 \cdot 10^2$ | $2,5 \cdot 10^2$ | $2,6 \cdot 10^2$ |
| Nitrate mixture (melted salts) | — | $2,3 \cdot 10^2$ | $3,0 \cdot 10^2$ | $3,3 \cdot 10^2$ | $3,2 \cdot 10^2$ |
| Mercury | $1,2 \cdot 10^3$ | $1,3 \cdot 10^3$ | $1,3 \cdot 10^3$ | — | — |
| Alloy (25% Na + 75% K) | $8,9 \cdot 10^2$ | $8,2 \cdot 10^2$ | $7,9 \cdot 10^2$ | $7,3 \cdot 10^2$ | $7,0 \cdot 10^2$ |
| Sodium | — | $1,3 \cdot 10^3$ | $1,2 \cdot 10^3$ | $1,2 \cdot 10^3$ | $1,1 \cdot 10^3$ |
| Alloy (56.5% Bi + 43.5% Pb) | — | $1,1 \cdot 10^3$ | $1,1 \cdot 10^3$ | $1,0 \cdot 10^3$ | $1,1 \cdot 10^3$ |
| Lithium | — | $1,8 \cdot 10^3$ | $1,8 \cdot 10^3$ | $1,8 \cdot 10^3$ | $1,8 \cdot 10^3$ |
| Tin | — | — | $1,6 \cdot 10^3$ | $1,5 \cdot 10^3$ | $1,5 \cdot 10^3$ |
| Bismuth | — | — | $1,1 \cdot 10^3$ | $1,1 \cdot 10^3$ | $1,2 \cdot 10^3$ |

TABLE 2

Economic Coefficients of Heat Transmission for Various Heat Carriers

| Heat carrier | Economic coefficients of heat transmission (based upon 43 kcal · $sec^{1.05}$ kg/ $m^{0.1}$ hr · degree as the unit point) | | | | |
|---|---|---|---|---|---|
| | 100 | 200 | 300 | 400 | 500 |
| Air (p = 1 atm) | 1,0 | 1,0 | 1,0 | 1,0 | 1,0 |
| Carbonic acid (p = 1 atm) | 0,9 | 0,9 | 1,0 | 1,1 | 1,1 |
| Steam (at the saturation point) | 1,7 | 2,3 | 3,8 | — | — |
| Water (at the saturation point) | 2,9 | 4,6 | 5,8 | — | — |
| Dowtherm (liquid diphenol mixture) | — | 0,18 | 0,28 | 0,35 | 0,37 |
| Nitrate mixture (melted salts) | — | 0,17 | 0,30 | 0,37 | 0,41 |
| Mercury | 0,34 | 0,37 | 0,39 | — | — |
| Alloy (25% Na + 75% K) | 2,5 | 2,6 | 2,6 | 2,6 | 2,7 |
| Sodium | — | 0,37 | 0,37 | 0,39 | 0,39 |
| Alloy (56.5% Bi + 43.5% Pb) | — | 0,31 | 0,33 | 0,31 | 0,37 |
| Lithium | — | 7,2 | 7,7 | 8,0 | 8,2 |
| Tin | — | — | 0,66 | 0,68 | 0,70 |
| Bismuth | — | — | 0,36 | 0,39 | 0,41 |

transfer as a function of the choice of heat carriers and the temperature. We will take as unity the coefficient of heat transfer of air at 100°C equal to 2.8 C (in kcal × × $sec^{0.8}/m^{2.6}$hr × degrees).

The computed data regarding the thermophysical properties of carbonic acid, Dowtherm and the nitrate mixture are taken from the questionnaire [2], and the data regarding the thermophysical properties of the remaining substances are taken from [3].

The energy carried away by the heat carriers during the time while passing through a pipe of length L for a temperature drop $\Delta t$, is given by

$$W = A\alpha\pi\, dL\, \Delta t\tau, \tag{4}$$

where A is the mechanical equivalent of heat. At the same time the mechanical energy expended in driving the heat carrier through the pipe is given by

$$P = \frac{G\Delta p\tau}{\varrho\eta}, \tag{5}$$

where $G = \rho v \frac{\pi d^2}{4}$ is the weight expenditure of the heat carrier, $\Delta p$ is the pressure drop, $\rho$ is the weight density of the heat carrier, and $\eta$ is the pump efficiency. The drop in pressure may be expressed in the form

$$\Delta p = \xi \frac{L}{d} \frac{\varrho v^2}{2g}, \tag{6}$$

where $\xi$ is the coefficient of hydraulic resistance and g is the acceleration due to gravity.

We find, using formulas (4)-( 6), the following expression for the economic coefficient of heat transfer

$$\beta = \frac{W}{P} = \frac{8Ag\eta}{v^3} \frac{\alpha}{\varrho\xi}. \tag{7}$$

The changes in the coefficient of hydraulic resistance

are independent of whether the heat carriers are gases, the usual liquids or molten metals and are well described by Blasius' formula

$$\xi = 0{,}316\,(vd)^{-1/4}\nu^{1/4}. \qquad (7)$$

Substituting this value in (7) we get

$$\beta = D\frac{\alpha}{\varrho\nu^{1/4}}, \qquad (9)$$

where $D = \frac{25.3\ Ag\eta}{v^{2.75}d^{0.25}}$ is a coefficient which depends upon the particular constructional details of the reactor.

In Table 2 we give the results of the calculation of the economic coefficient of heat transfer. We take as unity the economic coefficient of heat transfer of air at 100°C, equal to 43 CD (in kcal · $sec^{1.05}$ g/ $m^{0.1}$hr · deg).

We see from Tables 1 and 2 that there is significantly less difference between the values of the economic coefficients of heat transfer for the different heat carriers than between the values of the customary coefficients of heat transfer.

When making the final selection of the heat carrier one should take account of the other technico-economic indices (for example corrosiveness, value, etc.), in addition to the index developed in this article.

LITERATURE CITED


1. Scientific and Technical Bases of Nuclear Power, Edited by K. Gudman [Russian translation] (IL, Moscow, 1948, 1950) Vol. 1, p. 287; Vol. 2, p. 124.
2. Thermophysical Properties of Substances, Questionnaire, Edited by N. B. Vargaftika [in Russian] (Gosénergoizdat, Moscow, 1956).
3. M. A. Mikheev, Bases of Heat Transmission [in Russian] (Gosénergoizdat, Moscow, 1956).
4. S. S. Kutateladze, Basic Heat Exchange Theory [in Russian] (Mashgiz, Moscow, 1957) p. 145.


* * *

# TURBULENT TEMPERATURE PULSATIONS IN A LIQUID STREAM


V. I. Subbotin, M. Kh. Ibraginov, and M. N. Ivanovskii



Translated from Atomnaya Énergiya, Vol. 8, No. 3, pp. 254-257, March, 1960
Original article submitted October 12, 1959


Under conditions of heat exchange the pulsations in the speed of a turbulent liquid stream cause turbulent pulsations in the temperature. The experimental study of the turbulent pulsations in temperature is very important.

In the present work, the temperature in the liquid stream was measured by low intertia movable thermocouples of various designs with an open junction of 0.2 mm and a junction placed in a thin-walled case with an external diameter of 0.5 or 0.8 mm. One of the designs of the movable thermocouple is shown in [1]. The designs of the experimental sections and the control systems ensured both smooth movement of the thermocouples and recording at any point along the diameter of the tube. The experimental sections in the contour were placed vertically and horizontally. The thermal stream was provided by electrical heaters. The thermocouple readings were recorded by means of fast-acting class 0.5 ÉPP-09 potentiometers which took 1 sec to cover the whole scale. The limit of the scale was 0.5 mv.

Figures 1 and 2 show the distribution of temperature along the diameter of the tube during turbulent flow of molten metal and water. The development of temperature pulsations with time, typical for a stream of molten metal, is shown in Fig. 3. The development of pulsations had a similar character in water. The experiments showed that the amplitude and frequency of the temperature pulsations depend on the size of the thermal stream, the physical properties, the system of liquid flow and the dimensionless distance from the wall. Temperature pulsations were also observed in the wall of the tube, differing somewhat from the temperature pulsations in the liquid (Fig. 4). The temperature pulsations in the wall of the tube decayed with distance from the surface of heat exchange.

Experiments on the recording of temperature pulsations showed the following:

1. Change in the value of thermal loading leads to a change in the temperature pulsations. When the heating was stopped the temperature pulsations carried on for a certain length of time (2-5 sec) and then gradually decayed. During heating the reverse position was observed: gradual increase in pulsations up to normal values corresponding to the given system.

2. Switching on various sections of the heater along the length of the experimental section showed that the temperature pulsations both in the liquid and in the wall of the tube occurred only in the presence of a temperature gradient in the liquid stream in the sections being investigated. At a distance of five diameters from the start of heating there were temperature pulsations in the wall and liquid near the wall and there were no pulsations in the center of the liquid. At a distance greater than fifteen diameters from the start of heating the pulsations were observed over the whole section of the stream and in the wall. At a distance of ten diameters after the end of heating there were still temperature pulsations in the center and there were no pulsations in the wall of the tube.

3. The liquid circulation through the experimental sections was provided by various pumps: centrifugal and electromagnetic. The fluctuations in the liquid flow with time were very small (1-3% of the average value).

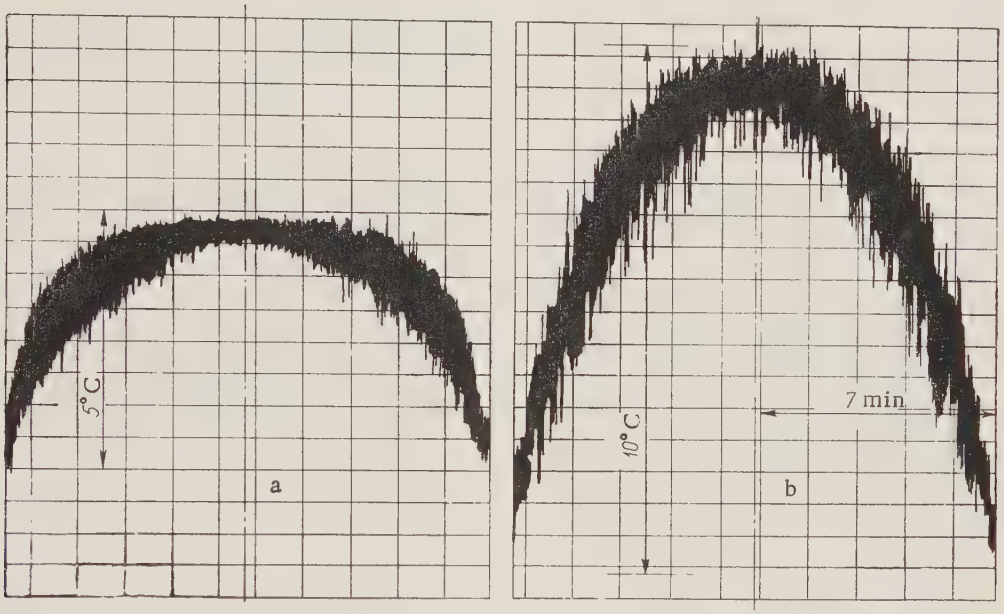


Fig. 1. Profile of temperature in a molten metal stream: a) Re = 230,000, q = 50,000 kcal/m$^2$·hr; b) Re = 30,000, q = 20,000 kcal/m$^2$·hr.

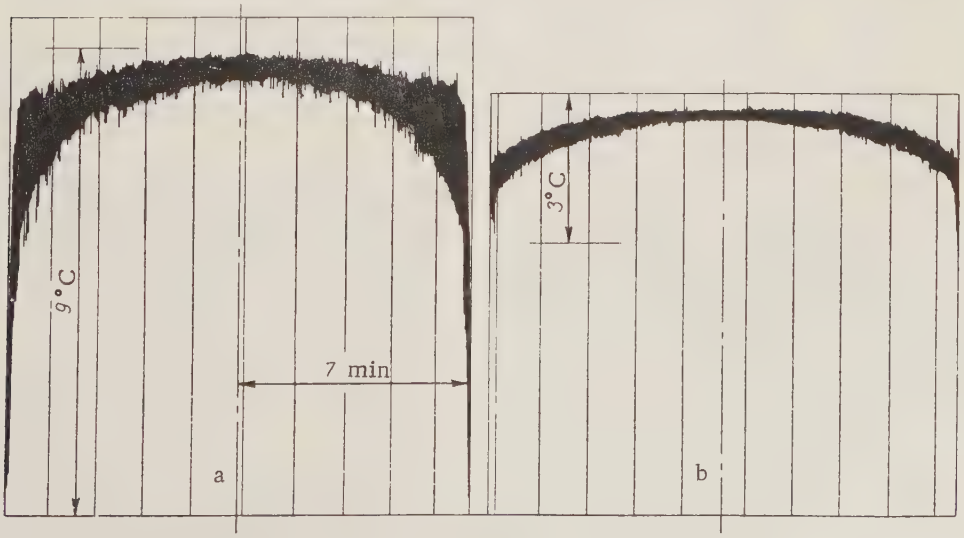


Fig. 2. Temperature profile in water stream: a) Re = 8,900, q = 30,000 kcal/m$^2$·hr; b) Re = 35,000, q = 50,000 kcal/m$^2$·hr.

A number of experiments was carried out without fluctuations in the flow (with a header tank to maintain a constant level of liquid). In these experiments the character of the pulsations was the same as when operating with pumps.

4. The frequency of the alternating current (50 cps) and the fluctuations in the power of the heater (3%) had no effect on the character of the temperature pulsations. The same pulsations were observed when the heater was fed with stable direct current. The temperature pulsations were also observed in the walls of the working heat exchanges where there was no electrical heating.

5. During the operation of the pumps there was mechanical vibration of the contour and experimental section, to eliminate which the section was connected with flexible hoses during the experiments with water. When the water flowed under gravity the vibration was completely absent. The temperature pulsations were the same both in the presence of mechanical vibrations from the operation of the pumps and without them. The absence of vibrations in the movable thermocouple was specially checked in the flow of water in a transparent channel.

6. Change in the system of liquid flow leads to a change in the temperature pulsations. With a transitional system of the flow there were considerable reductions in the frequency and amplitude of the pulsations. With laminar flow temperature fluctuations continued in the central part of the stream with a low frequency. These pulsations can be explained by natural convection of the liquid. The fluctuations were absent over a fairly wide layer of liquid adjacent to the wall and in the wall of the tube.

All experiments showed that the temperature fluctuations recorded by the instruments were caused by turbulent temperature pulsations in the stream.

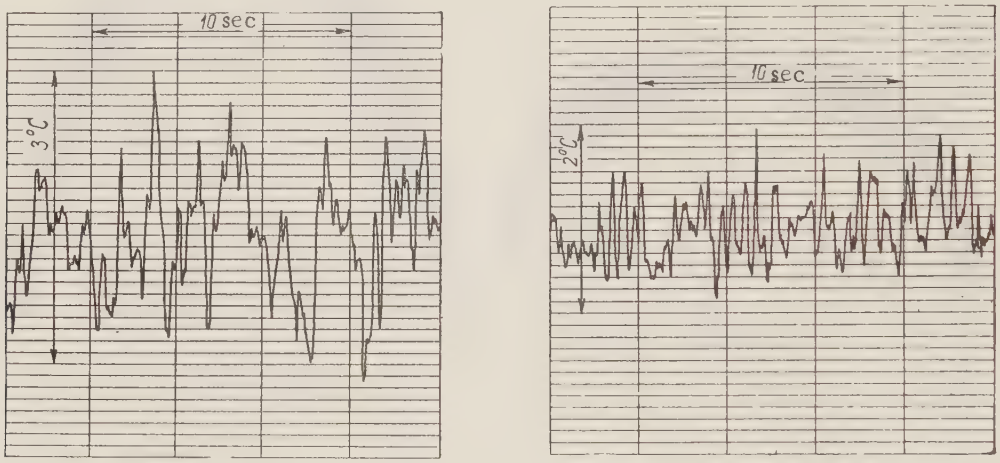


a b

Fig. 3. Development of temperature pulsations in time for a molten metal stream in the region of maximum amplitudes: a) Re = 30,000, q = 20,000 kcal/m$^2$·hr; b) Re = = 230,000, q = 50,000 kcal/m$^2$·hr.

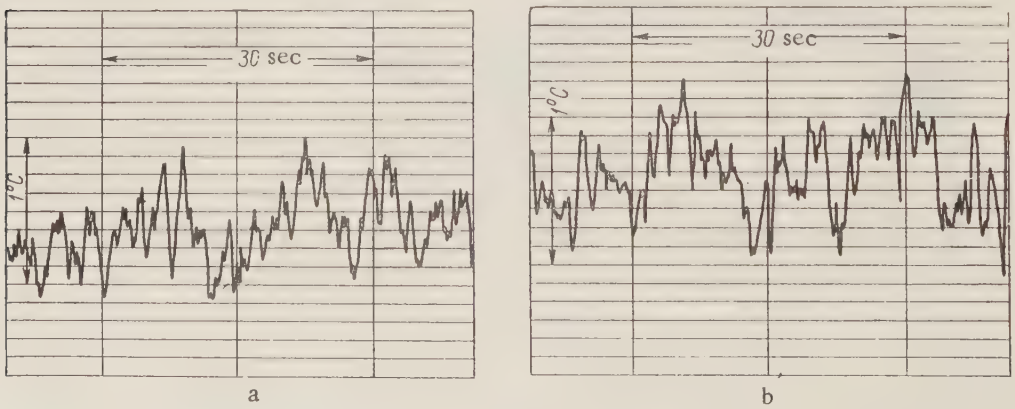


a b

Fig. 4. Development of temperature pulsations in the wall of a tube at a distance of 0.5 mm from the surface of heat exchange: a) with flow of water Re = 8,900, q = 30,000 kcal/m$^2$·hr; b) with molten metal flow Re = 90,000, q = 30,000 kcal/ /m$^2$·hr.

As can be seen from Fig. 1, for molten metals with a sufficiently regular change in the temperature gradient across the section of the tube, maximum pulsations were observed at about halfway between the center and the wall of the tube. For water, having a sharp change in the temperature gradient in the layer adjacent to the wall, the maximum pulsations were observed near the wall (see Fig. 2). This change in amplitude of the temperature pulsations along the radius of the tube agrees qualitatively with the hypothesis that the value of the turbulent temperature pulsations is proportional to the length of the path of displacement $l$ and the temperature gradient $d\bar{t}/dr$ [2].

$$t' = l\frac{d\bar{t}}{dr}.$$

At the same time, the experiments showed that the temperature pulsations on the axis and the wall of the tube are not equal to zero although it follows from the relationship given that in these cases $t' = 0$.

The temperature pulsations of the liquid recorded near the wall under conditions of stationary heat exchange and also the temperature fluctuations of the wall itself show that the process of heat transfer through the liquid layer adjacent to the wall and the surface of heat exchange is, strictly speaking, not stationary.

The thermocouples used in the experiments have low inertia and can react to fluctuations over a wide range of frequencies (up to 100 cps) almost without distortion in amplitude. The recording instruments (ÉPP-09) can react to fluctuations with a frequency up to 20 cps.

The fluctuations recorded in the experiments obviously do not represent the whole spectrum of temperature fluctuations. In later investigations the authors intend to use more advanced low-inertia instruments.

Those taking part in the construction of the equipment and the experiments were: E. V. Nomofilov, M. N. Arnol'dov and Yu. N. Prokrovskii. The authors would like to thank A. I. Leipunskii and A. P. Aleksandrov for their valuable advice and interest shown in the work.

LITERATURE CITED

1. P. L. Kirillov, V. I. Subbotin, M. Ya. Suvorov, and M. F. Troyanov, Atomnaya Énerg. 6, 4, 382 (1959).*
2. Problems of Turbulence, Collection edited by M. A. Velikanov [in Russian] (ONTI, Moscow, 1936).

* Original Russian pagination. See C. B. translation.

* * *

# ELECTROLYTIC PREPARATION OF LAYERS OF URANIUM COMPOUNDS WITH DENSITIES OF 1-3 mg/cm²

V. F. Titov

Translated from Atomnaya Énergiya, Vol. 8, No. 3, pp. 257-258, March, 1960
Original article submitted August 27, 1959

The electrolytic deposition of uranium compounds on to solid metal cathodes is one of the best methods for preparing strong uniform layers which can be used in nuclear physics for various types of work.

The preparation of layers of uranium compounds with densities up to 0.2-0.3 mg/cm² presents no difficulties using various baths and cathodes such as platinum, nickel, etc. [1].

With increase in the density of the layer, the adhesion of the uranium hydroxide deposit to the cathode surface becomes very weak and the layer is readily rubbed off. To obtain thick layers, therefore, a cathode is usually used with a more active surface, giving a good bond with the deposit. Thus, on aluminum it was possible to obtain layers of uranium with densities up to 2-3 mg/cm². However, existing methods either do not provide sufficient strength and uniformity in the layer [2], or are based on the deposition of only a small fraction of the uranium present in the solution [3]. In the latter case there is a reduction in the accuracy with which the layer is applied (10-15%).

To obtain strong uniform layers of uranium with densities of 1-3 mg/cm² the uranium was deposited quantitatively from ammonium oxalate solutions. The electrolysis was carried out in cells described in [4]. The cathodes were aluminum discs of 0.5-1.0 mm

thickness and areas of 10-20 $cm^2$. Before electrolysis the surface of the aluminum was carefully cleaned with emery cloth. The anode was a platinum disc with the appropriate diameter.

The electrolysis conditions were as follows: the electrolyte was a 0.2 M solution of $(NH_4)_2C_2O_4$; pH = 9; the volume of the solution was 1 ml per 1 $cm^2$ of the cathode surface; the concentration of uranium put into the solution in the form of uranyl nitrate was 1-3 mg/ml, depending on the required density of deposit; the temperature was 80°C.

The heated solution was poured into the cell and the current density was fixed at 10 ma/$cm^2$, the electrolysis took 50-60 min. The cathode then received a deposit of 95+2% uranium. The percentage deposition can be greater but there is a deterioration in the surface of the layer.

Before the end of electrolysis methyl alcohol was poured into the cell, the whole solution was poured off, the cell washed out with alcohol and dismantled. The layer was dried in air.

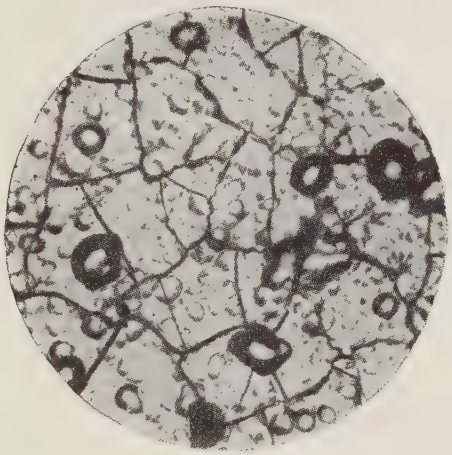

Fig. 1. Layer of uranium compound of density 1 mg/$cm^2$ (× 600).

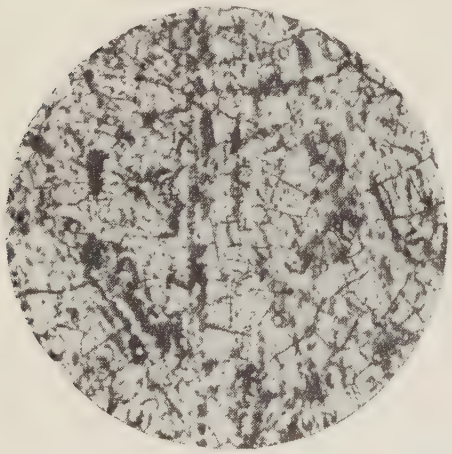

Fig. 2. Layer of a uranium compound of density 3 mg/$cm^2$ (× 600).

The layer of density 1 mg/$cm^2$ was smooth and bright (Fig. 1). After the layer had been rubbed with a cotton pad there were no traces of uranium oxides on it. With layers of density 2-3 mg/$cm^2$ the brightness was reduced and with a layer of density 3 mg/$cm^2$ traces of oxides remained on the pad, this being connected with the mechanism for deposition of uranium from oxalate solutions. It was found that the maximum rate of deposition is observed in a 0.2 M solution of $(NH_4)_2C_2O_4$ with a uranium concentration of 1 mg/ml. Further increases in the concentration both of uranium and of the ammonium oxalate leads to a gradual reduction in the rate of deposition of uranium. This is due to the fact that under these conditions the growth of the crystals of the deposit begins to predominate. There is presumably some polymerization here in the solution of the complex uranyl ions. Furthermore, as is known, increasing the concentration of electrolyte leads to a reduction in the number of crystals formed during electrolysis. It should be mentioned here that the uranium concentration used in [3] (4.76 mg/ml) could not give good layers with a sufficiently complete (> 50%) deposition of uranium.

Strong uniform layers of uranium with density 3 mg/$cm^2$ were obtained using aluminum coated electrochemically with zinc [2]. Instead of etching in acid this aluminum was cleaned with emery cloth and zinc was deposited on it from an alkaline solution (525 g NaOH and 100 g ZnO per 1 liter of water).

The conditions of electrolysis were as follows: the electrolyte was a 0.2 M solution of $(NH_4)_2C_2O_4$; pH = 9; the uranium concentration was 1 mg/ml; the volume of solution was 3 ml per 1 $cm^2$ of the cathode surface; the current density was 100 ma/$cm^2$ and the electrolysis lasted for 50 min. During this time 97 ±1% of the uranium in the solution was deposited. The structure of the surface layer is shown in Fig. 2. The uniformity of the layers was checked by a count of the α-particles emitted by each 1 $cm^2$ of the cathode surface. The maximum deviations did not exceed 10%. X-ray structural analysis of the deposit showed the presence of $UO_2$ structure.

## LITERATURE CITED


1. K. Kasto, The Analytical Chemistry of Uranium and Thorium [Russian translation] edited by P. N. Palei (IL, Moscow, 1956) p. 340.
2. C. Wilson and A. Langer, Nucleonics 11, 8, 48 (1953).
3. L. Koch, J. Nucl. Energy 2, 110 (1955).
4. G. N. Yakovlev, P. M. Chulkov, V. V. Dedov, V. N. Kosyakov, and Yu. B. Sobolev, Atomnaya Énerg. 5, 131 (1956).*


*Original Russian pagination. See C. B. translation.

# SOLUBILITY OF URANIUM (IV) HYDROXIDE IN SODIUM HYDROXIDE

N. P. Galkin and M. A. Stepanov

Translated from Atomnaya Énergiya, Vol. 8, No. 3, pp. 258-261, March, 1960
Original article submitted November 27, 1959

At the present time in a number of cases, uranium (IV) hydroxide is separated in a strongly alkaline medium in the processing of natural and irradiated raw material [1], though the behavior of this compound in the given medium has been studied little. In communications [2-4] there have been reports that uranium (IV) hydroxide has only basic properties and does not dissolve in excess precipitant. However, it was recently shown [5] that uranium (IV) hydroxide is amphoteric. The equilibrium constant of the reaction

$$U(OH)_4 + OH^- \rightleftarrows H_3UO_4^- + H_2O, \qquad (1)$$

equals $1.7 \cdot 10^{-4}$.

Since the solution of uranium (IV) hydroxide has been studied over a narrow range of alkali concentrations (up to 0.6 N), it was decided to check the accuracy of the derived rules in more concentrated alkali solutions.

Uranium (IV) hydroxide was precipitated from hydrochloric acid solution with aqueous sodium hydroxide solution. The hydrochloric acid solution of uranium (IV) was obtained by the action of hydrochloric acid on metallic uranium of 99.87% purity. The filtered solution (1.753 N with respect to HCl) contained 0.3595 g-ion/liter of uranium (IV). The amount of uranium (IV) was determined by titration with potassium bichromate [6].

The excess acidity was calculated as the difference between the "total" acidity, determined by neutralization of the medium to phenolphthalein, and the acidity created due to hydrolysis of uranium (IV) during neutralization of the solution. In order to exclude the oxidation of uranium (IV) during its precipitation, washing and treatment of its hydroxide with alkali, all operations were carried out in a "box" filled with oxygen-free argon [7]. The clear plastic tubes in which all the experiments were carried out had hermetic screw tops. The latter were fitted with rubber and Teflon gaskets on which even strong alkali solutions had no appreciable action.

Uranium (IV) hydroxide was precipitated in the following way. Into a tube was poured 2 ml of uranium chloride and then 30 ml of 0.34 N sodium hydroxide solution. The tubes were closed tightly and removed from the box and their contents mixed for 6 hr in an air thermostat at 20°C. The tubes were then returned to the box, there the mother solution was separated from the precipitate by decantation. The apparent volume of the precipitate was 1/14 of the clear part. Considerable purification was achieved by three washes with water by decantation. A qualitative test for chlorine ion with silver nitrate gave a negative result.

The opinion in [8] that potassium and sodium cannot be removed completely from uranium (IV) hydroxide by washing is apparently incorrect. Spectral analysis of the water-washed precipitate indicated the absence of sodium (less than 0.01%), for example, when the hydroxide was precipitated with sodium hydroxide solution.

The sodium hydroxide solution was prepared from a reagent of "chemically pure" grade. In order to avoid the harmful effect of carbonate ion, we dissolved the sodium hydroxide in boiled distilled water in an argon atmosphere. As concentrated sodium hydroxide dissolves normal silicate glass [9], clear plastic vessels were used in our experiments.

A coagulated portion of the uranium hydroxide pulp, washed free from mother solution, was treated with a definite amount of alkali and distilled water (Table 1). When all the components had been introduced into the tubes, 1-2 ml of free space remained. The tubes were tightly closed with tops and transferred to the air thermostat, where their contents were mixed for 6 days (8 hours per day) at 25±1°C (it was considered that equilibrium was reached after this time [5]). After the mixing, the solid phase was allowed to settle and the clear portion passed through a fine paper filter and the uranium and alkali content of the filtrate determined. The analysis results are given in Table 1 and the figure.

The experiments confirmed the results in [5] only at low alkali concentrations (up to 0.5 N). The linear relation between the uranium (IV) content of the solution and the alkali concentration was disrupted at high alkali concentrations. After reaching a maximum value in 2 N alkali, the uranium concentration began

TABLE 1

Data on the System Uranium (IV) Hydroxide– Aqueous Sodium Hydroxide Solution

| Experiment No. | Components in starting solution | | | Equilibrium concentrations | | | Constant of reaction (1), $K \cdot 10^5$ |
|---|---|---|---|---|---|---|---|
| | alkali | | water, ml | alkali, N | uranium | | |
| | volume, ml | concentration, N | | | g/liter | g-ion/liter $\cdot 10^5$ | |
| 1 | 50,0 | 8,50 | 0,0 | 7,40 | 0,015 | 6,3 | 0,85 |
| 2 | 25,0 | 8,50 | 25,0 | 4,40 | 0,020 | 8,4 | 1,91 |
| 3 | 10,0 | 8,50 | 40,0 | 1,75 | 0,020 | 8,4 | 4,81 |
| 4 | 5,0 | 8,50 | 45,0 | 0,85 | 0,020 | 8,4 | 9,90 |
| 5 | 2,0 | 8,50 | 48,0 | 0,35 | 0,015 | 6,0 | 18,0 |
| 6 | 1,0 | 8,50 | 49,0 | 0,20 | 0,007 | 2,9 | 14,7 |
| 7 | 50,0 | 0,85 | 0,0 | 0,075 | 0,005 | 2,1 | 28,0 |
| 8 | 10,0 | 0,85 | 40,0 | 0,021 | 0,003 | 1,3 | 62,0 |
| 9 | — | — | — | 0,632 | — | 5,9 | 14 |
| 10 | — | — | — | 0,484 | — | 7,0 | 17 |
| 11 | — | — | — | 0,266 | — | 4,5 | 19 |
| 12 | — | — | — | 0,215 | — | 4,1 | 19 |
| 13 | — | — | — | 0,144 | — | 2,7 | — |
| 14 | — | — | — | 0,080 | — | 0,63 | — |
| 15 | — | — | — | 0,000 | — | 0,3 | — |

Note: The data of experiments 9-15 were taken from [5].

TABLE 2

Chemical Composition of Precipitates Isolated with an Equilibrium Concentration of 7.0 N Alkali

| Wash liquid | Drying conditions | Element content of precipitate, % | | | Molar ratio of sodium to uranium |
|---|---|---|---|---|---|
| | | uranium | | sodium | |
| | | U (IV) | U (VI)+U(IV) | | |
| Water | In a drying cupboard at 200°C for 2 hr | 16,48<br>16,35 | 64,49<br>64,55 | 0,06<br>0,04 | $9,65 \cdot 10^{-3}$<br>$6,39 \cdot 10^{-3}$ |
| Acetone | In air for 1 day | 10,5<br>10,8 | 61,88<br>61,88 | 2,57<br>2,20 | 0,428<br>0,367 |
| Diethyl ether | In a drying cupboard at 180°C for 4 hr | 12,7<br>12,8<br>15,4 | 67,50<br>65,80<br>65,94 | 1,70<br>1,80<br>1,67 | 0,260<br>0,283<br>0,262 |
| Ethanol | In air for 1 day | 13,8<br>14,1 | 74,80<br>74,94 | 2,73<br>2,69 | 0,388<br>0,373 |

to fall, even though the alkalinity of the medium increased. Consequently, the processes occurring in the system cannot be described by equation (1) alone. In our opinion, the fall in uranium concentration in the solution may be explained by the salting-out action of sodium ions if it is assumed that a new compound whose formula corresponds to the formula $NaH_3UO_4$ forms in the precipitate. To check this hypothesis, we analyzed the solid phase chemically and the results are presented in Table 2.

Washing the precipitate with water led to complete removal of the sodium from the solid phase. The completeness with which the mother solution was washed from the precipitate was checked by the reaction of zinc uranyl acetate with the sodium ion present in the wash waters. Apparently, the proposed compound is stable only in strongly alkaline media; hydrolysis occurs under the action of water and this may be described by the equation.

$$NaH_3UO_4 + H_2O \rightleftarrows U(OH)_4 + NaOH \qquad (2)$$

Then, to reduce hydrolysis according to equation (2) to a minimum, we used acetone, diethyl ether, and absolute ethanol as wash liquids. However, even under these conditions we observed partial elution of sodium, i.e., hydrolysis of the salt $NaH_3UO_4$ was not eliminated.

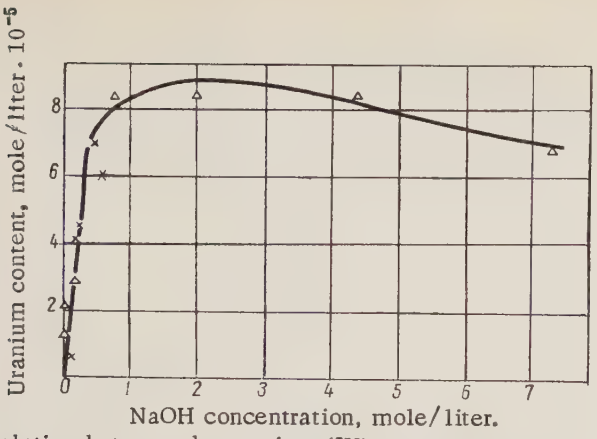


Relation between the uranium (IV) concentration and the alkalinity of the medium: △) data from our work; ×) data from [5].

As a result of this, the sodium content of the precipitate was considerably below theroetical values.

Consequently, a study of the chemical composition of the solid phase of the system uranium (IV) hydroxide–aqueous sodium hydroxide solution indicated the formation of a new compound $NaH_3UO_4$, which is capable of hydrolysis.

LITERATURE CITED

1. R. Gelin and H. Mogard, Proceedings of the Second International Conference on the Peaceful Uses of Atomic Energy (Geneva, 1958). Selected Works of Foreign Scientists, Technology of Atomic Raw Material [Russian translation] (Atomizdat, Moscow, 1959) Vol. 7, p. 417.
2. B. V. Nekrasov, Course in General Chemistry [in Russian] (Goskhimizdat, Moscow-Leningrad, 1954).
3. N. I. Blok, Qualitative Chemical Analysis [in Russian] (Goskhimizdat, Moscow-Leningrad, 1952).
4. J. Katz and E. Rabinowitch, Chemistry of Uranium [Russian translation] (IL, Moscow, 1954).
5. K. Gayer and H. Leider, Canad. J. Chem. 35, 1, 5 (1957).
6. Analytical Chemistry of Uranium and Thorium, Edited by C. J. Rodden [Russian translation] (IL, Moscow, 1956).
7. K. V. Chmutov, Techniques in Physicochemical Investigation [in Russian] (Goskhimizdat, Moscow-Leningrad, 1948).
8. M. Aloy, "Recherches sur l'uranium et ses composés," Theses Toulouse, Nos. 21, 23 (1901) (cited in Gmelins. Handbuch der Anorganischen Chemie, Auflage 8, Hr. 55-Uran.and Isotope, (Berlin, 1936) p. 100).
9. Yu. V. Karyakin and I. I. Agelov, Pure Chemical Reagents [in Russian] (Goskhimizdat, Moscow, 1955).

* * *

# CATALYTIC EFFECT OF IRON COMPOUNDS IN THE OXIDATION OF TETRAVALENT URANIUM IN ACID MEDIA

Vikt. I. Spitsyn, G. M. Nesmeyanova, and G. A. Alkhazashvili

Tranlsated from Atomnaya Énergiya, Vol. 8, No. 3, pp. 261-262, March, 1960
Original article submitted July 17, 1959

The oxidation of tetravalent uranium in the presence of $Fe^{3+}$ salts has not been studied quantitatively up to now. There is a report in the literature [1] that the oxidation of uranium is accelerated by the presence of soluble iron compounds. It was shown [2] that the $Fe^{3+}$ concentration in the solution should not be less than 2 g/liter for successful oxidation of uranium, regardless of the type of oxidant used and $Fe^{2+}$ content in the solution. In [3] it is assumed that $MnO_2$ is the primary oxidant in this process and that the $Fe^{3+}$ ions act as a catalyst; in other papers, for example [4], the necessity for having a certain amount of $Fe^{3+}$ ions in the solution to give the medium the required oxidation potential is reported.

The effect of iron compounds on the oxidation of uranium was studied with pure uranous-uranic oxide and $Fe^{2+}$ and $Fe^{3+}$ sulfates. Sulfuric or nitric acids various concentrations was used as the solvent and $MnO_2$ and $KClO_3$ were used as the oxidants. A sample of the oxide was placed in a reaction vessel and a stoichiometric

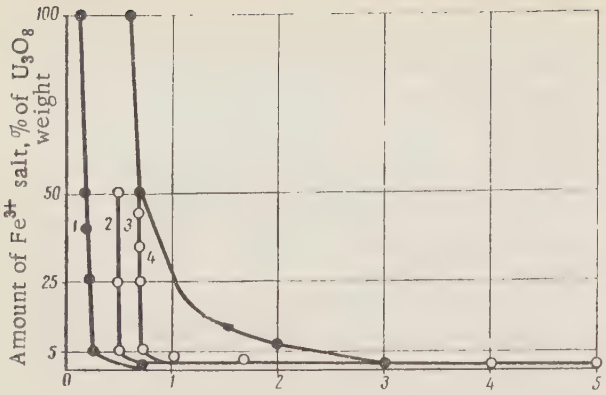


Fig. 1. Relation between the uranium solution time and the amount of $Fe^{3+}$ salt added in the solution of uranous-uranic oxide in solutions of nitric and sulfuric acids with $MnO_2$ and 100% solution of the oxide at t = 90°C.
1, 4) Nitric acid (50 and 5 g/liter, respectively);
2, 3) sulfuric acid (5 and 150 g/liter, respectively).

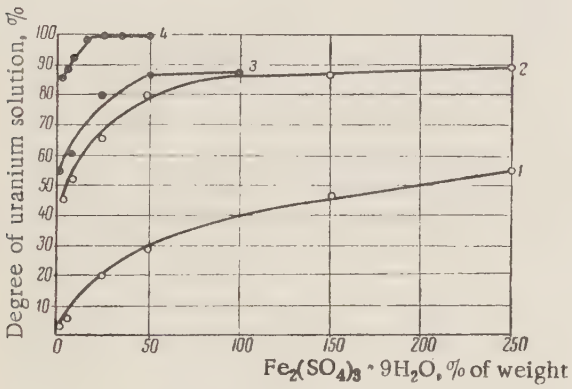


Fig. 2. Effect of added $Fe^{3+}$ salt on the degree of uranium solution in nitric acid and sulfuric acid with $MnO_2$ at various concentrations: 1, 2) Nitric acid (5 and 50 g/liter, respectively); 3, 4) sulfuric acid (5 and 50 g/liter, respectively). At t = 20°C, $\tau$ equals 72 hr for nitric acid and 48 hr for sulfuric acid with $MnO_2$.

amount of oxidant and acid added. The experiments were carried out in an air thermostat at 20 and 90°C. Figure 1 gives data on the effect of $Fe^{3+}$ ion concentration on the time for complete solution of uranium in nitric and sulfuric acids in the presence of the oxidant $MnO_2$. As the Figure shows, the addition of $Fe^{3+}$ salt in an amount equal to 0.5% of the uranous-uranic oxide weight made it possible to dissolve all the uranium in one hour with a sulfuric acid concentration of 5 g/liter. An increase in the amount of $Fe^{3+}$ salt to 5% decreased the uranium solution time from 3 hr to 40 min at a sulfuric acid concentration of 150 g/liter and to 30 min at a concentration of 5 g/liter.

The addition of $Fe^{3+}$ salt in an amount equal to 0.5-5% of the uranous-uranic oxide weight made it

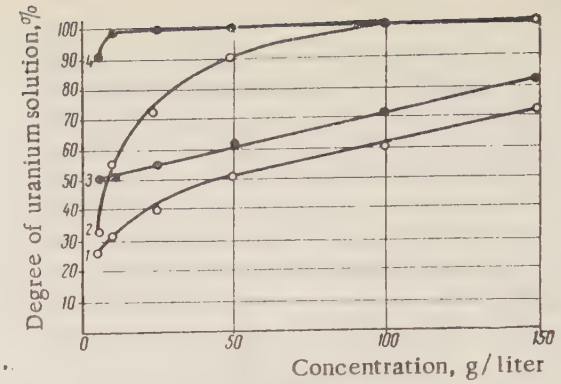


Fig. 3. Effect of microamounts of $Fe^{3+}$ salt on the degree of uranium solution during the solution of $U_3O_8$ in sulfuric acid solutions of various concentrations with $KClO_3$ (curves 1 and 2) or $MnO_2$ (curves 3 and 4) as oxidant (t = 90°C, $\tau$ = 1 hr).

possible to reduce the uranium solution time from 3 hr to 40 min with a nitric acid concentration of 5 g/liter and from 30 to 8 min with a concentration of 50 g/liter.

The introduction into the reaction mixture of a ferric salt in an amount equal to 0.5-250% of the sample weight in the solution of uranous-uranic oxide in nitric or sulfuric acid with $MnO_2$ at 20°C considerably increased the degree of solution of uranium (Fig. 2).

Data on the effect of microamounts of $Fe^{3+}$ salt on the solution of uranous-uranic oxide in sulfuric acid with $KClO_3$ or $MnO_2$ as oxidant are given in Fig. 3. The Figure shows that the introduction of $Fe^{3+}$ salt into the reaction mixture in an amount of $5 \cdot 10^{-3}$ g-ion/g-ion of U considerably increased the degree of uranium solution. The uranous-uranic oxide was completely oxidized by $KClO_3$ or $MnO_2$ at sulfuric acid concentrations of 100 and 10-25 g/liter, respectively.

From the results presented it follows that iron ions accelerate the solution of uranium severalfold, reducing the the starting acid concentration. Salts of $Fe^{3+}$ are strong oxidants for tetravalent uranium. The effect of large amounts of $Fe^{3+}$ is particularly characteristic for dilute solutions of nitic acid (see Figs. 1 and 2), which is a very weak oxidant in this case. On the other hand, as $Fe^{3+}$ ions do not react with $MnO_2$ or $KClO_3$, $Fe^{3+}$ acts as a catalyst until there is no $U^{4+}$ in the reaction mixture.

At the moment that they are oxidized, $Fe^{2+}$ ions have a catalytic effect on the oxidation of uranium. The mechanism of the catalytic acceleration of uranium oxidation by iron compounds may be represented as follows:

$$Fe^{2+} \xrightarrow{\text{oxidant}} Fe^{3+} \xrightarrow[U^{4+}]{} Fe^{2+} \xrightarrow{\text{oxidant}} \rightarrow Fe^{3+} \xrightarrow[U^{4+}]{} Fe^{2+} \text{ etc.}$$

i.e., iron ions transfer electrons between the oxidants and the uranium.

LITERATURE CITED

1. T. Arden, Industr. Chemist. 32, 376, 202 (1956).
2. I. Arthur and R. Wheeler, J. South African Institute of Min. and Met. 57, 11, 631 (1957).
3. A. Gaudin and R. Schuhmann, J. Metals, 8, 8, 1065, 1956).
4. A. Thunaes, Canad. Mining. J., 77, 6, 123 (1956).

* * *

# EFFECTS OF GAMMA RADIATION ON THE ELECTRODE PROPERTIES OF LITHIUM GLASS

N. A. Fedotov

Translated from Atomnaya Énergiya, Vol. 8, No. 3, pp. 262-264, March, 1960
Original article submitted November 27, 1959

Measurement of the pH of solutions using glass electrodes is currently meeting with increasingly greater favor in industry, engineering, scientific research etc. The problem of the effect of $\gamma$ radiation on readings of a glass electrode in measurements of the pH of solutions comes up in connection with the production of radioactive isotopes, as well as the widespread use of such isotopes in investigations of processes occurring in aqueous solutions.

The aim of the present note is to shed some light on the effect of $\gamma$ radiation on the electrode properties of a glass commonly used in the manufacture of glass electrodes. The problem of radiation effects on an auxiliary electrode, and that of the accuracy of emf measurements of circuits bearing some similarity to that case, in the case of an intense $\gamma$ field, will not be discussed here.

The glass electrode involved is a glass tube 12 mm in diameter (of No. 23 glass) with a bulb made of lithium-base electrode glass of the following composition (in molar percentages): $Li_2O$ – 27; $Cs_2O$ – 3; $La_2O_3$ – 3; $SiO_2$ – 67. Electrodes made of this glass show excellent linearity over the pH range 0.5-12.5 (at room temperature), exhibit relatively low resistivity, and possess a reasonable chemical stability in acid and alkaline solutions (at room temperature and elevated temperatures). A detailed description of the properties of electrodes and means of manufacturing them may be found by consulting references [1-3].

The three most important electrode characteristics, the sensitivity gradient, asymmetry potential, and resistivity, were determined.

A 0.1 N solution of hydrochloric acid was poured into the electrode in taking the characteristics. Potential measurements of the glass electrodes in standard buffer solutions were carried out with reference to a saturated calomel electrode placed at the same tempera-

Values of Asymmetry Potential of the Electrodes Before and After Irradiation.

| Electrode number | pH of solution | | | | | | | | | | | |
|---|---|---|---|---|---|---|---|---|---|---|---|---|
| | 1,2 | | 3,10 | | 5,05 | | 7,35 | | 8,85 | | 10,35 | |
| | prior to irradiation | after irradiation | prior to irradiation | after irradiation | prior to irradiation | after irradiation | prior to irradiation | after irradiation | prior to irradiation | after irradiation | prior to irradiation | after irradia- |
| 1 | 10 | 11 | 16 | 12 | 12 | 10 | 7 | 9 | 9 | 14 | 10 | 14 |
| 2 | 11 | 8 | 16 | 10 | 12 | 8 | 7 | 11 | 9 | 13 | 10 | 12 |
| 3 | 9 | 8 | 16 | 10 | 12 | 8 | 7 | 9 | 10 | 12 | 10 | 13 |

ture. The experimental arrangement for measuring emf is shown in the accompanying diagram.

The asymmetry potential was measured over the pH interval 1-10. An accuracy of ± 2 mv was achieved in the determination of asymmetry potential. The resistivity of the walls of the electrode bulb was determined by measuring the current passing between two silver electrodes immersed in the solution on both sides of the bulb of the glass electrode.

The external current source had a voltage of 90 v. The error in the determination of electrode resistivity did not exceed ± 1%. To prevent the values of the abovementioned characteristics from being affected by the walls of the cylindrical portion of the electrode, the inner and outer surfaces of the cylindrical portion were coated with a tenuous layer of vaseline during all measurements, thus rendering the surface of the glass nonwettable.

We began by taking all of the characteristics prior to irradiating the electrodes. The solution held within the electrode was then poured out, and benzene was applied to remove traces of grease from the outer and inner surfaces of the cylindrical portion of the bulb. After this all three electrodes were placed into a receptacle which was placed in a $Co^{60}$ γ source of 20,000 gm-eq Ra. The electrode bulbs were placed at equal distances (7 cm) from the center of the source. Irradiation proceeded for 48 hours. The integral irradiation dose was 25 million r. After irradiation, the electrodes had acquired a dark-brown coloration. Post-irradiation measurements of the electrode characteristics were carried out in the same manner as the pre-irradiation measurements.

The pre-irradiation sensitivity gradient of the three electrodes (at t = 23°C) was 59.0 mv/pH, while the post-irradiation value (at t = 21°C) was 58.0 mv/pH.

The accuracy achieved in the determinations was ± 0.3 mv/pH. All three electrodes had the same

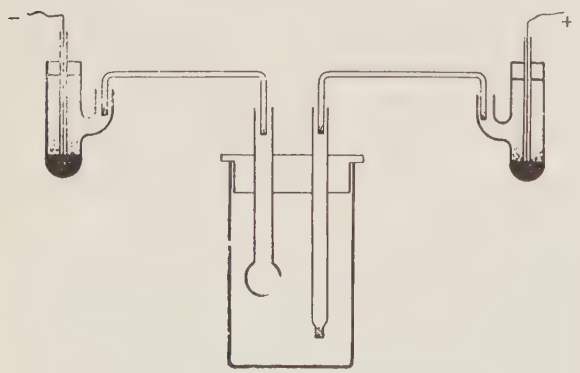


Experimental arrangement for measuring the potential of the glass electrodes.

| Resistance, megohms | |
|---|---|
| pre-irradiation (t = 23° C) | post-irradiation (t = 21° C) |
| 165 | 169 |
| 361 | 384 |
| 148 | 153 |

a) Resistance, megohms; b) pre-irradiation; c) post-irradiation.

characteristics both prior to and subsequent to irradiation.

An observed insignificant decrease in the sensitivity gradient is related to a slight change in temperature between measurements. The sensitivity gradient of 58.0± 0.3 mv/pH at temperature 21°C is a characteristic value for glass electrodes manufactured from many grades of electrode glasses.

Values of the pre-irradiation and post-irradiation electrode asymmetry potentials, in solutions with different pH values, are tabulated (in millivolts). As is apparent from the tabulated data, the post-irradiation asymmetry potential averages a drop of 3 mv in absolute value over the pH interval 1-7, and increases by the same amount over the pH region > 7 (relative to the value of the asymmetry potential of nonirradiated electrodes placed in the same solution).

Above, we present the results of resistance measurements of the three electrodes before and after irradiation, at temperatures 23° and 21°C, respectively.

After introducing corrections for the temperature dependence of the resistance of lithium-base glass [3], the difference in the pre-irradiation and post-irradiation values of the electrode resistance did not exceed ± 1 megohm, i.e., remained within the limits of accuracy of the measurement.

The investigations accordingly show that even following intense γ irradiation of the electrode glass, the sensitivity gradient and electrode resistance remain constant (within 0.5-1.0%), while the variation in electrode asymmetry potential averages about 3 mv in absolute value. We infer from these findings that electrodes of lithium-base glass may be widely used for pH measurements of solutions with high content of γ-active isotopes.

## LITERATURE CITED

1. G. Perley, Analyt. Chem. 21, 394 (1949).
2. N. A. Fedotov, Zavodskaya Lab. 4, 498 (1958).
3. N. A. Fedotov, Zhur. Fiz. Khim. 32, 10, 1951 (1958).

# MEASUREMENT OF GAMMA-RADIATION DOSE BY THE CHANGE IN OPTICAL ACTIVITY OF CERTAIN CARBOHYDRATES

S. V. Starodubtsev, Sh. A. Ablyaev, and V. V. Generalova

Ttranslated from Atomnaya Énergiya, Vol. 8, No. 3, pp. 264-265, March, 1960
Original article submitted October 21, 1959

Several techniques are available for measuring large doses of gamma radiation, taking advantage of such chemical effects as: oxidation of bivalent iron in solution [1, 2], the change undergone by cerium sulfate in solution [3], decomposition of sodium benzoate solutions [4], decoloration of methylene blue [5], and many other reactions [6-10].

A common and important limitation to these chemical techniques of dosimetry is their complexity, and the time required for chemical processing of the solutions following exposure to radiation, as well as ambiguities and low level of precision in the results.

In order to single out those methods which do not require subsequent complicated processing and are yet sensitive to very large doses, we carried out a study of the effect of intense beams of $\gamma$ rays on aqueous solutions of carbohydrates. A particularly detailed investigation was made of the radiation effects on sucrose and glucose in solution [11]. Aqueous solutions of both sucrose and glucose are optically active, so that a change in the activity is evidence for some change in glucose or sucrose concentration in the solution, as a result of exposure of solutions of glucose and sucrose, sealed into glass cuvettes, to $\gamma$ irradiation.

ChDA brand glucose and sucrose were used in the investigation, with twice-distilled water employed as solvent. Irradiation of the prepared sepecimens (7 ml of each) was carried out on a water-shielded $Co^{60}$ $\gamma$ source of 2,100 C activity.

The solutions were irradiated with doses ranging from 0 to 200 million roentgens. The maximum dose rate employed was 1.1 million r/hr. The specific rotation of the solutions was sensed by a sensitive polarimeter, and the dose value found by any particular method was checked by the ferrosulfate method or the methylene blue method.

Prior to irradiation, the angle of rotation of the plane of polarization of all of the specimens prepared was measured with the polarimeter. Some of the specimens were used as controls and not exposed to irradiation. The remaining specimens, after being irradiated with a specific dose, were again run through the polarimeter. The irradiation and all of the measurements were carried out at controlled temperatures.

The measurements indicated a considerable decrease in angle of rotation of the plane of polarization in response to $\gamma$ irradiation of solutions of glucose and sucrose, the decrease being found by experiment to be a function of dose level and concentration of the solution.

Figure 1 shows a typical run of variation of angle of rotation of the plane of polarization $\alpha$ in solutions of sucrose and glucose of 45% concentration (curve 1) and 20% concentration (curve 2), in response to increased irradiation doses up to 200 million roentgens (length of measuring cuvette: 10 cm).

Figures 2 and 3 show the variation in angle of rotation $\Delta\alpha$, referred to unit concentration C and to unit path length of light ray $l$, in sucrose and glucose solutions. This run of the rotation-angle curves as a function of irradiation dose was also observed at other concentrations.

It becomes apparent from inspection of the accompanying graphs that the angle of rotation of the plane of polarization for glucose and sucrose solutions varies over a wide range in linear fashion, as a function of

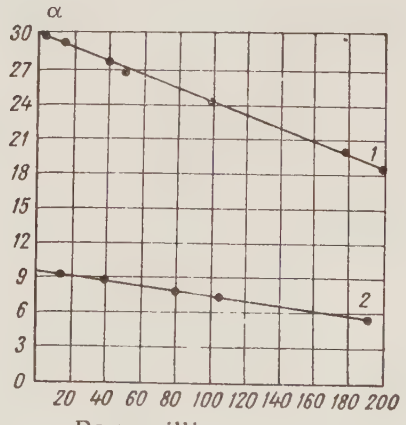


Fig. 1. Variation in angle or rotation of plane of polarization, plotted against irradiation dose.

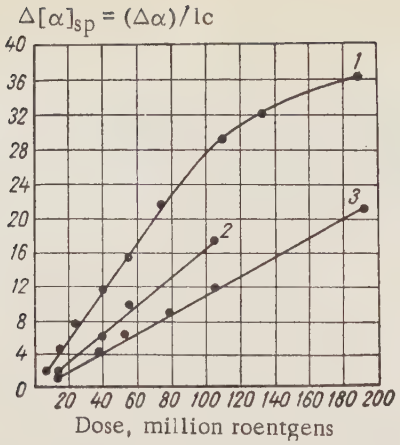


Fig. 2. Change in angle of rotation of plane of polarization of glucose solutions, as a function of irradiation dose (in percent): 1) 5; 2) 10; 3) 20.

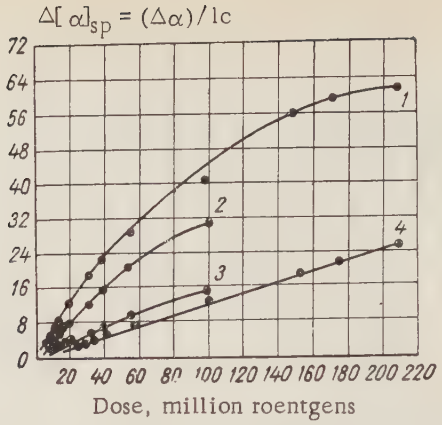


Fig. 3. Variation in angle of rotation of plane of polarization of sucrose solutions as a function of irradiation dose (in percent): 1) 5; 2) 10; 3) 30; 4) 45.

irradiation dose (up to 200 million roentgens and higher). It was also noted that the radiation effects are independent of dose rate over the range $10^4$ to $10^6$ r/hr, and that the reproducibility of the results is very stable.

The simplicity of the post-irradiation experimental technique in studying the solutions, the broad range of applicable doses (up to $10^8$-$10^9$ r), and the independence of radiation effect from dose rate over a wide range, combine to render aqueous solutions of glucose and sucrose an excellent dosimetric liquid. The use of glucose solutions is more convenient and more feasible in view of the longer shelf life and service life of ampules containing the solutions, once prepared and duly sterilized, and moreover on account of the tendency of changes occurring in the solution in response to irradiation to remain constant, added to the insensitivity of those changes to the temperature at which the exposure took place (up to 80°C inclusive).

The stability of sucrose solutions is much lower; they decompose appreciably on prolonged standing, and aftereffects appear following irradiation, besides which variations in angle of rotation as a function of irradiation dose are found to be directly dependent on the temperature of irradiation, and to increase sharply as that temperature is raised.

## LITERATURE CITED

1. H. Fricke and S. Morse, Am. J. Roentgenol. 18, 430 (1927).
2. H. Fricke, Philos. Mag. 7, 129 (1929).
3. T. Hardwick, Canad. J. Chem. 30, 23 (1952).
4. M. Day and G. Stein, Nucleonics 8, 2, 34 (1951).
5. Ya. L. Shekhtman, et al., Doklady Akad. Nauk SSSR 74, 767 (1950).
6. L. Mongini and E. Zimmer, J. Chim. Phys. 50, 491 (1953).
7. E. Weber and R. Schuler, J. Amer. Chem. Soc. 74, 4415 (1952).
8. I. Draganic, J. Chim. Phys. 52, 512 (1955).
9. S. Goldblith, and B. Proctor, Nucleonics 7, 2, 83 (1950)
10. H. Andrews and P. Shore, J. Chem. Phys. 18, 1165 (1950).

# VII SESSION OF THE LEARNED COUNCIL OF THE JOINT INSTITUTE FOR NUCLEAR RESEARCH (DUBNA)

M. Lebedenko

The scheduled VII session of the Learned Council of the Joint Institute for Nuclear Research was convened at Dubna, November 21 to 25, 1959

Leading physicists from the member nations of the Institute took part in the deliberations of the session. These included the head of the Tirana University faculty Petrak Pilika, the Director of the Sofia Physics Institute Academician Georgi Nadzhakov, the Director of the Central Institute for Physical Research in Budapest Academician Lajos Jánosi, the Director of the Nuclear Research Institute of the Polish Academy of Sciences Academician Andrzej Soltan (since deceased), the Director of the Nuclear Physics Institute in Bucharest Prof. Horia Hulubei, the Director of the Central Nuclear Physics Institute Prof. Heinz Barwich (German Democratic Republic), the vice director of the Atomic Energy Institute of the Chinese Academy of Sciences Peng Huan-wu, and many other prominent scientists from the socialist countries. Also participating in the deliberations of the Learned Council were the Embassy representative of the Democratic Republic of Vietnam Nguyen Van Sao, and the representatives of the Main Control Board on the Uses of Atomic Energy, attached to the Council of Ministers of the USSR, Prof. D. V Efremov and Prof. K. N. Meshcheryakov.

During the session, the chair was shared alternately by D. I. Blokhintsev, Director of the Joint Institute and Corresponding Member of the USSR Academy of Sciences, Prof. Wang Hang-ch'ang (Chinese People's Republic), Vice Director of the Joint Institute, and Emil Dzhakov, Corresponding Member of the Bulgarian Academy of Sciences.

Following a report by D. I. Blokhintsev and the fulfillment of the decisions reached at the V and VI sessions of the body, the Learned Council adopted an ample resolution summarizing the important successes achieved by the directors and staff of the Institute during 1959. The resolution singled out for emphasis the principal trends to be followed in the development of the research activity of the scientists assembled from the 12 socialist countries working at Dubna on problems within the scope of the peaceful uses of the energy contained within the atomic nucleus.

The main point on the agenda at the VII session of the Learned Council was the presentation and discussion of reports on the scientific activities of the Institute laboratories during 1959, and their plans for 1960.

Of outstanding interest was the report on the results of research work conducted at the High-Energies Laboratory, by the now vice director of that laboratory Prof. V. A. Petukhov. Information on the research conducted at the laboratory with the aid of the 10 Bev proton synchrotron had been made public at Kiev, on the occasion of the IX International Conference of High-Energy Physics. The research efforts deal primarily with problems of interaction between high-energy protons or pi-mesons and nucleons or nuclei, the generation and interactions of "strange" particles, and the structure of nucleons. Plans for 1960 call for diversified studies along the principal trends in high-energy physics, including search efforts to find new particles, and the study of unknown or little-known interactions between elementary particles. New methods and techniques will be developed. Further design improvements are in store for the proton synchrotron.

V. P. Dzhelepov, Doctor of Physical and Mathematical Sciences, delivered a report on the work of the oldest laboratory of the Institute, the Nuclear Problems Laboratory, of which he is the head. This laboratory only recently celebrated its tenth anniversary (the synchrocyclotron, at that time the world's most powerful particle accelerator, was commissioned in 1949).

During the year covered under the report by Dr. Dzhelepov, over 100 research studies were completed, and in particular valuable results were secured on problems of weak interaction, generation of mesons, and interactions between pi-mesons and nucleons. Articles dealing with 75 of these studies have already been published in Soviet and foreign scientific publications. The commissioning of the world's first accelerator with spatial variation of the magnetic field, built at this laboratory, and the development of new specimens of research equipment attracted considerable attention on the part of the participants at the International Conference on Accelerators and Experimental Equipment (Geneva 1959).

A report on the work in progress at one of the new laboratories of the Institute, the Neutron Physics Laboratory, was delivered by its Director, Corresponding Member of the USSR Academy of Sciences I. M. Frank. Construction work is largely complete on the building which is to house the novel-design research reactor. Assembly of the reactor is nearing completion. Tests have been performed with success on the basic reactor

components and the control equipment. Research facilities and instrumentation are being checked out. Work on automating the processing of results of measurements is being advanced. The laboratory is undertaking a program of research in collaboration with other scientific institutions. According to the opinion expressed in the report by the Director of the Nuclear Reactions Laboratory, Corresponding Member of the Academy of Sciences of the USSR G. N. Flerov, the role assigned to the physics of multiply charged ions will take on increasingly greater importance in the overall development of nuclear physics. In an effort to speed the day when the accelerator of multiply charged ions will be inaugurated, the scientific staff of the laboratory, on their own initiative, devoted some of their free time to helping the workers assigned to assemble the machine in place.

In collaboration with the Institute of Atomic Energy of the USSR Academy of Sciences, a good deal of work was carried out on the properties of element 102, produced for the first time in the Soviet Union. Notable successes were scored in the development of techniques of express physical analysis of short-lived elements.

Following a report by Academician N. N. Bogolyubov, the session of the Learned Council took note of the fact that the Theoretical Physics Laboratory had carried to completion a program of scientific research work during 1959. Significant accomplishments were registered in the development of the theory of dispersion relations, the structure of nucleons, and theories of elementary particles.

After a vigorous discussion participated in by many Soviet and foreign physicists, the Learned Council adopted a resolution based on the reports of the laboratory directors, and confirmed their provisional programs for 1960.

The report of the Vice Director of the Institute, E. Dzhakov, was devoted to the development of work on automating the processing of photographic plates obtained by means of chambers and thick-layer photographic emulsions. The staffs of the experimental-design bureaus of the Joint Institute and the Nuclear Problems Laboratory have developed two facilities for automatic processing of plates. These machines yield systematized measurements data in a form suitable for feeding into high-speed computers. An instrument designed for the same purposes was built as a result of joint work on the part of Hungarian and Polish institutes. All three machines will be in operation at Dubna. They are presently being given an operational checkout.

The Learned Council adopted a resolution on the further expansion of work related to automating the processing of experimental materials.

Vice Director of the Joint Institute Wang Hang-ch'ang presented a report to the session on the Institute's international relations and ties. During 1959, the international contacts of the Institute were successfully broadened primarily in the following aspects:

1) the holding of international workshop meetings at the Institute;

2) participation in international and national scientific conferences;

3) tours of research staff members to the member-nations of the Institute for the purpose of giving lectures and reports;

4) rendering aid to specific scientific teams working in the member-nations of the Institute on topics of common interest to the Institute;

5) exchange of scientific information with the leading scientific institutions of the world.

In the resolution adopted on the basis of the report, the Learned Council outlined a program of measures for the further development of the Institute's international ties.

As a result of the Institute's successful activities, the number of applications on the part of member-nations of the Institute for the admission of scientists an and engineers of their respective countries to the Dubna staff has increased. This was reported by Prof. Dzhakov in a report on the composition of the staff. The number of foreign physicists from the socialist countries is increasing. These scientists are actively engaged in all of the basic research efforts of the Institute. The Learned Council adopted a resolution,the gist of which is to double the number of scientists and engineers from those countries working at the Institute during 1960.

The deliberations of the VII session of the Learned Council, proceeding in an atmosphere of friendship and creative discussion, were successfully brought to completion. The fulfillment of the resolutions adopted by the session will provide the Joint Institute for Nuclear Research with the opportunity to carry forward and on high the banner of socialist science in peaceful competition with the scientists of the capitalist countries.

* * *

# CONFERENCE OF REPRESENTATIVES OF 12 GOVERNMENTS

M. Lebedenko

On November 26-28, 1959, at Dubna, a session of the Committee of authorized representatives of the governments of member-nations of the Joint Institute for Nuclear Research was convened. This constitutes the highest governing body of the Institute.

The session was opened by the Director of the Joint Institute, Corresponding Member of the USSR Academy of Sciences D. I. Blokhintsev. On the suggestion of the Hungarian delegation, representatives of Albania, the Chinese People's Democratic Republic, and Mongolia were elected to the presidium.

Prof. Sondom (Mongolian Democratic Republic), who chaired the first session, gave the floor to Prof. Blokhintsev for a report summarizing the activities of the Institute during the outgoing year.

In his report, the Director of the Institute subjected to analysis the most important research investigations in the field of nuclear physics completed at Dubna by dint of the joint efforts of scientists from all the socialist countries. He noted that the scientific activities of the Institute during 1959 were greatly expanded thanks to the development of work on the proton synchrotron of the High-Energies Laboratory. Several of the experimental and theoretical investigations completed here throw some light on problems concerning the structure of nucleons and the laws governing the generation of "strange" particles. One of the new laboratories, the Neutron Physics Laboratory, has worked out a plan for an interesting experiment aimed at verifying the general theory of relativity. This is the first experiment of its kind under conditions existing upon the earth. In the Nuclear Problems Laboratory, which is marking its tenth year of existence, investigations were conducted on nucleon and meson physics.

During 1959, the international associations of the Institute were greatly broadened.

The Administrative Director of the Joint Institute, V. N. Sergienko, delivered a report on the Institute's budget, program of capital outlays, and staff membership for the year 1960.

Representatives of 12 governments put their signatures to a Protocol acknowledging their high estimate of the activities of the management and staff of the Joint Institute for 1959, and taking note of similar problems for 1960. The financial report of the Institute for the outgoing year, and the budget and staff expenditures for 1960 were confirmed.

This session of the Committee also took up another question of paramount importance. The authorized representatives of the 12 governments exchanged views of the need for further widening the scope of diversified collaboration between the socialist countries in the field of the peaceful uses of atomic energy. Most of the lands of socialism presently have at their disposal ample cadres of highly trained scientists, nuclear reactors, accelerators, and other experimental facilities built with the aid of the USSR, i.e., favorable conditions have been created for research work in the field of the peaceful uses of atomic energy. This renders imperative an expansion of scientific collaboration.

Taking into account the desires expressed by the scientists of the socialist countries, the authorized representatives adopted an appropriate resolution; the idea of utilizing the bodies of the Joint Institute for Nuclear Research to facilitate this collaboration was approved.

By decision of the Committee of authorized representatives article 18 of the by-laws of the Joint Institute for Nuclear Research were amended by addition of the following clauses:

Directorship and Learned Council:

a) shall be empowered to organize, in response to the request of any member-nation of the Joint Institute for Nuclear Research, consultations on research programs in the field of the peaceful uses of atomic energy;

b) shall be empowered to convene, in case of necessity, sections of working commissions of the Learned Council, general-scientific and specialized scientific and enginnering conferences and colloquia of specialists from member-nations of the Institute for the purpose of exchange of experiences, and shall also be empowered to organize the exchange of individual specialists on problems of scientific research within the field of the peaceful uses of atomic energy;

c) shall present for approval, before a meeting of the authorized representatives of the governments of the member-nations of the Joint Institute for Nuclear Research, plans involving joint development of scientific problems within the scope of the peaceful uses of atomic energy, on those occasions judged convenient by the Learned Council;

d) shall be empowered to set up provisional working commissions or permanent sections of the Council to expedite preliminary work on proposals pertinent to specific scientific research problems within the scope of the peaceful uses of atomic energy.

The resolutions of the Committee of authorized governmental representatives is an important landmark in the struggle of the scientists of the lands of socialism to broaden the scope of possibilities open to the peaceful utilization of atomic energy.

* * *

# III ALL-UNION TECHNICAL-SCHOOL CONFERENCE ON ELECTRON ACCELERATORS

Yu. M. Ado and K. A. Belovintsev

On the initiative of the Tomsk Polytechnic Institute, the III All-Union Intertechnical-School Conference on Electron Accelerators was held at Tomsk in September 1959. Representatives of educational institutions, scientific research institutes, and industrial enterprises took part in the Conference.

The papers delivered at the Conference were devoted not only to the theory and engineering design of accelerators, but also to problems concerning the applications of electron accelerators in the various branches of the national economy, e.g., in metallurgy, machine manufacture, geology, and medicine.

The urgent problem of increasing the intensity of electron accelerators found its reflection in several papers. A report was heard on the inauguration of the 25 Mev double-chamber pulsed stereobetatron. Increased dimensions of the operational region and the use of exterior high-voltage injection made it possible to increase the radiation dose in a single pulse to two or three orders of magnitude above the radiation dose obtainable from a conventional betatron of the same energy.

Problems widely discussed at the Conference included the process of capture into a betatron orbit, scattering of electrons by residual gas during acceleration, the use of external injection, increasing the energy of injected particles, investigations into the behavior of electrons undergoing acceleration, new accelerator designs and experiments on the use of powerful cathodes related to the problem of increasing the intensity of electron accelerators.

Some of the papers touched on problems of dynamics of particle motion inside accelerators. One report was read on new results obtained in the solution of the problem of the effect of quantum radiation fluctuations on the motion of electrons in a cyclic accelerator. It was shown that the quantum fluctuations lead to increased amplitude of betatron oscillations without building up synchrotron oscillations. An analysis of the motion of electron beams with polarized spins in a cyclic accelerator showed that acceleration should be accompanied by precessing of the spin.

New information was contained in the papers discussing experiments on the polarization properties of radiation from the "radiating electron," and on the study of coherent electron radiation.

Some reports touched on the theory of elementary particles. For example, the questions of generation of an electron-positron pair by a $\gamma$ photon with spin effects and the finite dimensions of the nuclei taken into account were analyzed, as were interaction between nonrelativistic baryons with their structure taken into account, longitudinal polarization of Dirac particles in weak interactions. A paper discussing nonconservation of parity drew particular attention.

Participants at the Conference gave serious attention to problems of control, monitoring, and stabilization of the performance of accelerator facilities, and to research and development work on auxiliary equipment and instrumentation. Papers on techniques for stabilizing the intensity level and energies of accelerated particles launched a lively discussion.

Extensive material was presented in papers dealing with engineering and design projects for electron accelerators with energies up to 30 Mev, intended for work under specific conditions in some particular branch of the national economy. Particularly deserving of note are projects on the design of specialized miniature induction accelerators for geologic applications, especially bore-hole logging. The use of betatrons in geophysical investigations in the ore-processing and petroleum industries has made possible improved techniques in prospecting for minerals. In semiconductor physics and metallurgy, a method for the effective determination of oxygen content in semiconductors and metals based on the photonuclear reaction of oxygen has been successfully developed. In the physics of dielectrics, valuable data on the radiation stability of several properties of solid dielectrics have been obtained from the study of the effects of betatron bombardment of matter.

The Conference also heard a report on applications of a betatron radiation in nondestructive testing of thick metal parts.

Much interesting information was garnered from the papers presented by the Tomsk Medical Institute, on betatron applications in therapy, the study of the effects of large and small radiation doses on various body organs, on metabolism and on the nervous system. Experiments have demonstrated that the betatron is in a number of cases a most effective instrument for therapy of malignant tumors.

In a paper dealing with the effects of betatron radiation on the organism, the pathological action of small doses of ionizing radiation acting over a protracted time interval were stressed.

In conclusion, we should take note of the fact that the need for electron accelerators in the various branches of science, engineering, and medicine, greatly increased of late, puts a premium on mass production of machines of that type. The resolutions adopted by the Conference

stressed the need to design a ~30 Mev model betatron for industrial applications.

The Tomsk Polytechnic Institute took on the responsibility of publishing the proceedings of the Conference in the form of a symposium.

* * *

# SYMPOSIUM ON EXTRACTION THEORY

I. V. Seryakov

A symposium of the theory of extraction processes was held December 3-4, 1959, at the V. I. Vernadskii Institute of Geochemistry and Analytic Chemistry of the USSR Academy of Sciences. The purpose of this symposium was to discuss the most important questions in extraction theory. Problems of the chemistry and thermodynamics of extraction equilibria, the effect of the nature of the extracting agent and salting-out agents, composition of the extractable compounds and their interaction with water and extractant molecules were discussed. Five papers were read on these questions.

A paper delivered by V. I. Kuznetsov, "The Chemistry of Extraction Processes," dealt with chemical conceptions of extraction processes. These concepts are based largely on facts lodged in the theory of the action of analytical organic reagents. The reporter holds the view that loss of hydrophilic properties by an element falls little short of being a basic precondition for efficient extraction of the element. His paper reports an attempt in this vein to correlate the tendency of ions to form extractable compounds with the amount of charge $z/n$ on each atom of the ion, $z$ being the ionic charge, and $n$ the number of atoms forming the ion. In those cases where ionic radius is known, it must be taken into account and the proclivity to extraction must be characterized by the charge density, i.e., by the amount of charge per unit surface. Extractability of ions shows improvement in inverse proportion to charge density and accordingly, has better chances the weaker the hydration. This relationship was illustrated by a few examples of extraction of large-molecule colored complexes of thorium and uranium with organic reagents.

This correlation of extracting power with value of $z/n$ brought on an animated discussion. K. B. Yatsimirskii drew attention to the need to secure more precise information on the range of applicability of the relationship postulated by Kuznetsov, in view of the possible examples which could be cited in contradiction to the latter's assertions. M. M. Senyavin remarked that the complexities inherent in the extraction process, including the variegated processes of intermolecular and chemical effects and solvation, make it difficult to single out any one simple quantity which could effectively characterize degrees of extractability; taking the number of atoms in the ion into account appears especially promising where it is a question of extracting compounds with complex organic molecules, when the role of disperse-phase intermolecular interaction is paramount.

V. V. Fomin, in a paper entitled "Extraction Equilibria," reviewed extraction processes from the standpoint of those chemical reactions in which the extractable element participates in both phases. Following this approach, he divides extraction processes into two groups. The first group has assigned to it processes of extraction of metal cations based on simple exchange reactions between cations and reagent, the latter being a weak acid (hydroxyquinoline, cupferron, dithizone) and sometimes taking on the role of extractant (acetylacetone, butyric acid, etc.). The second group combines extraction of inorganic anions by those extractants (which could double as reagents) capable, by interacting with acid, of forming cations preferentially to entering into an interaction with an inorganic anion (amines, etc.). It was noted in the report that the element need not always lose its hydrophilic properties in the extraction process. It was proved, for instance, that the dissolving of the chloride anion of iron by ethers proceeds in the presence of a minimal and necessary amount of water.

An interesting discussion ensued, stimulated by the mention in Kuznetsov's and Fomin's papers of the oxonium mechanism of extraction of elements, suggesting a transition of the organic oxygen-containing extractants in a strongly acidic medium to oxonium cations which, by interacting with inorganic anions, form extractable oxonium salts. This view, widely propagated in the literature, is, in Fomin's opinion, difficult to reconcile with the transfer to the organic layer of oxygen-containing extractants in amounts larger than

required for the formation of oxonium salt. A. A. Lipovskii and V. A. Mikhailov took the floor in this discussion. The latter cited some highly interesting data from the literature on the extraction of protactinium, of pertinence to the oxonium mechanism.

A paper submitted by A. V. Nikolaev, N. M. Sinitsyn, S. M. Shubina, "Donor-Acceptor Properties of Extractants," was devoted to the effect of the nature of the organic solvent on extraction. Based on the example of a single class of compounds containing phosphoryl oxygen, the dependence of their extractive properties on the value of the dipole moment of the P. . .O bond, which is in turn altered by the introduction of various substituents into the extractant molecule, was investigated. According to data cited by the reporters, the increase in the dipole moment contributes to an enhanced degree of extraction of the elements.

N. N. Basargin, on taking the floor, noted that it is not only the nature of the extractant which plays a great role in extraction, but also the nature of the extractable element. Extraction of elements which manifest primarily a proclivity to yield compounds with a covalent bond may lead to an opposite result. From the point of view of the dependence of total bond energy on the ionic character of the bond, enhanced ionic character of the bond may sometimes not only fail to contribute to extraction, but may even impede it.

An interesting paper on the extractive properties of of phosphorus-containing extractants of different classes was submitted by V. G. Timoshev, who took note of the decisive role of the donor-acceptor properties of the given extractant species.

The phenomenon of salting-out in extraction processes was discussed in a paper read by O. Ya. Samoilov and V. I. Tikhomirov, who, on the basis of a statistical treatment of the thermal motion of water molecules, made an attempt to account for differences in the action of salting agents found in the principal (Ca, Sr) and side (Zn, Cd) subgroups of the Mendeleev periodic table. The explanation offered by the authors took into account the dehydrating action of salting cations in connection with the covalent character of the bonds they formed. A. A. Nemodruk, who took the floor in the discussion, drew attention to the fact that, in order to explain the salting-out process, not only dehydration, but also the concentration of the anion of the salting agent, the variation in the mutual solubility of both phases introduced by the presence of the salting agent, and several other factors must be taken into account.

A report delivered by A. M. Rozen was devoted to the use of thermodynamics in describing extraction equilibria. Resting on examples of extraction processes classified by the reporter in accordance with the character of the dissociation involved, the nature of the interaction with the solvent, and the state of the elements in the aqueous phase, the reporter demonstrated the possibility of using activity constants to arrive at a type of extraction process and a correct interpretation of the mechanism responsible for that process and, by drawing upon the theory of regular solutions, also the possibility of accounting for the effect of many solvents (in the case of tributylphosphate extraction). The reporter adduced some interesting examples where neglect of activity constants would result in the discovery of nonexisting compounds and other gross errors. Yatsimirskii emphasized the need for a thermodynamical approach to study of extraction systems, took note of the limited scope of known thermodynamical data and consequently of the need to determine such data, particularly from experiments conducted at different temperature levels. In the discussion, Kuznetsov noted a disadvantage inherent in the use of activity constants, namely the need to determine these quantities experimentally, which excludes the possiblity of predicting degree of extraction on the sole basis of a knowledge of the chemical composition of the element, reagent, and extractant.

V. M. Vdovenko, A. K. Babko, D. D. Sublobov, I. R. Krichevskii, and A. A. Chaikhorskii were among those participating in the general discussion.

The symposium defined the principal trends apparent in further research on the theory of extraction processes, particularly: shedding light on the causes of selective solubility of inorganic and organic compounds in various solvents; expansion of investigations into solvation, expecially hydration of ions and molecules; further study into the chemical mechanism and thermodynamics of extraction equilibria; expansion of investigations aimed at determining the composition and nature of extracting compounds.

The symposium recommended the organization of a permanently active seminar on extraction theory.

The basic materials of the symposium will be published in the form of a collection of articles on extraction, to be put out by Atomizdat (Atomic Press) in 1960.

* * *

# DEVELOPMENT OF NUCLEAR POWER IN SWEDEN

M. Sokolov

The water power resources of Sweden were being used to 36% potential in 1958; Swedish hydroelectric power stations produced 29 billion kw-hr of electric power. With the extrapolated annual increase in production of electric power at hydroelectric stations mounting by 2.0-2.5 billion kw-hr (the 1958-1959 increment), the utilization of the hydropower resources of the country should arrive at their practical limit in some 20-25 years, in the opinion of Swedish power specialists.

Electric power stations fired by fossil fuels serve in Sweden as a back-up to cover periods of peak load. In years of low rainfall, the share of these stations in the over-all production of electric power was 10-12%. The further development of this type of power utilities could proceed only through increasing the already staggering imports of fossil fuels. At the present time, the cost of a single kw-hr of electric power is 0.02-0.03 krona, while the cost of a single kw-hr of electric power produced at a fuel-fired power plant is more than double (0.05-0.07 krona).

Under these conditions, nuclear power in Sweden is assured a competitive status. It can draw upon existing uranium reserves in the country. Sweden's uranium ores are low-grade, but reserves are adquate to provide a source of nuclear raw material for industrial-scale uranium production. Uranium is contained in the Swedish clay shales. The uranium content of the shales varies from 100 to 300 g/ton. Uranium reserves in the form of shale beds are currently estimated at 500 thousand tons minimum [1]. Highest uranium content is found in shales from the Kvarntorp (Närke Province) and Billingen (Västergötland Province) occurrences (200-300 g/ton). The Kvarntorn shale fields have the added advantage of being accessible to open-pit working.

The AB Atomenergi company, under joint private and government ownership, was set up in 1947 to carry through experimental work on utilization of nuclear power [4]. After 1950, Atomenergi and firms subcontracted to it proceeded to lay the foundations of the uranium industry. A plant for processing of uranium concentrates from shales went into operation in Kvarntorp in 1953. The initial output of the processing plant was 5 tons yearly, converted to uranium metal, and increased to 10 tons yearly by 1957 [5, 6]. Mining of uranium-containing shales at Kvarntorp went hand in hand with the development of underlying bituminous shales, which went to liquid fuel on an industrial scale, at a special processing plant [7]. This combined venture made it possible to appreciably scale down uranium concentration costs. Subsequent processing of concentrate containing 20-30% uranium, yielding uranium dioxide, took place at chemical facilities in Stockholm. Part of the uranium dioxide was used directly in reactors, the rest was reprocessed to yield uranium metal [8, 9].

In 1958, construction was started on a large-scale uranium plant at Ranstad, for processing shales from the Billingen beds. The plant was built to handle 120 tons of metal uranium production annually at peak output. Plans call for completion of construction work in 1962-1963 [10]. Scaled-up production schedules combined with the use of by-products for manufacture of sulfuric acid, and combustion of the shale residues in the kilns of a cement factory brought uranium costs down to roughly the same level as that produced in the higher-grade deposits in the USA and Canada.

Parallel with its uranium manufacturing activity, Atomenergi undertook construction of nuclear research reactors. The first heavy-water research reactor R-1 (see Table) was started up in 1954 in Stockholm. The reactor was nested in a 35-meter deep underground gallery hollowed out of granite rock. Its thermal power rating was initially 300 kw, and has now been brough up to 600 kw. The reactor is employed for production of radioactive isotopes for scientific, industrial, and medical applications [6, 8].

A second heavy-water research reactor, R-2, designed for materials testing, has been built at Studsvik (started up in late 1959) on the Baltic seacoast

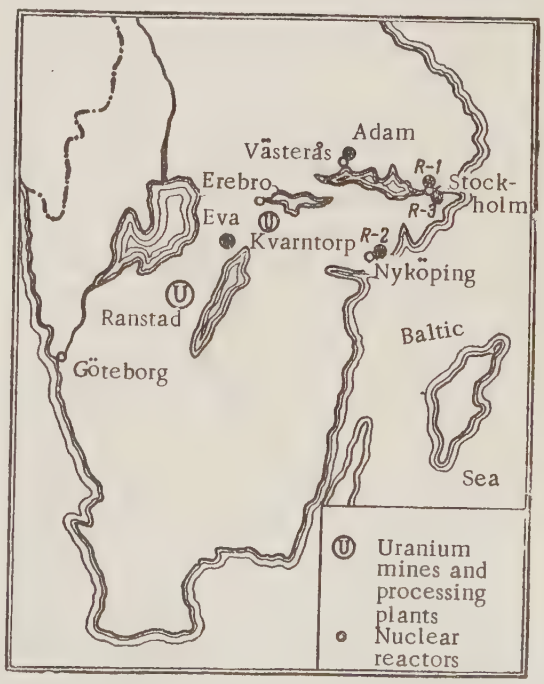


Nuclear reactors and uranium mines and processing plants in Sweden.

Nuclear Reactors Built, Under Construction, or in Planning Stages, in Sweden

| Name, location, and purpose of reactor | Year started up | Fuel used; loading | Moderator (heavy water), tons | Coolant; inlet and exit temperatures, °C | Power, Mw |
|---|---|---|---|---|---|
| R-1, Stockholm, research | 1954 | Natural uranium; 3 tons | 5 | Heavy water | 0.6 (th) |
| R-2, Studsvik, research | 1959 | Enriched (20%) uranium $U^{235}$ | No available data | Heavy water | 30 (th) |
| R-3, Farsta, heat power | 1962-1963 | Uranium dioxide; 11 tons | 30 | Heavy water; 205-220 | 125 (th)<br>15 (e) |
| "Adam", Västeras, heat power | 1960 (?) | Uranium dioxide; 9 tons | 26 | Heavy water; 80-140 | 75 (th) |
| "Eva", central Sweden, steam power station (planned) | 1963 | Uranium dioxide; 42 tons | 75 | Carbon dioxide gas; 100-150 | 444 (th)<br>135 (e) |
| Reactor project for a steam power station | No available data | Uranium dioxide; | No available data | Carbon dioxide gas; 115-410 | 525 (th) |
| Same | No available data | Natural uranium metal | No available data | Carbon dioxide gas; 156-400 | 525 (th) |

near Nykoping, at the site where the National Scientific Research Center of Nuclear Power Problems is being built by Atomenergi. The reactor was purchased in the USA. The enriched uranium (20% $U^{235}$) to feed the reactor was also obtained from the USA. Other plans for Studsvik include building a zero-power reactor R-0 to facilitate studies of different fuel-element designs and coolants, a 5 Mev Van de Graaff accelerator, and a pilot plant for reprocessing spent nuclear fuel. Construction of the Scientific Research Center at Studsvik is slated for completion by the mid-sixties [6, 11].

In 1956, the first Swedish ten-year development program for nuclear power, covering the period 1956-1965, was made public; this program calls for building five or six nuclear power plants of 75-100 Mw(th) rating for space heat and process heat, and one nuclear electric power station of 100 Mw(e) rating. Within the framework of this program, design and construction work has been started by Atomenergi and the State Power Control Board on three nuclear facilities: "Adam," R-3, and "Eva." Funds were allocated in the state budget for the building of these facilities [12].

All of the facilities are being planned as underground installations, sunk several tens of meters deep into solid granite and granite-gneiss bedrock, allowing for exceptionally reliable shielding from radiation and for localization of hot ejecta in the event of an accident. This makes it possible to build reactors in the direct vicinity of cities and industrial sites, a very important consideration where reactors function as space-heat and process-heat utilities. The "Adam" reactor is designed to satisfy heat-power needs in Västeras (70,000 inhabitants). The cost of 1 kw-hr of thermal power for a plant working 5,000 hours yearly will be 0.003-0.004 krona, while the cost of 1 kw-hr of thermal power produced in Sweden by combustion of imported fossil fuels in conventional heat-power stations is 0.013-0.14 krona [13]. The R-3 reactor is being built in the southeast suburbs of Stockholm. It is designed to provide h heat power for the new residential complex of Farsta (40,000 inhabitants). The electric power generated by the turbogenerators of the power plant (15 Mw) will be fed into the Stockholm power system [14].

The development of nuclear power for space-heat and process-heat applications gets top priority in Sweden. Besides supplying heat for household and community needs, nuclear reactors will also provide steam to numerous enterprises in the paper and pulp industry, which occupies a prominent place in the country's economy.

Construction of the "Eva" facility was the first step in the program for building nuclear-fired steam-condensation electric power stations. The construction site selected, tentatively, consists of granite cliffs on the banks of Lake Unden, southwest of the town Askersund in Central Sweden. Construction costs have been tentatively set at 180 million kronor [6]. In the opinion of Swedish specialists, an economically feasible heat power level for the nuclear steam-condensation electric plant is 300-500 Mw (th), corresponding to electric power 75-125 Mw(e) [15]. One of the projects elaborated by the ASEA company for the "Eva" electric power station involves a reactor rated at 444 Mw (th) and 135 Mw (e) [16]. At the Second International Conference on the Peaceful Uses of Atomic Energy (Geneva, 1958), the Swedish delegation presented two reactor projects for nuclear-fired electric power stations with ratings of 525 Mw (th) each [17].

A heterogeneous-type thermal neutron reactor burning natural uranium fuel was selected for the nuclear power facilities now under construction or on the planning boards. Plans for a further stage in the development of nuclear power envisage use of plutonium as secondary nuclear fuel. After the techniques for regenerating spent uranium will have been worked out at the Studsvik pilot plant, construction will begin on a scaled-up plutonium plant capable of providing the fuel needed by the nuclear electric power stations slated for construction in 1966-1975 [15].

Heavy water is the choice for moderator for all of the Swedish reactors. The R-3, "Adam," and "Eva" reactors require about 150 tons of heavy water (in the initial loading), which will be bought in the USA, price fixed at 320 kronor/kg by bilateral agreement [18]. The ASEA plans to build a heavy-water manufacturing plant of 20 tons annual capacity in Sweden [19]. However, since the net costs of heavy water production in Sweden run very high, Swedish nuclear power will be centered on imported heavy water in the foreseeable future.

In a number of articles published in Swedish technical journals [1, 15], calculations are adduced for uranium consumption and electric power costs extrapolated to nuclear electric power stations now being planned. At a cost of 384 kronor/kg for natural uranium, the fuel component in electric power costs will be 0.011 krona/kw-hr. The cost of 1 kw-hr electric power at Swedish nuclear-fueled electric power stations of 400-500 Mw (th) rating and 25% thermal efficiency would be 0.02-0.04 krona, i.e., slightly higher than the current cost of electric power developed at Sweden's hydroelectric power stations.

In 1959, the State Power Control Board and the Atomenergi company adopted the decision to temporarily halt work on building the "Adam" reactor at Västeras, because of sizable financial and engineering complications, and to redouble efforts in the construction of the R-3 reactor at Farsta, with the start-up date for the latter postponed from 1960-1961 to 1962-1963 [20].

LITERATURE CITED


1. E. Svenke, Iva Tidskr. 26, 3, 75 (1955).
2. E. Svenke, P/782 (Geneva, 1955).*
3. Nucleonics 14, 1, 15 (1956).
4. Statistik årsbok för Sverige 1958 (Stockholm, 1958) p. 326.
5. E. Svenke, P/784 (Geneva, 1955).*
6. Nucleonics 15, 12, 22 (1957).
7. E. Svenke, P/782 (Geneva, 1955).*
8. H. Brynielsson, 5th World Power Conference (Vienna, 1956) Paper 128 J/4, 4.
9. B. Hargö, Nucl. Engng 2, 16, 271 (1957).
10. Teknik för alla 19, 4, 6, (1958).
11. Engineering 183, 4764, 826 (1957).
12. G. Cederwall, P/2342 (Geneva, 1958).†
13. I. Wivstand and C. Mileikovsky, P/136 (Geneva, 1958).†
14. P. Margen, P/136 (Geneva, 1958).†
15. Tekn. tidskr. 86, 15, 351 (1956).
16. R. Liljeblad, Nucleonics 15, 11, 165 (1957).
17. R. Liljeblad and K. Madsen, P/2419 (Geneva, 1958).†
18. Dagens Nyheter (September 6, 1957).
19. Atomwirtschaft II, 11, 383 (1957).
20. Nucleonics 17, 6, 30 (1959).


*Reports from the First International Conference on the Peaceful Uses of Atomic Energy.

†Reports from the Second International Conference on the Peaceful Uses of Atomic Energy.

* * *

# PLASMA RESEARCH ON THE STELLARATOR

The Institute of Atomic Energy of the USSR Academy of Sciences had the honor of a visit by a group of American specialists. Included in this group was the prominent American astrophysicist Prof. L. Spitzer, renowned as the inventor of the Stellarator and as leader of a scientific research team on thermonuclear problems at Princeton University. Below we present a brief talk by L. Spitzer before the seminar of the Institute of Atomic Energy on October 16, 1959, as reconstructed from the notes of D. A. Frank-Kamenetskii.

## Organization of the Research Work

Work on the thermonuclear problem conducted at Princeton University under the designation of "Project Matterhorn" is associated with use of the apparatus now known as the Stellarator. The work is being carried out

at the university under contract with the Atomic Energy Commission. As a rule, detailed contracted work is carried out in the educational subdivisions of the university. In this case, because of the great scope and complexity of the work, an exception was made: a special research group was assembled at the university. The organizational set-up for project Matterhorn is indicated in the accompanying diagram (Fig. 1).*

The chairman of the supervisory committee H. D. Smyth is known to all as the author of a book describing the development of work on atomic energy in the USA during the second world war; at the present time he is a professor of physics at Princeton. Second in charge of the project is Dr. Gottlieb.† The Director has five subdivisions under him: a theoretical section (15 men) headed up by Dr. Frieman, an experimental section (40 men) under Dr. Gottlieb, an engineering section (40 men), a research and development section for stellarator design (15 men) and an administrative section. The figures in parentheses indicate the number of scientists and engineers, whereas the total number of persons involved in the project numbers some 350. About half of the volume of efforts are directed toward solving the problem of high-temperature plasma containment over a protracted period by means of the stellarator, while the other half is aimed at research on fundamental problems in plasma physics, which is also being carried out primarily in the stellarator configuration.

## Plasma Equilibrium in the Stellarator

The theoretical foundations of plasma containment in the stellarator have been reported on and published on repeated occasions. Here we shall give only a brief rundown on the work done. The Stellarator is a toroidal configuration (not necessarily a simple circular torus, rather any closed system) with an external applied magnetic field, with what is known as a rotational transform being effected within the system (see Fig. 2). The essence of the transform is that a line of force emerging from point A and circulating around the torus does not return to the same point, but intersects the original transverse section at point A'. After making several loops, the line of force will have covered an entire closed surface. These surfaces are known as magnetic surfaces. It is their existence which makes the equilibrium state of the plasma possible. The rotational transform may be realized in practice by a variety of methods. In the early work in Project Matterhorn we resorted to the simplest method, that of a torus twisted into a figure-eight. At the present time another technique has gained preference: additional helical stabi-

* All of the drawings, except for Fig. 4, were reproduced from memory by L. Spitzer, and are purely heuristic in character.

† The author of the talk, L. Spitzer, is the director of Project Matterhorn.

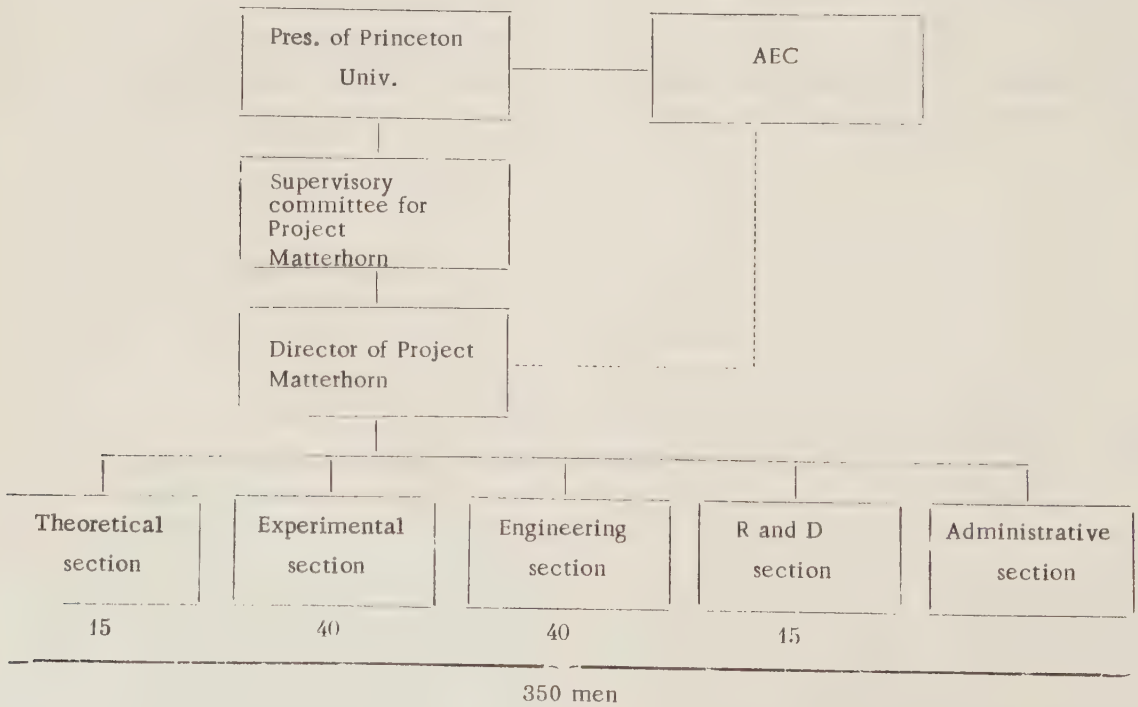


Fig. 1. Organizational structure of Project Matterhorn (figures indicate number of engineers and scientists assigned to each section).

lizing windings are placed beneath the basic winding of the constant magnetic field.

The properties of the plasma equilibrium configuration in the Stellarator and in the first instance plasma stability are determined by the value of the parameter $\beta = \frac{nkT}{H^2/8\pi}$, which is the ratio of the plasma gas pressure to the magnetic pressure. The basic requirement is that the values of $\beta$ not run too high. In studies of conditions of magnetohydrodynamic stability based on a conducting-fluid model, it was found that stable configurations are possible when $\beta$ does not exceed a certain critical value which closely approximates 0.1, and that stability conditions are extremely sensitive to the presence of helical stabilizing coils. At the present time, Kruskal and Rosenbluth are studying stability conditions with the aid of Boltzmann equations, using a free-particle model, while Frieman and Rothenberg are examining the effect of ordered velocities. In their general features, the stability conditions have remained the same. To date, the effect of finiteness of the Larmor radius has not been probed.

The Stellarator has, in addition to its value as a technical apparatus for high-temperature plasma containment, some other advantages, as a research tool for studying plasma physics problems. The advantages of the Stellarator over other facilities in this context are the following. In relation to "mirror machines," its advantage is the absence of particle losses through either end. The self-constricted discharge (pinch) has the disadvantage, from the standpoint of research work, that too many of its parameters vary simultaneously. The magnetic lines of force in a pinch are continuously displaced, velocities and even accelerations are variable, and the dynamical character of the process leads to various side effects. In the Stellarator, where the energy imparted to the plasma is small compared to the energy of the external magnetic field, the magnetic lines of force can be assumed to be practically fixed, while the field configuration inside the plasma can be taken as given.

One drawback of the Stellarator is complexity in design, and the difficulty attendant upon experimental work. This is probably the reason why the Stellarator is being used, as far as available information indicates, for plasma research only at Princeton and at the Max Planck Institute in Munich.

## Study of Plasma Activity

The basic content of work on plasma physics is the study of the as yet somewhat obscure processes associated with instabilities and their ultimate consequences. These processes have been termed "collective phenomena," or plasma activity. Depending on the method used for heating the plasma, different types of plasma activity are distinguished.

To-date the most widely used method of plasma heating is the simplest: ohmic heating. A technique of heating by means of ion cyclotron resonance has been developed by a group working under T. Stix. The Stellarator research program calls for the study of other heating techniques, including fast-particle injection.

Experimental arrangement. The experimental studies discussed in the present report were carried out on the B-3 stellarator, whose design is similar to that of the B-2 facility seen on display at the Second Geneva Conference on the Peaceful Uses of Atomic Energy. The basic parameters of the B-3 device are the following: tube diameter 5 cm, tube length 600 cm, magnetic field from 10 to 40 kilogauss for 30 msec, pressure $10^{-3}$ mm, ohmic heating voltage about 100 v for a loop traversal of 0.5 msec.

Kruskal limit. Theory predicts the onset of magnetohydrodynamic instability beginning at some critical value of current density which has been given the name of Kruskal limit. For disturbances of azimuthal number m = 1, the Kruskal limit predicts an instability region at a current density

$$j \geq 5\ H/L,$$

where $j$ is in amp/cm$^2$, H is in gauss, and L is in centimeters.

Illustration of the process. Figure 3 gives a schematic representation of the time variation of the basic parameters characterizing the discharge process. A current $\gg$ 1000 amp corresponds theoretically to the

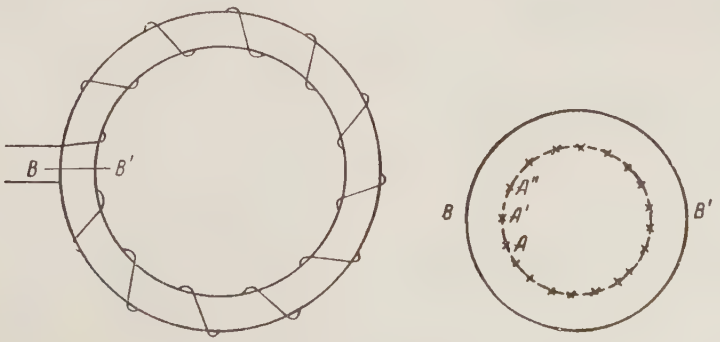


Fig. 2. Rotational transform.

Kruskal limit. The observed current maximum falls much below this theoretically predicted limit. Spectral observations were conducted through a window along the tube axis. The electron concentration was found by using a microwave interferometer at 4.8 mm wavelength.

Particle diffusion. The initial rise in electron concentration is due to the ionization process. After total ionization is reached, the particle concentration begins to fall off, and the ions and electrons drift out of the discharge.

Maximum electron concentration coincides with the instant when total ionization is reached, a fact which is confirmed by the sharp attentuation of the hydrogen line $H_\beta$ in the spectrum (cf. Fig. 3).

The electron concentration later drops approximately exponentially with time as $n_e \sim e^{-t/\tau}$ with time constant $\tau$. Repeated experiments have demonstrated that the graph of $1/\tau$ vs. initial pressure p is a straight line (Fig. 4). The following explanation is offered for this result. Electrons diffuse out of the discharge with a characteristic time $\tau_0$, but, upon arriving at the tube wall, knock out adsorbed hydrogen from the wall, the concentration of adsorbed hydrogen meanwhile being proportional to the initial pressure p.

Neutral hydrogen atoms knocked loose from the walls and entering the volume of the discharge are

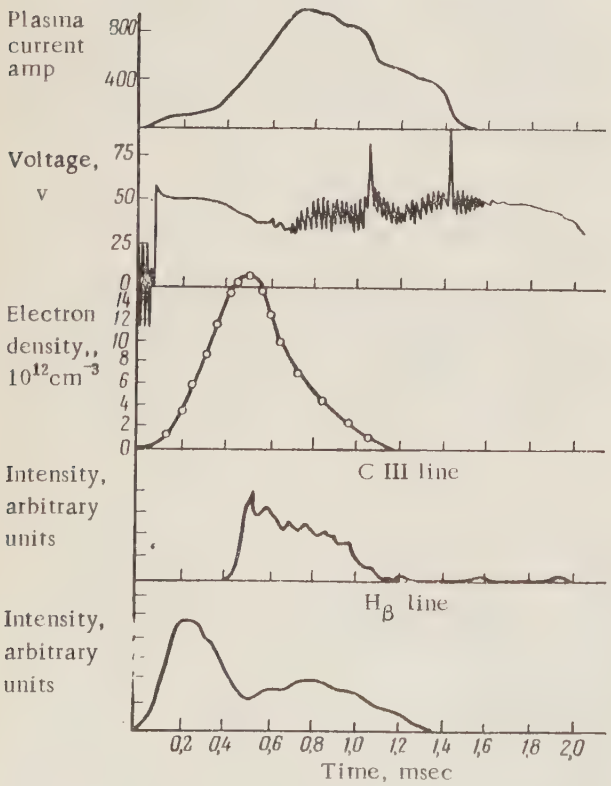


Fig. 3. Time variation of basic parameters characterizing the discharge process.

there ionized, increasing the electron concentration. This process is expressed by the equation

$$\frac{dn_e}{dt} = -\frac{n_e}{\tau_0} + \frac{n_e}{\tau_0}\alpha p = -\frac{n_e}{\tau},$$

and hence $$\frac{1}{\tau} = \frac{1}{\tau_0}(1 - \alpha p).$$

Experiments have shown that $\tau_0$ varies as a function of the magnetic field intensity, viz. as $H^{\frac{1}{2}}$. This result is unexpected, since a more pronounced dependence had been presupposed. It is possible that $\tau_0$ is proportional to the tube diameter. This will be verified on the C-Stellarator, now being built with a tube diameter of 20 cm.

The rate of diffusion of the particles does not change when stabilizing coils are added, from which we infer that observed diffusion bears no relation to magnetohydrodynamic instability. It may be supposed that electrostatic instability associated with low-frequency oscillations of the positive ions is involved.

The following scheme is suggested by way of explaining the proportionality observed between $\tau_0$ and the square root of the field intensity. From dimensionality considerations we see that if diffusion across the magnetic field is independent of the number of collisions, then the simplest formula for the diffusion coefficient will be of the form

$$D \sim \frac{c}{e}\frac{E}{H},$$

where E is the particle energy. Let us assume that the energy picked up by a particle is proportional to the time $\tau$ it dwells in the field, which is in turn inversely proportional to the diffusion coefficient. Then

$$\tau \sim \frac{1}{D} \sim \frac{H}{\tau},$$

and hence

$$\tau \sim \sqrt{H}.$$

Electrostatic instability. Directly following the current maximum on the voltage oscillogram we see sharp oscillations indicative of an instability. These oscillations are obvisouly unrelated to the magnetohydrodynamic instability studied by Kruskal, since current is much less than the critical value predicted by theory. However, the theory proves that an instability of electrostatic origin is possible, due to a drop in electron density, and the observed oscillations may be the result.

We learn from theory that mean free path length should vary inversely with charged-particle concentration. The electron acquires more energy per path length from the electric field, and electron velocity consequently builds up. The Coulomb collision cross section falls sharply as electron velocity rises. As a result, path length and electron velocity increases progressively and more and more electrons become runaways, i.e., move freely in the plasma as in a vacuum. Velocity distribution in the presence of runaway elec-

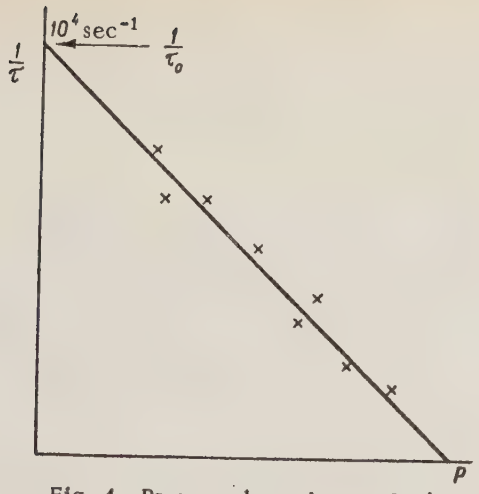


Fig. 4. Pressure dependence of $1/\tau$.

trons has been calculated by Bernstein and co-workers. In this case the distribution function shows two humps. As is known from the writings of Landau and other theoreticians, this velocity distribution is unstable and leads to a build-up of electrostatic oscillations.

The role of runaway electrons may be characterized by the value of the parameter

$$\gamma = \frac{\text{energy acquired in flight}}{\text{mean kinetic energy}} = \frac{kTE}{2\pi ne^3 \ln \Lambda}$$

The value of $\gamma$ at current maximum is approximately constant (0.10-0.20) and independent of H. The appearance of runaway electrons may be revealed by x rays, which emerge in the later stages of the discharge (cf. Fig. 3). The time elapsed from the commencement of the current drop till the appearance of the x rays corresponds more or less to the time required to accelerate the electrons to an energy matching the sensitivity threshold of the x-ray detectors used in the experiment.

## Impurity Problems

Significance of contaminants. Presence of contaminants is not especially important during the ohmic heating stage, but is of decisive nature when further heating is applied by other techniques. After the heating current is turned off, the rate of particle diffusion out of the plasma drops, but the plasma temperature drops simultaneously on account of impurities present. When the level of impurity content is successfully reduced, the the plasma remains hot and, probably, quiescent. It is then possible to employ the magnetic pumping technique for further heating, a method which in princple makes it possible to heat the plasma to very high temperatures, albeit relatively slowly.

Physical impurity level. Impurity content is determined spectroscopically. Basic measurements are carried out on lines of doubly ionized carbon. Regulated amounts of such gases as methane and carbon dioxide are introduced into the gas for calibration purposes. Measurements showed that the plasma's carbon content amounted to 1-10% of the number of hydrogen atoms.

Minimizing content of wall impurities. To minimize the contribution of contaminants from the walls of the facility, the following measures may be resorted to: stainless steel vacuum-melt tubes, and allowing the discharge itself to clean the walls. In the presently accepted systems, pulse repitition rate is 1 pulse per 30 sec.

The wall contribution to the impurity level is lowered when working with a higher pulse frequency. The "Etude" experimental set-up, now being tested out, which functions at a pulse rate of 10 discharges per sec, gives the same results, without warm-up, as the B-3 facility after warming up. The possibility of working with conventional equipment with a pulse rate of one discharge per sec is now being studied. There is hope for eliminating or at least curtailing warming up of the walls by this procedure.

Minimization of impurities contributed by the vacuum system. Mercury pumps are to be relied upon for stellarator outgassing in future work. The feasibility of converting the B-3 stellarator to a mercury system with fore-vacuum pumps using water is under study.

Minimization of impurities due to increased tube diameter. This problem will be looked into when the results of the experiments with the B-3 and C model stellarators are correlated.

## Conclusion

The stellarator, as may be grasped from the above, is a convenient research tool for probing various problems of plasma physics. The results already secured in this area are of indubitable scientific interest, and serve as evidence of the feasibility of improving this approach from all aspects.

* * *

# NEW SHIELDING MATERIALS

The problem of radiation shielding of reactor facilities is one of the fundamental engineering problems in reactor design.

This problem acquires a particular prominence in the design of mobile and transportable nuclear radiation facilities. The complexity of the problem facing the designer materializes in the variety of specifications for shielding against neutron radiation and gammas. Materials for neutron shielding must contain elements of low atomic weight (hydrogen, carbon, beryllium) needed to slow down fast neutrons, and elements with a large absorption cross section for thermal neutrons; it is also desirable to secure thermal neutron absorption unaccompanied by emission of hard gammas. Gamma radiation shielding requires heavier elements (lead, iron, tungsten).

Shielding of portable facilities is usually achieved with a mixture of heavy and light elements: iron-water shielding, lead-water, lead-polyethylene, and iron-graphite shielding combinations [1-4]. However, use of combinations of shielding materials often involves added difficulties in assembly and operation (corrosion, stability to heat load, impact strength, and other problems). Close attention is therefore required in developing new shielding materials combining the properties of "heavy" and "light" shielding. Reports on specimens of such combinations were delivered at the 1958 Geneva Conference on the Peaceful Uses of Atomic Energy [5]. Some papers have also appeared more recently in the foreign literature on new forms of shielding materials.

The Radiation Laboratory of the University of California, working with a private firm, has developed a method for producing a homogeneous dispersion of very fine powdered lead in a paraffin matrix [6]. This material has a density of 4 g/cm$^3$ and possesses the following mechanical (at 32°C temperature) and physical properties:

| | |
|---|---|
| Tensile strength | 14-17 kg/cm$^2$ |
| Shearing strength | 14.9 kg/cm$^2$ |
| Compressive strength | 2.1 kg/cm$^2$ |
| Relaxation length of gamma rays of energy 1.3 Mev | 10.2 cm |
| Relaxation length of neutrons of energy range 2-4 Mev | 10.2 cm |

Goodyear Corp. has developed a new material consisting of synthetic rubber with high hydrogen and powdered boron content [7]. This material is light, readily cast, and withstands temperatures from minus 50°C to +90°C, with a high radiation stability. The fact that the material is serviceable only as neutron shielding is a limitation.

A neutron shielding material consisting of boron-impregnated paraffin has been developed at Columbia University, USA [8]. This material successfully replaces the heavy concrete sheets used as neutron shielding at stationary nuclear facilities.

As a result of research financed by the US lead industry, lead-cemented alloys have made their appearance.

One of these alloys is a boron-lead alloy which has seen successful service as shielding against mixed (neutron and gamma) radiations from nuclear reactors.

I.S.

LITERATURE CITED


1. V. I. Kukhtevich and S. G. Tsypin, Atomnaya Énerg. 5, 4, 393 (1958).*
2. T. Rockwell, Reactor Shielding Design Manual, (New York, 1956).
3. B. T. Price, C. C. Horton, and K. T. Spinney, Radiation Shielding (Harwell, 1958).
4. Yu. V. Sivintsev and B. G. Pologikh (Geneva, 1958) P/2518.
5. E. Blizzard (Geneva, 1958) P/2162.
6. Missiles and Rockets 5, 11 (1959).
7. Missiles and Rockets 5, 28, 47 (1959).
8. Chem. Eng. 66, 14 (1959).


*Original Russian pagination. See C. B. translation.

# BRIEF NOTES

USSR. The workshops of the Ministry of Health and Sanitation of the Moldavian SSR have entered into mass production of a portable automatic facility for counting in work with radioactive isotopes. The facility automatically counts and simultaneously records on paper tape the number of radioactive decays in 50 specimens of soil and microorganisms.

East Germany. A treaty was drawn up and signed in November 1959 with the Rumanian Peoples Republic on collaboration in the area of nuclear engineering and nuclear research.

Finland. A uranium ore processing plant is under construction in the Kola region. Work is tentatively scheduled for completion in 1960.

The annual output of the plant will be 30,000 tons of ore with 0.2% uranium oxide content included in the composition of pitchblende and secondary uraniferous materials. After crushing, the ore is processed with sulfuric acid.

# NEW LITERATURE

## Books and Symposia

Power Reactors of the USA. Translated from English. Moscow, Atomizdat, 86 pages. 6 rubles, 10 kopeks.

Uses of Radioactivity in Engineering. E. Broda and T. Schönfeld. Translated from German. Moscow, Fizmatgiz, 1959. 443 pages. 13 rubles, 75 kopeks.

This book gives a survey of work on radioactivity applications in industry, covering publications to 1956. The first three chapters provide the basic information on radioactivity, measurements of radioactive radiation, and chemical processing of radioactive isotopes. The subsequent chapters consider applications of radioactive isotopes in various branches of industry. A table of radioactive isotopes useful for practical applications appears at the end of the book. A detailed bibliography is assigned to each chapter.

The book is written for college-level readership.

Kernverfahrenstechnik (Nuclear engineering techniques, in German). W. Mialki. Berlin, Spring-Verlag, 1958. 472 pages.

Many important problems in nuclear engineering are approached. The basics of nuclear physics are reviewed briefly, theory is outlined, and a classification of thermal reactors is provided. Materials used in reactor design are discussed. The basic control principles in nuclear reactor control are described. Methods for producing and enriching fissionable materials are shown, and manufacturing methods for fuel elements plus processing of radioactive wastes are discussed. Problems of heat transfer in reactors receive ample attention. The book is profusely illustrated. Data useful in practical calculations are tabulated for engineers working in the area of nuclear industry.

Lexikon der Kern- und Reaktortechnik. (Explanatory dictionary on nuclear and reactor science, in German). Publ. by K. Hocker and K. Weimer, Stuttgart Franckhische Verlagshandlung. 1959, 1688 pages.

The dictionary has over 3000 entries on nuclear physics, reactor engineering, and related branches of physics, engineering, chemistry, biology, and medicine. Besides terms in German, equivalents in English and French are provided. Many of the definitions relating to design, processes, etc., are illustrated by drawings, diagrams, graphs, figures. Tables of the most important physical constants are numerous, and a complete table of isotopes is presented. Basic data on reactors in operation, under construction, or planned are brought up to mid-1958. The dictionary offers copious references to the literature. It may prove useful as a reference, or as a translating medium to and from German, English, and French: in two volumes.

## ARTICLES FROM THE PERIODICAL LITERATURE

### I. Nuclear Power Physics

Vestnik Akad. Nauk SSSR 29, No. 11 (1959).

I. D. Rozhanskii, pp. 79-82. Problems of high-energy physics.

Doklady Akad. Nauk SSSR, 128, No. 6 (1959).*

B. M. Gokhberg et al., pp. 1157-1159. Effective cross sections and anisotropy of fission of $Np^{237}$ and $Th^{230}$.

Zhur. Éksp. i Teoret. Fiz. 37, No. 5 (11) (1959).

L. I. Rudakov and R. Z. Sagdeev, pp. 1337-1341. Oscillations of an inhomogeneous plasma in a magnetic field.

B. M. Bolotovskii and A. A. Rukhadze, pp. 1346-1351. Field of a charged particle in a nonstationary medium.

B. B. Kadomtsev, pp. 1352-1354. Plasma equilibrium in helical symmetry.

L. M. Kovrizhnykh, pp. 1394-1400. Velocity distribution of electrons in a strong electric field.

A. A. Vorob'ev et al., Uses of ratio of intensities of transitions to first excited levels of daughter nuclei in decay of $U^{238}$ and $U^{234}$.

A. P. Kazantsev, pp. 1463-1464. Motion of a charged particle in a rotating magnetic field.

Zhur. Éksp. i Teoret. Fiz. 37, No. 6 (12) (1959).

B. B. Kadomtsev, pp. 1646-1651. On stability of a low-pressure plasma.

L. M. Kovrizhnykh, pp. 1692-1696. On the oscillations of an electron-ion plasma.

N. V. Fedorenko and V. A. Belyaev, pp. 1808-1810. On the maximum cross section for nonresonance charge-transfer.

G. N. Smirenkin, pp. 1882-1824. Comparison of effective temperatures of spectra of neutrons emitted in fission of $U^{235}$ and $Pu^{239}$ by fast neutrons and thermal neutrons.

Izv. Vyssh. Ucheb. Zavedenii. Priborostroenie, No. 2 (1959).

O. P. Korovin et al., pp. 47-51. Stabilization and control of peak energy of $\gamma$ radiation of the 100 Mev synchrotron.

E. M. Belov, and V. M. Razin, pp. 52-55. Extremum-type (bang-bang) control device for intensity of betatron radiation.

Izv. Vyssh. Ucheb. Zaved. Radiofizika 2, No. 4 (1959).

B. N. Gershman, pp. 654-656. On longitudinal waves excited in a nonisothermal plasma.

Izv. Vyssh. Ucheb. Zaved. Fizika, No. 5 (1959).

B. N. Rodimov et al., pp. 6-13. Buidling up large betatron currents.

B. S. Kaz'min, pp. 14-18. Accelerator drift tube for producing a beam of high-intensity electrons.

G. I. Dimov and Yu. K. Petrov, pp. 19-25. On computing tolerances of magnetic field for a weak-focusing accelerator with magnet sectors.

V. A. Moskalev and Yu. M. Akimov, pp. 16-30. Commissioning of the 10 Mev double-chamber stereo-betatron.

Yu. M. Akimov et al., pp. 31-34. On extraction of an electron beam from the betatron chamber.

B. A. Moskalev et al., pp. 35-44. A high-current pulsed stereobetatron.

P. A. Cherdantsev, pp. 45-50. Effect of external disturbances on the behavior of space-charge density in a betatron vacuum chamber.

Yu. I. Remnev, pp. 81-85. On stresses in a solid under neutron bombardment.

Radiotekhnika i Électronika 4, No. 11 (1959).

M. D. Gobovich and L. L. Pasechnik, pp. 1850-1853. Plasma electron resonance.

Pribor. i Tekh. Éksper. No. 5 (1959).

V. I. Kotov et al., pp. 19-22. On the theory of a ring synchrocyclotron with radial sectors.

A. A. Kolomenskii and A. P. Fateev, pp. 22-26. Determination of tolerances for parameters of magnetic field in accelerators, using eigenfunctions.

E. L. Burshtein and A. D. Vlasov, pp. 26-28. Design of klystron buncher for a linear electron accelerator.

B. M. Golovin et al., pp. 33-35. A device incorporating an annular scatterer for improving small-angle scattering on high-energy neutrons.

A. P. Komar et al., pp. 36-40. Controllable diffusion chamber.

G. A. Vasil'ev, pp. 75-80. Traveling-wave cascade voltage multiplier.

G. E. Levin, pp. 80-85. New types of electrostatic generators: induction and tribo-induction machines.

V. N. Logunov and S. S. Semenov, pp. 122-123. Contractor device for a betatron.

Trudy Radiev. Inst. Im. Khlopina 8 (1959).

Yu. N. Artem'ev et al., pp. 78-83. Investigation of $\gamma$ rays accompanying fission of $U^{235}$ by thermal neutrons.

M. A. Bak, pp. 87-90. Analysis of a neutron field of uniform density.

M. A. Bak, pp. 192-206. Wall effect in ionization chambers.

K. K. Aglintsev et al., pp. 253-257. Effective electronic spectra in air-equivalent ionization chambers.

Kernergie 2, Nos. 10-11 (1959).

M. Ardenne and S. Schiller, pp. 893-899. A universal electron-ion source for Van de Graaff accelerators.

Nucl. Sci. and Eng. 6, No. 4 (1959).

W. Conkie, pp. 260-266. Polynomial approximations in neutron transplant theory.

W. Conkie, pp. 267-271. An iterative method in neutron transplant theory.

Nucleonics 17, No. 10 (1959).

S. Colgate, pp. 82-84. Report on the Uppsala Conference. Fusion, one year after Geneva.

Nucleonics 17, No. 11 (1959).

D. Hughes, pp. 132-133. New world-average thermal cross sections.

Physica 25, No. 10 (1959).

H. Brinkman, pp. 1016-1020. On the motion of a charged particle in an inhomogeneous fluid.

## II. Nuclear Power Engineering

Inzh.-Fiz. Zhur. 2, No. 9 (1959).

Ya. Malak and I. Shmid, pp. 12-23. Study of heat transfer in a homogeneous BWR.

Teploénergetika, No. 12 (1959).

V. A. Kirillin and S. A. Ulybin, pp. 77-80. On the thermodynamical properties of ordinary water and heavy water.

Trudy Radiev. Inst. Im. Khlopina, 9 (1959).

Yu. L. Khazov et al., pp. 91-103. Energy distribution of neutrons in water surroudning a source.

Atompraxis 5, Nos. 10-11 (1959).

S. Lacey, pp. 416-419. Control system at nuclear power stations.

Chem. and Process Eng. 40, No. 10 (1959).

pp. 397-398, 404. Atomic energy in China.

Energia Nucleare 6, No. 11 (1959).

A. Ascari, pp. 702-706. Estimation of damage during start-up of a reactor.

Jaderná Energie 5, No. 10 (1959).

J. Cockcroft, pp. 326-330. Program for development of nuclear power in the UK.

Jaderná Energie 5, No. 11 (1959).

J. Drásky, pp. 362-366. Power engineering problems arising in the building of nuclear electric power stations.

J. Kvasnička and Z. Lát, pp. 367-372. Ventilation and heating principles in nuclear engineering enterprises.

J. Nucl. Energy. Part A. Reactor Sci. 11, No. 1 (1959).

A. Waltner and B. Leonard, pp. 1-7. Measurement of neutron output during spontaneous fusion of natural uranium.

N. Pattenden and V. Rainey, pp. 14-18. Cross section of $Pu^{240}$ for slow neutrons.

K. Singwi, pp. 19-20. On the theory of diffusion cooling of thermal energy neutrons.

A. Jaffey, pp. 21-30. The value of $\bar{\nu}$ on thermoneutrons for $Pu^{241}$ in solid inhibitors.

D. Littler, p. 34. The intensity of neutron emission during spontaneous fission of natural uranium.

D. Hone, p. 34. Magnitude of the mean free transport mileage for $D_2O$.

Kernenergie 2, No. 7 (1959).

K. Meyer, pp. 597-601. Calculations for critical state of a special model of boiling-water reactor.

Kernenergie 2, No. 8 (1959).

K. Meyer and E. Griepentrog, pp. 693-698. Calculations of fuel-element burnup in thermal reactors with a hard spectrum. II. Calculations of extent of burnup at nonideal reactor performance.

Kernenergie 2, No. 9 (1959).

H. Spindler and F. Thummler, pp. 781-794. The problem of corrosion in water-cooled high-temperature reactors.

Nucl. Energy Engr. 13, No. 137 (1959).

pp. 489-490. Atomic electrostations in Trawsfynydd.

pp. 491-495. Research in the field of neutron physics.

pp. 496-497. Receiving overheated steam from a sodium experimental reactor.

pp. 499-501, 510. Research work of the firm "Hawker-Sidley Nuclear Power."

pp. 502-506. Utilization of organic retarders and thermocouples in power reactors.

Nucl. Energy Eng. 13, No. 138 (1959).

pp. 534-537. Reasearch reactor "Merlin".

I. El-Ibiary, pp. 545-549. Conversion of power in a heavy-water reactor during accidental stoppage.

pp. 552-555. The Dresden reactor brought to the critical stage.

Nucl. Eng. 4, No. 43 (1959).

D. Jubb, pp. 431-434. Condensation in a reactor containment vessel.

pp. 435-438. The Marcoule reactor G-2.

p. 441. Research at Culcheth.

R. Forbes, pp. 442-445. Radiographic inspection.

A. Gifford and B. Litting, pp. 446-447. Inspection of nuclear components.

R. Beech, pp. 448-449. Testing graphic struts.

W. Steckelmacher, pp. 450-453. Leak detection.

J. Cole, pp. 454-455. Unconventional methods.

Nucl. Power. 4, No.44 (1959).

p . 93. Fast neutron breeder-reactor in Dunrea brought to critical condition.

J. Phillips, pp. 94-100. The triggering of the reactor in Dunrea.

H. Sandiford, pp. 100a-102a. Control by a fast reactor.

I. Everson, pp. 103-108. Water-loop of the high pressure reactor DIDO.

pp. 109-111. Proposals on the development of atomic power in the USA.

A. Gray, pp. 112-116. Ionization chambers with gamma-compensation for the regulation of a reactor.

J. Ayre, pp. 117-118. Thermocouple for the control of a reactor.

Nucl. Power. 4, No. 44 (1959).

C. Grove-Palmer and H. Pass, pp. 118-121. Characteristics of the organic thermocarrier Santovax R.

Nuclear Sci. and Eng. 6, No. 4 (1959).

R. Stone et al, pp. 255-259. Transient behavior of TRIGA, a zirconium-hydride water-moderated reactor.

Nucl. Sci. and Eng. 6, No. 4 (1959).

C. Walter, pp. 279-283. A fuel element for an elevated-temperature crtical assembly.

C. Cohn, pp. 284-287. Errors in reactivity measurements due to photoneutron effects.

A. Rotenberg, pp. 288-293. A Monte Carlo calculation of thermal utilization.

A. Sola and W. Managan, pp. 294-297. Flux perturbation produced by ion chambers and fission chambers.

Y. Fukai et al., pp. 298-305. Calculations of flux distributions in a boiling water reactor.

S. Fultz, pp. 313-319. The time-dependent thermal neutron flux from a pulsed subcritical assembly.

G. Baldwin, pp. 320-327. Kinetics of a reactor composed of two loosely coupled cones.

C. Zucker and L. Haring, pp. 328-332. Measuring the release time and total drop time of a control rod.

H. Smets, pp. 341-349. The application of topological methods to the kinetics of homogeneous reactors.

Nucleonics 17, No. 8 (1959).

S. Baron, pp. 60-62. Advanced power reactor studies. Engineering comparisons.

G. Hoveke and J. Felice, p. 63. $D_2O$ - Natural uranium reactor.

Nucleonics 17, No. 9 (1959).

J. Kenton, pp. 73-81, Atomic sea trials. pp. 82-85, Building the nuclear navy.

A. Liebshutz and M. Miller, pp. 126-127. The Georgia reactor. New faculty for dynamic irradiation testing.

Nucleonics 17, No. 10 (1959).

N. Triner, pp. 78-81. Structural design in high-temperature reactors.

J. Wilson. pp. 90-96. Instrument development at Savannah River. I. Nondestructive testing equipment.

pp. 98-101. Simple relations describe reactor power bursts.

J. Thie, pp. 102-111, Statistical analysis of power. Reactor noise.

Nucleonics 17, No. 11 (1959).

C. Trilling, pp. 113-117. OMRE operating experience.

pp. 124-131. Test reactor futures. A panel discussion.

G. Safford and W. Havens, pp. 134-138, 205-206. Fission parameters for $U^{235}$.

Nucleonics 17, No. 12 (1959).

pp. 65-75. Rebuilding Dresden.

p. 104. Nuclear engineering. Task force sums up fluid-fuel reactors.

R. Hammond et al., pp. 106-109. Turret. A test of unclad fuel.

C. Kroeber and J. Welch., pp. 110. Control-rod drive for HTGR.

Science 130, No. 3382 (1959).

L. Farr, pp. 1067-1071. Brookhaven reactor for medical research.

## III. Nuclear Fuel and Materials

Geokhimiya, No. 7 (1959).

E. K. Gerling and Yu. A. Shukolyukov, pp. 608-618. Accumulation of the isotope $A^{38}$ in uraniferous minerals.

Doklady Akad. Nauk SSSR 129, No. 2 (1959).

K. I. Sakodynskii and N. M. Zhavoronkov, pp. 391-393. Effect of $\gamma$ radiation on rate of hydrogen exchange between water and isoamylthiol.

Zhur. Anal. Khim. 14, No. 5 (1959).

Yu. A. Chernikhov et al., pp. 567-570. Complexometric assay of thorium in monazite concentrates.

D. I. Ryabchikov et al., pp. 581-587. Study of interaction between hexavalent uranium and Complexon III (EDTA).

Izv. Akad. Nauk SSSR. Otdel Tekh. Nauk. Metallurgiya i toplivo No. 3 (1959).

B. V. Sharov, pp. 148-150. Structure of surface layer of uranium resulting from electric-spark erosion treatment.

Izv. Akad. Nauk SSSR, Ser. Geol. No. 11 (1959).

A. Ya. Krylov, pp. 8-14. Distribution of uranium and thorium in some single-phase intrusions of the Tien-Shan.

Izv. Akad. Nauk. SSSR, Ser. Fiz. 23, No. 10 (1959).

I. Ya. Kachkurova et al., pp. 1253-1255. Study of radiolysis of alkanes with the aid of ultraviolet and infrared spectroscopy.

Radiokhimiya I, No. 5 (1959).

S. E. Bresler et al, pp. 507-513. Zirconium-based ion-exchange resins.

I. E. Starik et al., pp. 545-547. Use of phenylarsonic acid to separate neptunium and plutonium.

M. E. Krevinskaya et al., pp. 548-561. Properties of nitric-acid solutions of plutonyl nitrate.

M. E. Krevinskaya et al., pp 562-566. Isolation of plutonyl nitrate, and its properties.

A. M. Gurevich and L. P. Polozhenskaya, pp. 567-572. Investigation of the solid phase in the system $UO_2(NO_3)_2 - ROH - H_2O_2 - H_2O$.

V. I. Kuznetsov and S. B. Savvin, pp. 583-588. Rapid photometric determination of throrium with the reagent thoron II.

V. I. Kuznetsov and S.B. Savvin, pp. 589-595. Rapid photometric determination of uranium with the reagent arsenazo II.

K. F. Lazarev, pp. 603-612. Methods for determining the limiting leachability of radioelements from minerals.

Trudy Inst. Geol. Rudnykh Mestorozhdenii, Petrografii, Mineralogii i Geokhimii No. 28 (1959).

I. G. Chentsov, pp. 43-82. Problems in the mineralogy and geochemistry of some sedimentary uraniferous ore showings.

I. G. Chentsov, pp. 142-147. On uranium intrusions in some rock-forming minerals.

Uspekhi Khimii 28, No. 11 (1959).

A. K. Lavrukhina, pp. 1310-1340. The role of nuclear processes in the formation of the chemical elements.

E. Segrè, pp. 1392-1398. New forms of atoms and anti-matter.

Khim. Nauka i Promyshlennost' 4, No. 5 (1959).

B. D. Stepin et al., pp. 681-682. Latest techniques in the production of some thorium salts.

E. Cerrai and C. Testa, pp. 707-716. Extraction and determination of zirconium and hafnium by a method of flowing anion exchange in hydrochloric acid.

Jaderná Energie 5, No. 10 (1959).

J. Pluhar and J. Vrtel, pp. 331-335. Fuel elements, fuel-element cladding, and reactor structural materials. II. Structural materials.

J. Ruziska, pp. 340-344. Production of heavy water by hydrogen distillation.

M. Ardenne, pp. 345-348. An electronic oscillator for the radiochemical laboratory.

Jaderná Energie 5, No. 11 (1959).

M. Pasek, pp. 373-377. Study of liquid metals at the Nuclear Research Institute of the Czechoslovak Academy of Sciences, 1956 to 1958.

J. Inorg. and Nucl. Chem. 11, No. 3 (1959).

H. Scherff and G. Herrmann, pp. 247-248. Zur Herstellung von $Nb^{95}$-freiem $Zr^{95}$ durch TTA-Extrakon.

J. Nucl. Energy. Part A. Reactor Sci. 11, No. 1 (1959).

J. Adam and B. Cox, pp. 31-33. Conversion of phase in solid solutions of zirconium due to illumination.

J. Nucl. Materials 1, No. 3 (1959).

W. Thurber and R. Beaver, pp. 226-232. Aluminum with scattered uranium carbide plate-like thermoemitting elements with a great concentration of uranium.

F. Ellinger et al., pp. 233-243. The system of uranium-plutonium.

P. Pfeil and L. Griffiths, pp. 244-248. The influence of insertion on the behavior of metals in an arc discharge.

D. Jansen and E. Hoffman, pp. 249-258. Alloy lithium-lead for protective installation. Metallurgical research.

A. Bel et al., pp. 259-270. Sintering of uranium oxide in hydrogen at 1350°C.

W. Yeniscavitch et al., pp. 271-280. Absorbtion of hydrogen by zirconium alloy-2 enriched by nickel.

D. Evans and G. Raynor, pp. 281-288. Transition of a thorium screen, dependent on solution.

B. Howlett, pp. 289-299. Alloys of systems uranium-titanium-zirconium.

Y. Adda, et al., pp. 300-301. Research on self-diffusion in the beta-phase of uranium.

R. Tuxworth and W. Evans, pp. 302-303. Plane emission of $U_4O_9$ in uranium dioxide.

Kernenergie 2, No. 10-11 (1959).

C. Weissmantel, pp. 909-919. A scintillation spectrometer for radiochemical research work.

Memoires Scient. Rev. Metallurgie 56, No. 6 (1959).

A. Boettcher, pp. 625-628. Critical limits of possible additives to uranium metal and uranium compounds, for fuel elements.

Memoires Scient. Rev. Metallurgie 56, No. 7 (1959).

L. Champeix, pp. 657-662. Analysis of small amounts of carbon in uranium.

L. Leach, pp. 675-680. Study of corrosion in manganese and uranium.

H. Coriou, pp. 693-703. Effect of carbon and its distribution on corrosion of zirconium in water at 315°C.

G. Sainfort, pp. 704-712. Mechanism and laws of corrosion of zirconium at high temperatures.

H. Martens et al., pp. 721-730. Resistance of graphites to extension at high temperatures.

Mining Eng. 11, No. 7 (1959).

A. Tanner, pp. 706-708. Meteorological influence on radon concentration in drill holes.

Nucl. Sci. and Eng. 6, No. 4 (1959).

O. Dwyer and A. Eshaya, pp. 350-360. On the removal of volatile fissionable products from uranium-bismuth reactor fuels.

A. Poindexter, pp. 162-168. Decreasing the cost of producing combustibles.

Nucleonics 17, No. 12 (1959).

R. Connally, pp. 98-100. Uranium analysis by gamma absorbtion.

Trans. Metallurg. Soc. AIME 215, No. 5 (1959).

W. Gruzensky and G. Engel, pp. 738-742. Division of yttrium and rare-earth nitrates with the help of the extracting system 3 n-butyl-3 methyl-2 butanone.

L. Porter and G. Diennes, pp. 854-863. Influence of neutron exposure on martensite transformation in ferronickel alloys.

N. Peterson and R. Ogilvie, pp. 873-874. The influence of radiation on the velocity diffusion of arsenic in germanium.

D. Deardorff and H. Kato, pp. 876-877. Temperature of the alpha-beta-transformation of hafnium.

## IV. Nuclear Radiation Shielding

Geokhimiya, No. 7 (1959).

V. I. Baranov and L. A. Khristianova, pp. 619-622. Radioactivity of the water of the Indian Ocean.

Zhur. Anal. Khim. 14, No. 5 (1959).

N. I. Gusev et al., pp. 606-611. New methods in packaging for handling radioactive materials.

Ivz. Timiryaz. Sel'sko-Khoz.,Akad. No. 5 (1959)

I. V. Gulyakin et al., pp. 29-46. Study of relationship between strontium-90 and calcium in soils and plants.

Med. Radiol. 4, No. 11 (1959).

J. Nosek and W. Chmelarz, pp. 74-76. Deactivation of skin in cases of contamination by radioactive materials.

Pribor. i. Tekh. Éksp. No. 5 (1959).

E. A. Zherebin et al., pp. 29-32. A fast neutron spectrometer.

V. V. Matveev et al., pp. 40-44. Determination of certain parameters of photomultiplier tubes and scintillators.

A. M. Ratner, pp. 44-47. Mean light output of scintillators.

G. A. Kirdina and N. K. Pereyaslova, pp. 47-51. Preparation of and properties of large scintillating plastics.

Yu. K. Gus'kov and A. V. Zvonarev, pp. 121-122. Thermocouple system for measuring fast neutron fluxes.

G. G. Aref'ev, pp. 123-124. Determination of corrections in beta measurements.

Radiokhimiya 1, No. 5 (1959).

V. K. Zinovleva et al., pp. 613-615. Procedure for isolating strontium from soil and for assay of $Sr^{90}$.

V. P. Shvedov et al., pp. 616-618. Determination of radioactive strontium in aqueous samples (rain and snow precipitates).

L. K. Ponomaseva and V. L. Zolotavin, pp. 619-621. Desportion of radiostrontium and radiocesium from suspended particles in the water in open reservoirs.

Trudy Radiev. Inst. im. Khlopina 9 (1959).

G. M. Gorodinskii, pp. 258-167. Method for measuring half-lives of short-lived radioactive elements.

Atompraxis 5, Nos. 10-11 (1959).

K. Franz, pp. 381-387. Single-channel and multi-channel pulse height analyzers.

K. Jordan, pp. 401-407. Use of coincidence circuits and gating circuits in scintillation spectrometry.

F. Rinn, pp. 407-415. Neutron detectors.

A. Wensel, pp. 419-421. Contamination of air by long-lived $\gamma$-decay products.

H. Kiefer and R. Maushart, pp. 431-433. Constant direct control of low-level $\beta$-activity in water.

E. Graul, pp. 434-443. Problems of safety and shielding in reactor design and in handling radioactive isotopes.

Jaderná Energie 5, No. 11 (1959).

V. Santholzer, pp. 378-382. Artificial radioactivity of air as a result of nuclear weapons testing.

Kernenergie 2, Nos. 10-11 (1959).

K. Schmidt and H. Zindler, pp. 900-903. On the problem of artificial radioactivity of the atmosphere.

R. Höhle, pp. 904-908. Differential calorimeter for β-activity measurements.

Jaderná Energie 5, No. 10 (1959).

Zezula, pp. 349-350. Approximate calculation of total beta-activity of decay products of $U^{235}$.

Nucl. Energy Engr. 13, No. 138 (1959).

H. Dunster, pp. 540-543. Disposal of radioactive wastes to the coastal waters.

Nucl. Sci. and Eng. 6, No. 4 (1959).

L. Ruby and J. Rechen, pp. 272-278. An efficient counting system for the detection of neutrons from low-yield pulsed neutron sources.

Nucleonics 17, No. 9 (1959).

J. Smit et al., pp. 116-123. AMP – Effective ion exchanger for testing fission wastes.

Nucleonics 17, No. 10 (1959).

M. Green, p. 77. Absorption of monoenergetic x- and γ-rays.

Nucleonics 17, No. 11 (1959).

J. Wilson, pp. 140-148. Instrument development at Savannah River. II. Reactor, process instruments.

M. Van Dila, pp. 150-155. Large-crystal counting.

W. George and L. Bacon, pp. 173-178. Application of present worth to waste-disposal economics.

Nucleonics 17, No. 12 (1959).

R. Domish, et al., pp. 76-79. Calcination of high-level wastes for ultimate disposal.

J. Wilson, pp. 86-96. Instrument development at Savannah River Laboratories. III. Health physics, laboratory instruments.

Sewage and Ind. Wastes 31, No. 10 (1959).

R. Schechter and E. Gloyna, pp. 1165-1174. Thermal considerations in the storage of radioactive wastes.

H. Swope, pp. 1191-1196. Radioisotope wastes handling.

## V. Radioactive and Stable Isotopes, Uses of Radioactive Radiations

Vestnik Akad. Nauk SSSR 39, No. 11 (1959).

V. K. Matveev, and V.V. Patrikeev, pp. 53-55. Luminescent labeled sands.

Doklady Akad. Nauk SSSR 128, No. 6 (1959).

I. N. Plaksin et al., pp. 1208-1209. Use of artificial radioactivity induced by α particles for quantitative inspection of products containing aluminum and boron.

Myasnaya Industriya SSSR No. 5 (1959).

G. Egiazarov, pp. 51-53. Radiolysis of animal fats under bombardment by low-level doses of gamma-rays.

Neftyanik No. 11 (1959).

T. Kh. Abramyan, p. 23. A device for introducing radioactive isotopes into the bore hole during casing work.

Trudy Nauchno-Issled. Inst. Kabel'noi Prom. No. 4 (1959).

E. E. Finkel', pp. 96-103. Effect of ionizing radiations on permeability to moisture of polythene.

Uchen. Zap. Leningrad. Univ. No. 278. Ser. Fiz. i Geol. Nauk No. 11 (1959).

A. N. Makarov, pp. 109-118. On the use of neutron gamma-logging in coal mines.

Khim. Prom. No. 6 (1959).

V. L. Karpov et al., pp. 6-12. Increasing the heat stability of polythene insulation of wiring by bombardment with ionizing radiation.

Energia Nucleare 6, No. 11 (1959).

F. Levi, pp. 693-695. Radiation effects in semiconductors.

Nucl. Energy Eng. 13, No. 137 (1959).

F. Paulsen, pp. 485-488. Application of radioactive isotopes to agriculture.

Nucl. Energy Eng. 13, No. 138 (1959).

F. Paulsen, pp. 531-533. Equipment for irradiating foodstuffs.

Nucleonics 17, No. 10 (1959).

pp. 112-113. Applied radiation. Food irradiators look to low-dose treatments.

Nucleonics 17, No. 11 (1959).

pp. 182-199. Analysis, tracing and radiation processes.

Nucleonics 17, No. 12 (1959).

C. Rosenblum, pp. 80-83. The chemistry and application of tritium labeling.

V. Guinn and R. Coit, pp. 112-117. Measuring of oil consumption with tritium tracers.